The
University
Of
Sheffield.

Access to Electronic Thesis

Author:	Meurig Thomas
Thesis title:	On the Characterisation of Subsurface Deformation Microstructures in Aerostructural Titanium Alloys
Qualification:	PhD

If this electronic thesis has been edited by the author it will be indicated as such on the title page and in the text.

On the characterisation of subsurface deformation microstructures in aerostructural titanium alloys

Meurig Thomas MEng ARSM

Department of Materials Science & Engineering

A thesis submitted for the degree of Doctor of Philosophy of the University of Sheffield, March 2012

The
University
Of
Sheffield.

"Though wise men at their end know dark is right
Because their words had forked no lightning they
Do not go gentle into that good night"

Dylan Thomas

Abstract

A research programme has been undertaken to investigate the subsurface deformation microstructures in aerostructural titanium alloys that result from industrial surface finishing processes. Microstructural analysis of the region immediately below the treated surface has been performed for high speed machined and shot peened material, with emphasis placed on characterising the mode of plastic deformation through high resolution scanning electron microscopy and electron backscatter diffraction. Both shot peening and high-speed machining result in a plastically deformed subsurface layer, with experimental evidence collected through electron backscatter diffraction suggesting that the mode of plastic deformation is influenced by local textural heterogeneities (microtexture) in addition to alloy chemistry and substrate temperature.

The stability of the deformed subsurface microstructure following exposure to elevated temperature is investigated for the near-alpha titanium alloy Ti-834. Here, shot peening leads to an increase in oxygen uptake kinetics during exposure to laboratory air in the temperature range 600°C to 700°C. The increased levels of subsurface oxygen versus the non-shot peened condition were measured by secondary ion mass spectrometry and fatigue testing has suggested a lowering of the high cycle endurance limit in shot peened Ti-834 following prolonged thermal exposure in air.

The outcomes of this research suggest that the mode (and magnitude) of the residual plastic strain introduced by shot peening and high speed machining may be predicted; should an improved understanding of microtexture evolution during the primary processing (such as hot-working) of titanium alloys be achieved.

Acknowledgements

Firstly, I would like to express my sincere thanks to Dr Martin Jackson and Professor Trevor Lindley for their continued guidance and support throughout the course of this research. I would also like to extend a thank you to Prof. Dave Rugg (Rolls-Royce) for his technical input into the project and expert knowledge. A special mention should also go to Mr Graham Hammersley (Metal Improvement Company) and Dr Sam Turner (AMRC with Boeing) for their respective efforts in facilitating the shot peening and high speed milling trials; without whom much of this research would not have been possible.

I would also like to thank all those who have assisted me through the course of this research programme, with a particular mention to Wayne van Rooyen, Michael Robinson, Andrew Cunliffe and Mark Richardson for their individual efforts as project students over the past years. For her assistance in collecting the electron backscatter diffraction data, I am grateful to Magda Lopez-Pedrosa and likewise for the secondary ion mass spectrometry data, I wish to thank Richard Chater at Imperial College.

Finally, I would like to thank my family and friends who have helped and supported me tremendously throughout the last few years.

Contents

List of Tables

List of Figures

2. Literature review

3. An investigation into the microstructure and properties of shot peened Ti-834

4. Deformation mechanisms during shot peening: The role of chemistry, temperature and microtexture

5. Microstructural Damage during High Speed Machining of Ti-834 and Ti-6Al-4V

Chapter 1

Introduction

The use of titanium alloys in the aerospace sector has grown rapidly throughout the latter half of the twentieth century and into the twenty-first. For example, approximately 120 tonnes of titanium alloy is used for the construction of the Boeing 787 Dreamliner; compared to less than 20 tonnes in similar size airframes from the 1970s such as the Boeing 757 and 767 [1]. For airframe gas turbine power plants, titanium has superseded steel alloys for use in the low and intermediate pressure compressor assemblies, with advanced high temperature near-α titanium alloys competing with nickel alloys in the "hot-end" high pressure compressor stages of the Rolls-Royce Trent 700 and RB211 engines [2].

The drive to improve aircraft gas-turbine efficiency has led to substantial development of lightweight titanium alloys capable of operating at high temperatures. Alloys such as Ti-834 provide medium strength, good creep, fatigue and oxidation resistance up to temperatures of 600°C. In order to further improve the mechanical properties of a component, surface treatments are often employed in the final stages of the manufacturing process, prior to assembly. The high strain rate, cold working process of shot peening, is one such example. In addition to improving environmental cracking and tribological properties, the introduction of compressive residual stresses up to a depth of 200-300 μm beneath the peened surface prolongs the service life of a component through retardation of microcrack propagation [3] and it is well documented that shot peening improves the ambient temperature fatigue properties of Ti-6Al-4V [4].

Prior to surface finishing processes such as shot peening, titanium alloy components are machined into net geometry from the condition of supply forging. Due to the difficulties in machining titanium at productive rates, there have been concerted efforts to advance the boundaries of high productivity machining with particular emphasis placed on high speed milling for finishing and semi-finishing applications. Finishing passes during machining and the shot peening process both introduce residual plastic strain into the surface of a component [5][6]. Although considerable research effort has focused on the resultant subsurface residual stress profiles associated with both the shot peening and machining process, less attention has been paid to characterising the micromechanisms of plastic deformation and the effect such deformation structures may have on the subsurface microstructural stability during service conditions. This is particularly pertinent to the high temperature class of near-α

titanium alloys, such as Ti-834, where in-service degradation such as surface oxygen embrittlement may occur.

Although the residual deformation structures following machining [7] and shot peening [8] have recently been studied for the classical engineering materials and nickel alloys, the purpose of this research programme is to characterise the microstructural response of structural titanium alloys to industrial surface finishing processes, namely shot peening and high performance milling. Whilst it may appear somewhat abstract to compare high speed machining and shot peening within the same package of research, there is considerable synergy in the characterisation methods employed to study the effects of these two processes. The intention of this research programme is to therefore use the shot peening and high speed milling processes as a means through which the mechanisms of subsurface plastic deformation are studied, rather than the optimisation and development of the individual operations, which would typically fall within the remit of the mechanical or manufacturing engineer.

The presentation and discussion of experimental results reported in this thesis is divided into three chapters: The first discusses the effect of shot peening on the subsurface microstructure and properties of the near-alpha titanium alloy Ti-834 following long-term high temperature exposure in air. Following this, the effect of alloy chemistry, temperature and microtexture on the mode of plastic deformation during shot peening of titanium alloys is considered. Finally, the microstructural damage during high speed milling of titanium alloys Ti-834 and Ti-6Al-4V is investigated. In this final chapter, finite element modeling of the orthogonal cutting process is performed using the finite element code DEFORM^{TM}-2D. The aim of the modeling is to provide an insight into the complex stress/strain distribution that occurs during the machining process and relate the finite element predictions to the observed deformation microstructures.

Since a multitude of research topics must be addressed within the course of this thesis, each results and discussion chapter provides an introductory section that places the research within the context of the current literature and metallurgical understanding. Rather than a single chapter dedicated to the experimental methods employed during the research, individual sections describing the experimental methodology are provided as subsections of the results chapters.

An over-arching literature review is also provided in the next chapter, which introduces the reader to the metallurgy of titanium alloys, the current art with respect to characterising plastic deformation modes and finally an overview of research into surface finishing procedures such as shot peening and machining. The purpose of the literature review is to describe some key concepts that are discussed later on in the thesis, with more specific details of related research provided in the introduction section to each chapter.

References

[1] R. Bolingbroke, Presentation to the IOM[3] Light Metals Committee, July 2010.

[2] R. Thomas, in: M. Winstone (Eds.), Titanium Alloys at Elevated Temperature: Structural Development and Service Behaviour, The Institute of Materials, London, 2001, pp:1-8

[3] P. J. Withers, Reports on Progress in Physics 70 (2007) 2211 – 2264

[4] L. Wagner, C. Gerdes, G. Lütjering, in: G. Lütjering, U. Zwicker, W. Bunk (Eds.), Titanium, Science and Technology, Deutsche Gesellschaft für Metallkunde e. V., Oberursel, 1985, pp:2147-2154

[5] M. A. S. Torres, H. J. C. Voorwald, International Journal of Fatigue 24 (2002) 877 – 886

[6] J. I. Hughes, A. R. C Sharman, K. Ridgway, Proceeding of the Institute of Mechanical Engineers, part B: Journal of Engineering Manufacture 218 (2004) 1113

[7] Y. Guo, R. M'Saoubi, S. Chandrasekar, CIRP Annals – Manufacturing Technology 60 (2011) 137 – 140

[8] D. J. Child, G. D. West, R. C. Thompson, Acta Materialia 59 (2011) 4825 – 4834

Chapter 2

Literature review

2.1   Titanium: An introduction

The practical exploitation of titanium as an engineering material became possible with the development of the Kroll process to extract titanium from its ore (TiO_2). Although novel reduction routes are currently being developed [1], the Kroll process remains the dominant method for extraction. Owing to its excellent corrosion resistance and high specific strength, the principal markets for titanium remain the petrochemical and aerospace industries.

   The allotropic phase transformation between the high temperature body-centre-cubic (BCC) β phase and the low temperature hexagonal-close-packed (HCP) α phase governs the physical metallurgy of titanium alloys [2][3]. In high purity titanium, this transformation occurs at approximately 882°C (depending of alloy purity) and the crystal structures of the β and α phase are illustrated in figure 2.1. The hexagonal-close-packed α-phase of titanium has an axial (c/a) ratio of 1.587 and a comprehensive review of the crystallography of HCP structures can be found in ref. [4].

   Upon slow to medium rate cooling through the β → α transformation temperature *viz.* β-transus, precipitation of the α phase initially occurs along the prior β grain boundaries. Diffusion driven growth of α lamellae into the β grains follows; with the individual α lath width being strongly controlled by the rate of cooling through the β-transus. Formation of a martensitic phase can occur following quenching (or fast cooling) of titanium through the β-transus. The military transformation structure is termed the α′ phase and can be described as either "massive" or "acicular" martensite, with the prior ordinarily observed in pure (or low alloy content) titanium only. Acicular martensite occurs in titanium alloys of higher solute content and for a more detailed description of the martensitic structures observed in titanium; the reader is directed to refs. [2][3][5].

   Similarly to the group IV element Zirconium, the β → α phase transformation in titanium is characterised by the Burgers orientation relationship {110}$_β$//{0002}$_α$ and <111>$_β$//<11-20>$_α$ [6]. A total of twelve discrete α orientations (or variants) can arise during the β → α transformation from an initial β orientation and efforts to fully characterise preferential selection of the variants are well documented in the literature for titanium [7-9] and zirconium alloys [10][11].
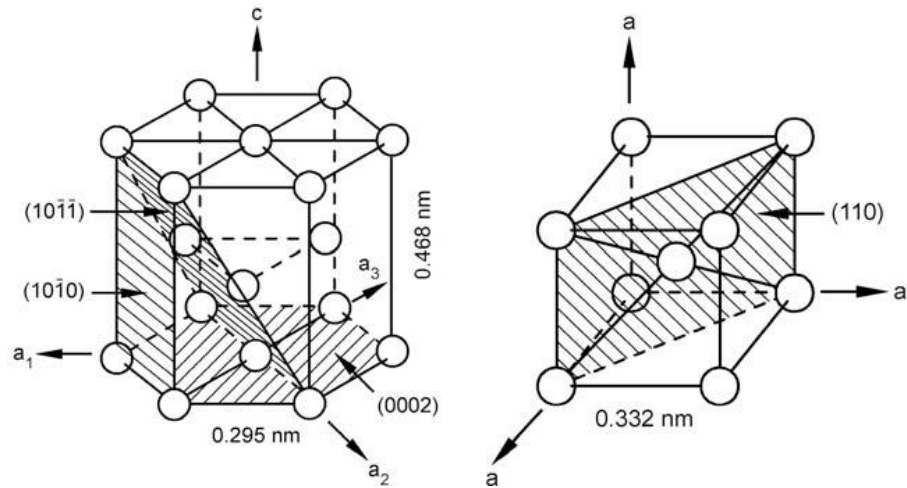
Figure 2.1: Crystal structures of the α and β phases of titanium. From ref. [5]

The addition of solute alloying elements to titanium has the effect of either increasing or decreasing the β-transus temperature [2][3] and an introductory review is provided by Margolin [12]. Elements such as aluminium, oxygen and nitrogen are soluble in the α phase and raise the allotropic phase transformation temperature and as such are often termed α-stabilisers. Molybdenum, vanadium, iron and niobium are examples of alloying elements that are soluble in the β phase, lower the β → α transformation temperature and are consequently referred to as β-stabilisers.

In addition to raising or lowering the β-transus, alloying titanium with the respective α or β-stabilising elements has the effect of increasing the temperature window within which the two phases are thermodynamically stable and are able to coexist [3]. The effect of alloy concentration on the thermodynamic stability of the α and β phases can be conveniently illustrated in the form of a pseudo-binary phase diagram. Figure 2 is an example re-drawn from Flower [3], which illustrates a narrowing of the temperature window for coexistence of the α and β phases with decreasing concentration of β-stabilising elements.
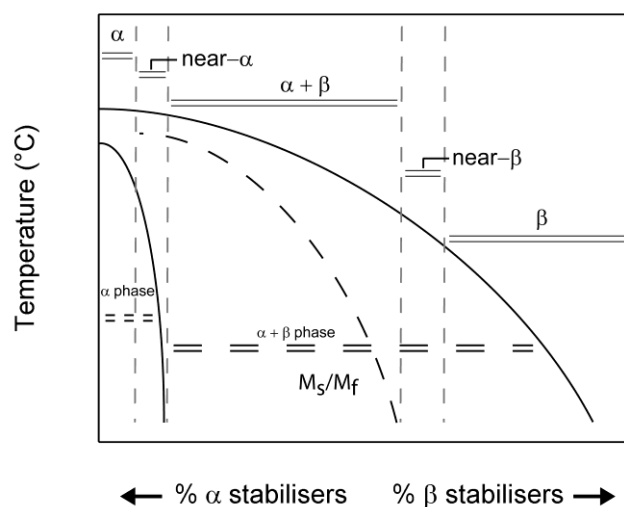
Figure 2.2: The pseudo-phase diagram for titanium alloys showing the position of the different alloy classes with respect to the allotropic transformation temperature. Re-drawn from Flower in ref. [3]

The pseudo-binary phase diagram is also useful for categorising titanium alloys as a function of their alloying additions and the respective effect such additions have on the physical metallurgy of titanium. Also labelled on the phase diagram in figure 2 are the respective positions of the alloy classes; from corrosion resistant single phase α alloys to the high strength near-β and metastable-β alloys. The metallurgy and engineering application across the range of titanium alloy classes is diverse, and a brief overview of the different classes is presented below.

2.1.1 *The α alloys*

These alloys are single phase, corrosion resistant and largely employed in the petrochemical industry. Alloys of this class are typically divided into two groups: Unalloyed titanium containing residual amounts of O and Fe, and those which are purposely alloyed with α stabilising elements, such as Al and Sn to increase strength. Typical α alloys include the binary Ti-O system and ternary Ti-5Al-2.5Sn. Slow cooling from above the β-transus leads to a serrated α microstructure, with growth of the α laths into the untransformed β grains along a selected number of habit planes.

Increasing the cooling rate firstly decreases the width of the individual lamellae and secondly increases the total number of habit planes along which the α phase grows. The number of habit planes that growth occurs on dictates the α colony size, with more rapid cooling rates leading to a basket-weave type microstructure. Hot working of α alloys below the β-transus results in a fine, equiaxed microstructure with the grain size controlled by the processing temperature. The most common of the α alloys is commercial purity titanium (CP-Ti). Depending on purity, CP-Ti grades of titanium posses yield strengths in the range 170 – 480 MPa and are typically employed in non structural applications [13].

2.1.2 *Near-α alloys*

Near-α alloys are forgeable alloys primarily used in the "hot end" compressor stages of gas turbine aero engines for rotating components such as discs, rings and blades. Near-α alloys possess good creep resistance and strength retention at elevated temperatures, with the most common example being Ti-6242S [13]. Other examples of near-α class include the β annealed alloy Ti-829 and α + β processed alloy Ti-834. Unlike alloys originating from the United States where the naming notation reflects the alloy composition, the British alloys Ti-829 and Ti-834 (previously IMI 829 and IMI 834) are not named after their chemistry, but rather by an internal number designation scheme developed by the now defunct IMI Titanium.[1]

Near-α alloys contain small quantities of β stabilising elements (up to 2 wt. %) to permit thermo-mechanical processing in the α + β phase. Alloys are ordinarily processed either above the β-transus to yield fully β-transformed microstructure or in the α + β phase to produce a bi-modal microstructure consisting of primary α grains in a β-transformed matrix [14].

---

[1] As part of restructuring in the 1990's, IMI divested it metal smelting and founding business units and the titanium manufacturing branch was taken over by Titanium Metals Corporation of America (TIMET). Alloys designed by IMI, such as IMI 829 and IMI 834, were subsequently re-designated Timetal®829 and Timetal®834 by TIMET. For the purpose of this thesis however, alloys of previous IMI designation will be referred to with the prefix "Ti". i.e Ti-829 and Ti-834.

2.1.3   *The α + β alloys*

α + β alloys contain alloying elements to stabilise and strengthen the α phase and retain significant proportions of the β phase at ambient temperatures [2]. Such alloys are often processed in the α + β phase to produce a fine equiaxed microstructure for high tensile and fatigue strength. As with the α and near-α alloys, cooling from processing above the β-transus leads to a fully β-transformed microstructure with the α colony size and lath width influenced by cooling rate [15]. The α + β alloy Ti-6Al-4V is the workhorse of the alloy class and constitutes approximately 40% of the total titanium tonnage manufactured per annum. Another example of an α + β titanium alloy is Ti-6246, which contains a significantly higher proportion of β-stabilising elements and exists towards the right-hand side of the α + β range in figure 2. The α + β class of alloys are widely used in engineering applications ranging from the rotating discs and fan blades in the aerospace sector [13], to its use in joint replacement implants for the biomedical industry [16][17].

2.1.4   *Near-β and Metastable-β alloys*

Alloys within this class sit to the right of M_s/M_f line in the pseudo-binary phase diagram in figure 2 and contain a large enough concentration of β-stabilisers to fully retain a β structure on quenching. The high β phase volume fraction facilitates hot working at lower temperatures than α + β alloys and the metastable-β phase can be significantly age hardened by the precipitation of fine α particles [18] to yield high strength alloys that are typically employed in the aerospace sector for landing gear applications [13].

The range in mechanical properties of titanium alloys from the commercial purity grades to the metastable β alloys are reflected in both chemistry and physical metallurgy. Whilst near-α alloys are generally optimised for high temperature creep resistance, the near-β alloys posses tensile strengths comparable to steels [13]. With a basic overview of titanium alloys complete, the next section of this chapter will review the elastic properties of α-titanium and the mechanisms which accommodate plastic strain. Following this, a review of methods to identify deformation mode using electron backscatter diffraction (EBSD) will be provided.

2.2   Mechanical behaviour of α-Titanium

The following section will provide an overview of the mechanical behaviour of Titanium. As the alloys investigated during the course of this study (CP-Ti, Ti-834 and Ti-6Al-4V) are situated towards the left hand side of the pseudo-binary phase diagram (figure 2.2), the focus will be on the response of the α-Titanium phase to the application of load. The elastic properties of α-Ti together with an overview of factors controlling yield strength are initially discussed in section 2.2.1, with the metallurgical mechanisms that facilitate plastic flow addressed in section 2.2.2. In section 2.2.3, the application of electron backscatter diffraction to identify deformation modes in hexagonal close packed alloys is reviewed.

2.2.1   *Elastic properties and yield strength*

In common with metals of hexagonal-close-packed crystal structure, such as Mg, Zr and Zn, α-titanium is mechanically anisotropic and its stress-strain response is strongly dependant on orientation of the crystals with respect to the direction of applied load. For single crystals of α-titanium, the elastic modulus varies with respect to the angle

between the *c*-axis and the loading direction, with the highest stiffness occurring when the stress axis is parallel to the *c*-axis [5]. In terms of its linear elastic behaviour with respect to temperature, the modulus of elasticity and shear modulus of α-titanium vary in an approximately linear manner; with values of both elastic constants decreasing with an increase in test temperature [5][19].

The elastic limit of α-titanium can be significantly increased by the addition of solute alloying elements. Oxygen is a potent solution strengthening element of the α phase and the addition of 0.1 wt. % oxygen to iodide titanium raises the tensile strength by approximately 120 MPa according to an early study by Ogden and Jaffee [20]. Nitrogen and carbon have similar strengthening effects to α-titanium, although addition of all three elements leads to concomitant decrease in tensile ductility [20].

Aluminium also has the effect of strengthening the α phase; either as a basic solid solution strengthening element, or through precipitation hardening caused by the formation of coherent Ti_3Al particles in Ti-Al alloys where Al concentration exceeds 5 wt. % [5]. As with other metallic systems, the yield point of titanium may also be increased through refinement of the effective structural unit size (Hall-Petch mechanism). The term "effective structural unit" is preferred over "grain size", as it is traditionally considered that dislocations can readily traverse across similarly orientated α laths in a β-transformed microstructure, with the lath boundary β phase offering little resistance to dislocation motion. According to a study by Savage [21] on the near-α alloy Ti-6-2-4-2 however, the ease of dislocation transmission across the α/β interface within differently orientated colonies is controlled by the misorientation of dislocations within the two phases.

2.2.2 *Mechanisms of plastic deformation*

Beyond the elastic limit of α-Ti, irrecoverable deformation is accommodated by a combination of dislocation slip and mechanical twinning [4][19][22-24]. There are a total of seven planes and directions that are considered potential slip systems in the HCP structure according to Rosembaum [25], although only six are possible according to Partridge [4]. A list of possible slip planes and directions according to Paton [22] is presented in table 2.1 and important planes and directions in the HCP structure are illustrated in figure 2.3. Of these, basal slip ({0001}<11-20>) and prism slip ({10-10}<11-20>) are considered to be the most common operable slip modes in high purity α-Ti [22]. As the HCP structure of α-Titanium has a c/a ratio of 1.587, a greater spacing between the prism planes exists than in an ideally packed HCP structure where the c/a ratio is equal to √3. The relative packing density of atoms on the {10-10} prism planes is therefore greater than on the {0002} basal plane [26]; resulting in a lowered prevalence for basal slip in α-Ti when compared with HCP structures of c/a ratio greater than √3 (such as Mg and Zn) [25][27].

Table 2.1: Dislocation slip modes in alpha titanium [22]

Slip Mode	
<*a*>-slip	{0001}<11-20>
	{10-10}<11-20>
	{10-11}<11-20}
<*c+a*>-slip	{10-11}<11-23>
	{11-22}<11-23>

Although both the prism and basal planes have three slip systems each, only two are independent of each other [5][26]. Accordingly, this means that the number of independent slip systems reported in pure titanium is insufficient to accommodate homogeneous plastic strain. Whilst the addition of aluminium to α-Ti is reported to promote <c+a> slip on the pyramidal planes [22][26][28], the prism and basal planes only permit slip along the a-direction.

<div align="center">Table 2.2: Mechanical twinning modes in alpha titanium [48]</div>

Mode	K_1 Plane	η_1	Misorientation (Angle/Axis)	Theoretical Shear
Tensile type-1	{10-12}	<-1011>	85°<1-210>	0.171
Tensile type-2	{11-21}	<-1-126>	35°<1-100>	0.629
Compression type-1	{11-22}	<11-2-3>	65°<-1100>	0.221
Compression type-2	{10-11}	<10-12>	54°<-12-10>	0.101

Since unalloyed α-Titanium is ductile at ambient temperatures, accommodation of plastic strain parallel to the c-axis in the absence of <c+a> slip must occur through deformation twinning [22-24] and a list of reported twin modes is provided in table 2.2. Unlike dislocation slip where a limited number of atoms move large distances, mechanical twinning involves the comparably small movement of a large number of atoms. The military-like movement of atoms during twinning results in mirror symmetry across a crystal plane. This plane is referred to as the composition plane, the twinning plane or the first undistorted plane and has the abbreviation K_1. The direction of shear is parallel to the K_1 plane and is referred to as shear direction or η_1. For an introduction to mechanical twinning in metals, the reader is referred to ref. [29].

As with dislocation slip, mechanical twinning can lead to extension or contraction of a crystal, although the magnitude of shear strain in an HCP structure is dependent on the mode of twinning and c/a ratio. With reference to figure 2.4, this can be illustrated for the {10-12} twin mode in HCP metals. The shear strain accommodated by {10-12} twinning can be calculated by the following equation [29]:

$$S = \left[\left(\frac{c}{a}\right) - 3\right]\frac{\sqrt{3}a}{3c} \qquad \text{Eqn. 2.1}$$

Where c and a are the respective lattice parameters of the HCP crystal and S is the strain accommodated by {10-12} twinning. If the c/a ratio is equal to √3, then it follows that the strain accommodated by this particular twin mode is zero. If the c/a ratio is less than √3, then the value strain is negative i.e. {10-12} facilitates a contraction along the c-axis as is the case with Cd and Zn. Conversely, if the c/a ratio is greater than √3 as is the case in α-Ti and α-Zr, then S is greater than zero and {10-12} twinning facilitates and extension of the crystal parallel to the c-axis.
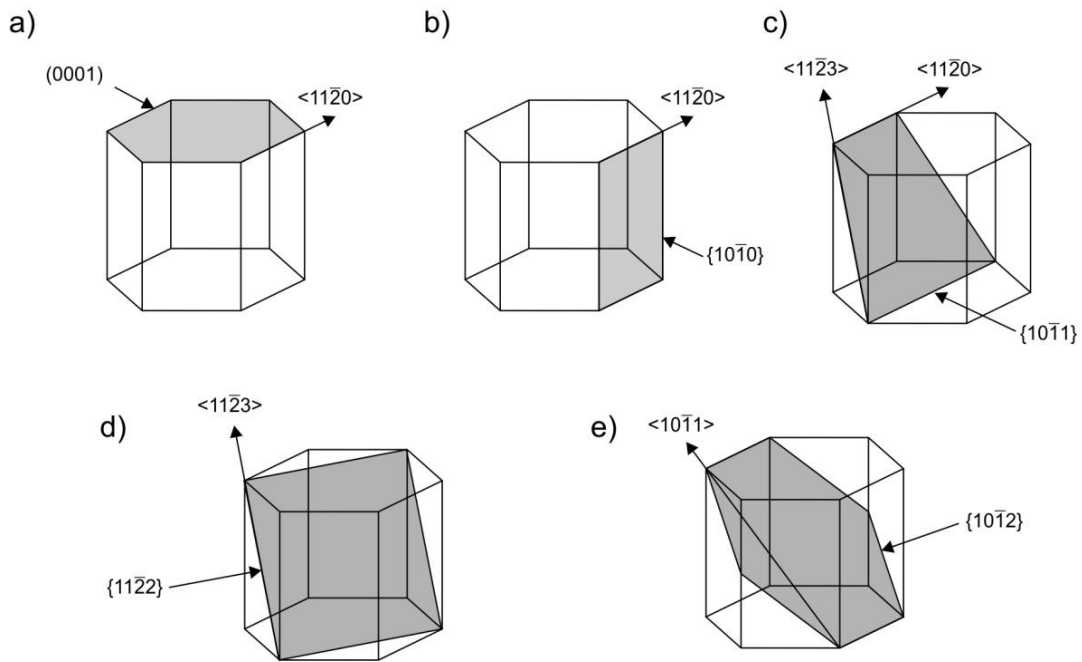
Figure 2.3: Important planes and directions in α-Ti. The basal and prismatic slip systems are illustrated in a) and b) respectively. The {10-11} and {11-22} pyramidal slip systems with both <a> and <c+a> slip directions are given in c) and d). The {10-12} twin plane and <10-11> shear direction is shown in e). [4][5][25]
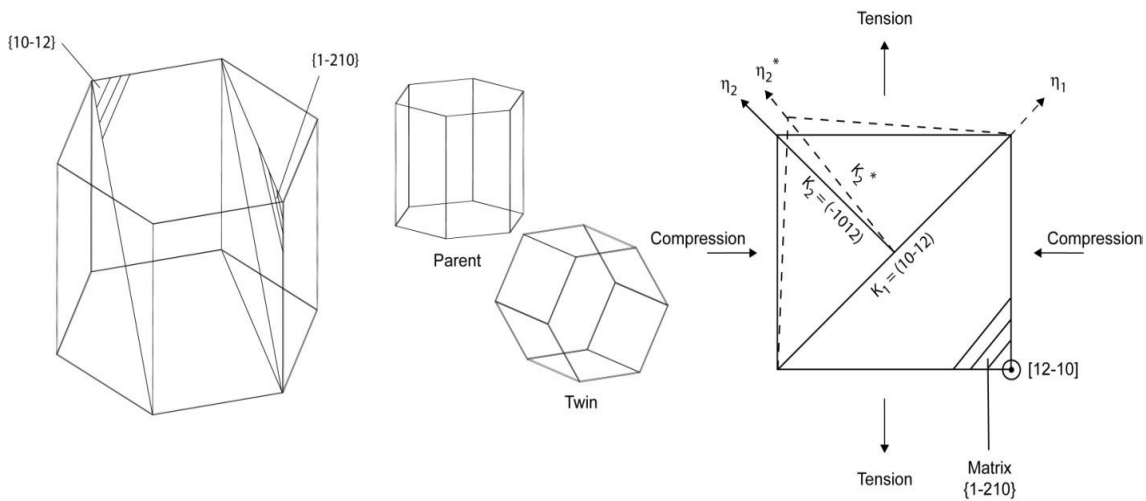
Figure 2.4: Geometry of {10-12} type mechanical twinning in α-titanium. Figure redrawn from Partridge [4].

The study of mechanical twinning in α-Ti has been a pertinent topic for the second half of the twentieth century and a general review of twin and slip systems from the 1970s is presented in ref. [19]. More recently, Salem *et al* [24] have investigated the role of deformation twinning on the strain hardening of α-titanium, whilst Chichili *et al* [30] have performed a series of experiments to examine the high-strain-rate mechanical response of α-titanium. Twinning is reported to contribute to strain hardening of titanium through both the Hall-Petch and Basinski mechanisms according to Salem *et al* [24], with twin density increasing with the applied plastic strain in CP-Ti. Chichili *et al* [30] obtained a similar result and it was also reported that the number density of mechanical twins in CP-Ti also increases with strain rate. This aligns with a review by Christian and Mahajan [31], who state that twinning is favoured by low temperature and high strain rates.

The strain rate sensitivity of the flow stress in α-Ti was also discussed in ref. [30], with higher strain rates leading to a measured increase in the flow stress during compression testing. Such strain-rate sensitivity on the flow stress is also observed deformation of titanium at elevated temperatures, with the flow stress increasing with increasing strain rate from 0.001 s^{-1} to 1 s^{-1} during hot-compression testing of Ti-6Al-4V [32].

Twinning can also contribute to textural softening during straining as the twinned volume becomes favourably orientated for dislocation slip. As discussed above, slip in α-Ti predominantly occurs on the {0002} and {10-10} planes in the <11-20> directions. The resolved stress acting upon a given slip system is calculated by [33]:

$$\tau_R = \frac{P}{A} \cos\varphi \cos\lambda \qquad\qquad \text{Eqn. 2.2}$$

Where τ_R is the resolved shear stress, P the load, A the area upon which the load acts, and φ and λ are the respective angles that the slip plane normal and the slip direction are with the loading axis. If the loading direction is parallel to the *c*-axis of an HCP crystal, the resolved shear stress on the prism and basal slip systems are zero. Here, plastic strain cannot be accommodated by dislocation slip on the basal and prism planes and such an orientation of the crystal with respect to the stress axis is considered a "hard" orientation. In the absence of <*c+a*> slip, strain will be accommodated by the formation of a mechanical twin in the crystal, if the resolved shear stress acting on a twin plane is sufficient.

As noted by Song and Gray, the nucleation of twins generally starts in crystal where the potential twinning planes are close to the plane of maximum local shear stress [34]. In the case of {10-12} twinning, a rotation of ~85° about the <1-210> axis will occur such the *c*-axis of the twinned volume becomes approximately normal to the loading direction. Such an orientation with respect to the loading direction is considered a "soft" one, as the both the prism plane and *a*-direction are oblique to the stress axis and the {10-10}<11-20> slip system has a high resolved shear stress acting on it i.e. high Schmid factor. This effect is often referred to as texture softening [35] and plastic deformation by dislocation glide occurs within the twinned volume.
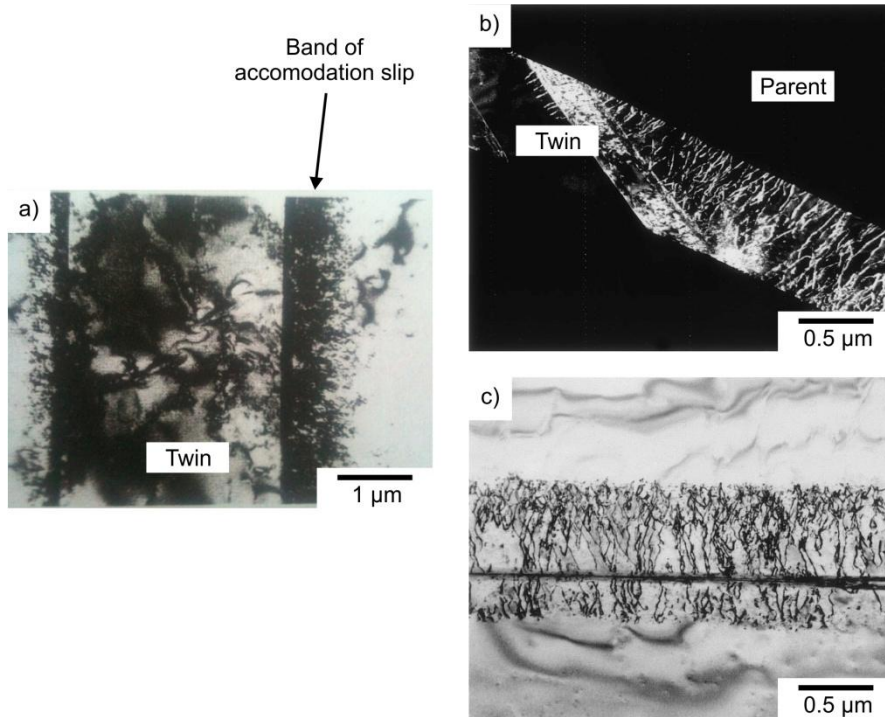
Figure 2.5: TEM observations of dislocations associated with mechanical twin in α-titanium. An example bright-field TEM micrograph showing the zone of accommodation dislocations at a twin boundary from Paton [22] is shown in a).

Figure 2.6: Bright field TEM micrograph of Hf quasi-statically compressed of a strain of 0.2 at room temperature. Deformation has predominantly occurred by mechanical twinning and dislocations within the twinned volume can be observed. Micrograph from ref. [38].
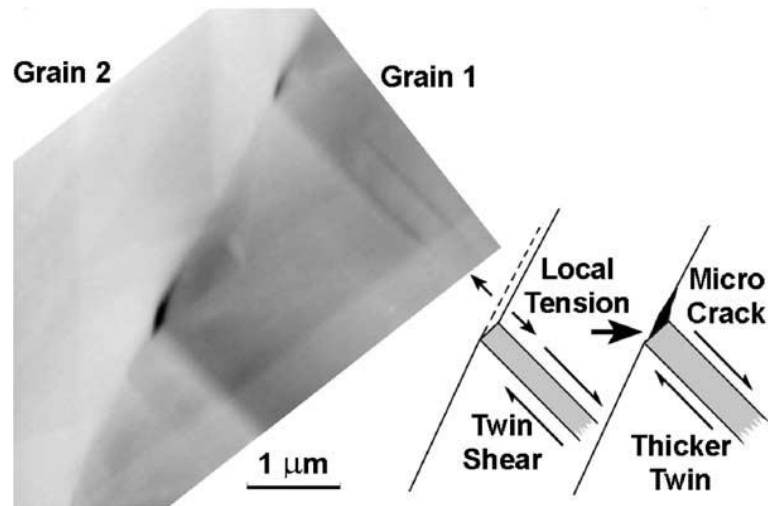
Figure 2.7: Microcracks developing between grains where twin shear causes a local tension opening force in a near-γ TiAl high temperature intermetallic material. Electron channelling constrict image and corresponding schematic illustration are from Bieler *et al*. [41]

In addition to the considerable dislocation activity observed within twins formed during compression tests of α-titanium, Paton [22] and Williams [26] have reported extensive <*c+a*> slip in the matrix immediately surrounding the twin boundary. Transmission electron micrographs from references [22] and [26] illustrating the narrow band of accommodation slip around a twin boundary are shown in figure 2.5. In [22], Paton also discussed the importance of this layer of accommodation slip in reference to the work of Partridge [36], who suggested that crack initiation could occur within the accommodation slip layer during cyclic loading. Similarly to the TEM studies of deformed α-titanium, *c*-type screw dislocation have also be observed within the twinned region in Hf [37] and a bright field TEM micrograph of Hf compressed quasi-statically at room temperature to 20% strain showing the twin boundary structure is presented in figure 2.6 [38].

In an early review by Armstrong [39], the role of twinning in the nucleation of fatigue cracks was discussed in reference to twin boundaries acting as barriers to dislocation slip. Here, it was proposed that cracks initiated at twin/matrix interfaces during cyclic loading due to the inability of the magnesium crystal to accommodate further slip across the boundary. It was proposed that a twin can act as a stress concentrator when it impinges on obstacles such as grain boundaries. It was stated however, that the precise role of twins in crack initiation was unclear, with certain experiments showing that twins were not associated with the production of cracks.
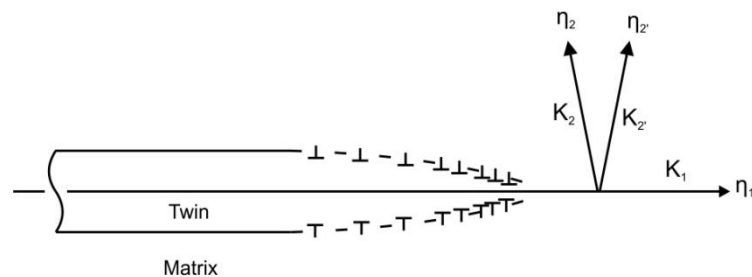
Figure 2.8: Schematic illustration of "Frank" type glissile edge dislocations at a twin boundary. The density of "Frank" dislocations is dependent on the deviation of the twin boundary from the K_1 plane. Illustration re-drawn from ref. [42]

A more recent study on the role of twinning during fracture under four-point bending in a near-γ TiAl has shown evidence of microcrack initiation at the intersection of mechanical twins with grain boundaries [40], which perhaps support the ideas of Armstrong concerning the capabilities of twins to produce internal stress concentrations. An illustration of the proposed mechanism for the formation of microcracks at the intersection of twins with grain boundaries in a near-γ TiAl is shown in figure 2.7 [41]. Here, the twinning shear was accommodated by the nucleation of microcracks at the twin/grain boundary interface, which is in contrast to more classical models for the accommodation of twinning shear. In a review of twinning by Cahn [42], the classical model of Eshelby, Frank and Nabarro for the occurrence of twin dislocations at the boundary was discussed. The configuration of twin boundary edge dislocations, which are glissile in the plane parallel to K_1, is shown in figure 2.8. In the case of the classical model for twin dislocations, the density of twin boundary dislocations depends on the deviation of the twin interface from the K_1 plane. That is, with increasing twin boundary curvature or a more lenticular shape, a higher local dislocation density is expected.

In summary, early and more recent studies have shown that internal stresses are associated with the presence of a twin boundary and that the twin boundaries themselves cannot be considered as perfectly coherent interfaces. Further to this, the works of Paton [22] and Partridge [36] have shown evidence through TEM, of dislocation pile-up at twin interfaces during straining, with a zone of high dislocation density in parent grain adjacent to a twin. In conjunction with the observed hardening due to the Hall-Petch mechanism, substantive evidence exists pertaining to the defective nature of a twin boundary, or at least the regions surrounding it.

2.2.3 *Identification of deformation mode through electron backscatter diffraction*

The identification of deformation mechanisms has traditionally been performed using transmission electron microscopy, and early work toward its application in titanium can be found in refs. [22][26][30]. Advances in electron backscatter diffraction however, have allowed the analysis of crystal structure over length scales considerable greater than TEM, although sufficiently small to capture crystallographic data on the micro-scale.

A study by Mason *et al* [43] has discussed the use of EBSD for identifying twinning mode and twin volume fraction in deformed alpha Zr. Figure 2.9 shows the methodology employed by Mason *et al* [43] to confirm the presence of a {10-12} type mechanical twin in a alpha grain. The coincident poles of the K_1 twin plane can be observed in the {10-12} stereographic projection in figure 2.9 with the corresponding twinned volume coloured in blue. The solid lines are the normal to the twin boundary trace and clear coincident between the boundary normal with the K_1 poles exists.

A similar approach for the identification of slip systems in Ti-6Al-4V deformed in tension through EBSD has been employed by Bridier *et al* [44]. Pre-polished specimens of a duplex Ti-6Al-4V alloy were subjected to in-situ scanning electron microscopy (SEM) tensile tests. The density of slip bands that became visible through the intersection of dislocations with the polished surface was correlated to EBSD analysis of the crystal structure. From the corresponding EBSD data, traces of the basal, prism and pyramidal slip planes were superimposed on the secondary electron SEM micrographs obtained during the *in situ* tensile straining. Further analysis of the deformed polycrystals demonstrated that the Schmid factor (eqn. 2.2) was a relevant parameter to the nature of the activated slip systems.
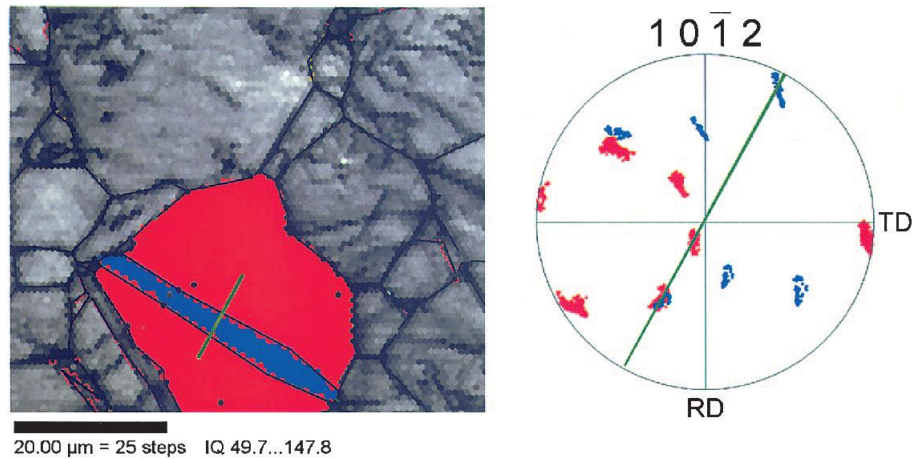
Figure 2.9: Methodology employed by Mason *et al* [43] to confirm the presence of a {10-12} twin in Zr. The parent grain is coloured red and the twinned volume blue. The corresponding {10-12} projection showing the pole of the K_1 twin plane is also shown (coincidence of the parent and twin {10-12} poles).
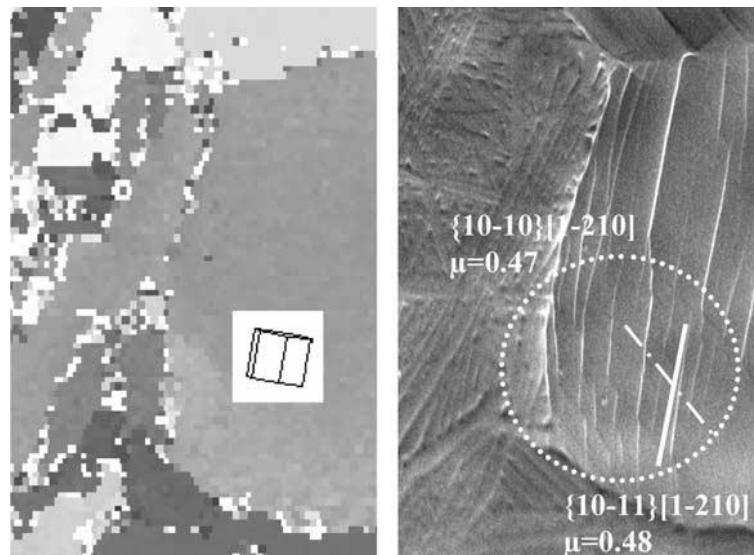
Figure 2.10: Local EBSD map (left) and corresponding secondary electron SEM micrograph (right) of a duplex Ti-6Al-4V alloy subjected to uniaxial tensile deformation. Traces of the {10-10} and {10-11} planes are superimposed on the secondary electron micrograph and show the activation of both prism and pyramidal glide. From ref. [44]

The study of deformation through EBSD has also been performed by Keshavarz and Barnett [45] for a Mg-3Al-1Zn alloy deformed in tension. As with the work of Bridier *et al* [44], the specimens were polished to a metallographic finish prior to the tensile testing and the mechanical testing was carried out in situ in a SEM with a tensile stage. Following testing, EBSD was performed and an example of the trace analysis is presented in figure 2.11. Here, the corresponding stereographic projections of the basal and prism planes are included, with the closet theoretical trace to the observed trace due to the intersection of dislocations with the sample surface shown.
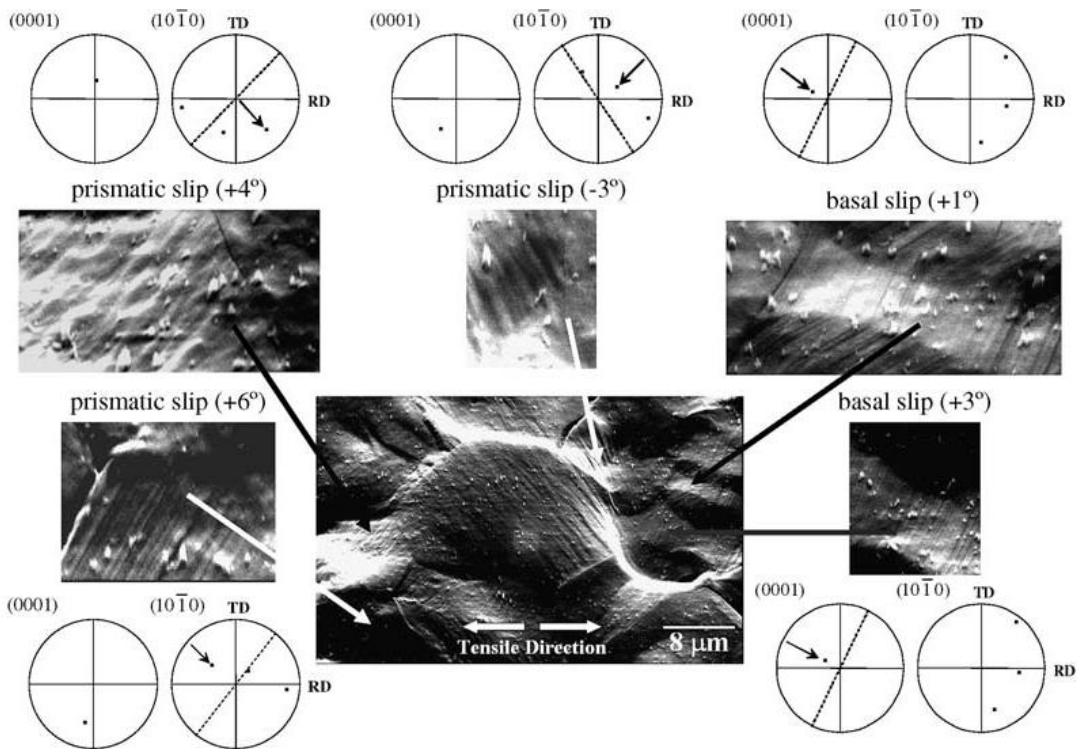
Figure 2.11: Slip traces and accompanying pole figures illustrating the method used by Keshavarz and Barnett [45] to identify the most likely active deformation mode after straining a Mg-3Al-1Zn alloy in tension.

Further examples of the use of EBSD to identify deformation mode exist e.g. references [24][46–49], with studies by Wang *et al* [48] showing evidence for a twin nucleation mechanism based on the transfer of {10-10}<11-20> slip across a grain boundary in deformed CP-Ti.

The ability of EBSD to capture crystallographic data across a comparatively large area (when compared with TEM) has demonstrated it to be an important tool in the study of deformation mode of crystalline solids. Emphasis can often be placed on the statistical analysis of deformation mode with respect to loading conditions owing to the larger sampling set that can be realistically attained when compared to TEM studies. For example, it is now common for the orientation of crystals containing a particular mode of deformation to be plotted on the unit stereographic triangle [44], or for histograms to be created showing the fraction of twins for a given average Schmid factor [49].

2.3   Processing of near-α and α + β titanium alloys

Wrought titanium alloys employed in the aerospace sector are subjected to a complex thermo-mechanical processing route that entails a number of hot working and heat treatment operations. An introductory review of the metallurgy and heat treatment of near-α and α + β titanium alloys is provided by Boyer in [13] and [50].

Similarly to steel alloys, processing of titanium alloys starts with casting into ingot, followed by a series of primary and secondary hot working operations to shape the material and develop a uniform microstructure across the billet [51]. During these processing operations, the microstructure and texture of the alloy are developed, with both having an important bearing on the final mechanical properties of the material. The importance of thermo-mechanical processing on the mechanical behaviour of near- α and α + β titanium alloys is aptly shown in figure 2.12 [52]. Here, ballistic impact testing of vehicle amour was performed by Kad *et al* [52] on Ti-6Al-4V that was plate annealed either above or below the β-transus. A marked drop in the ballistic impact limit was measured for Ti-6Al-4V material processed above the β-transus, with the ballistic response rationalised in terms of the different crystallographic textures of the two conditions. It was proposed that the strong basal texture resulting from rolling low in the α + β phase required greater external work during impact than the transverse-type texture obtained from super transus rolling.

The influence of thermo-mechanical processing on the microstructure, texture and mechanical properties of near-α and α + β titanium alloys extends well beyond the domain of dynamic impact testing. A review by Lütjering [53] discussed the dependency of high cycle fatigue (HCF) strength on the prior hot working and heat treatment temperature of Ti-6Al-4V, with the fine equiaxed microstructure showing the highest HCF strength. The lowest HCF strength was reported for coarse lamellar microstructures that result from slow cooling following annealing above the β-transus. In general terms, it was reported that a basal/transverse texture led to a higher HCF limit than a transverse type texture; although the direction of fatigue loading with respect to the rolling direction also had a strong influence on the fatigue strength.
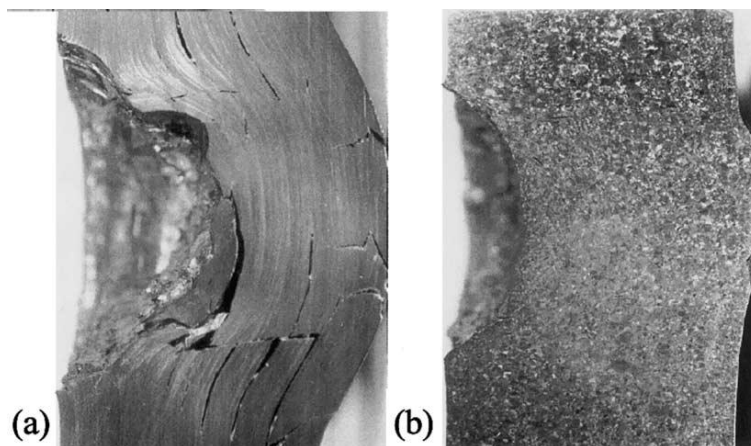
Figure 2.12: Cross-section view of the fragment simulated projectile impacted plates of Ti-6Al-4V annealed (a) below; and (b) above the β-transus temperature. From Kad *et al* ref. [52]

Microstructure and texture have a pronounced effect on the mechanical properties of titanium alloys. Since the origins of both microstructure and texture exist within the thermo-mechanical processing cycle, this section will briefly review processing of near-α and α + β titanium alloys with reference to mechanical properties. As the development

of microstructure and texture in α + β alloys has been comprehensively reviewed by Lütjering and Williams e.g. [5][15], only a brief discussion will be undertaken. Due to its limited use in the aerospace industry compared with alloys such as Ti-6Al-4V however, a more detailed overview of the development of the near-α alloy Ti-834 will be provided.

2.3.1 *Microstructure and texture development in Ti-6Al-4V*

Annealing any titanium alloy above the β-transus leads to a fully transformed microstructure on cooling. As discussed in section 2.1, the cooling rate through the β-transus effects the morphology of the subsequent α phase and figure 2.13 shows examples of the Ti-6Al-4V following cooling at different rates from above the β-transus [31]. Fast cooling (water quenching) results in a martensitic microstructure (diffusionless transformation) as shown in figure 2.13.a), whilst a colony microstructure (diffusional transformation) is obtained following air or furnace cooling as shown in figures 2.13 a) and b). The α phase lath width and colony size are related inversely to the cooling rate, with coarser laths associated with furnace cooling.

Such microstructures shown in figure 2.13 b) and c) are often termed "β-transformed" and result from the diffusional growth of α lamellae into the β-phase [3]. As briefly discussed in section 2.2.1, increasing the α colony size results in an increase in the effective distance a dislocation can travel (slip length) before being impeded by an obstacle such as a grain boundary, with the net effect being a reduction in tensile strength, ductility and high cycle fatigue strength [5][15].
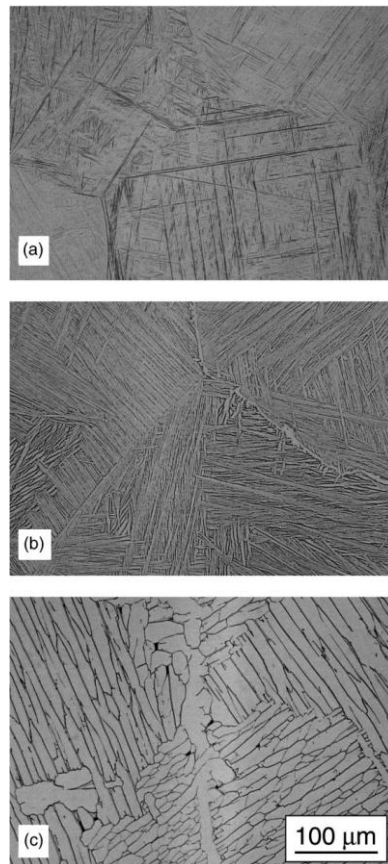
Figure 2.13: Light optical micrographs of β-annealed Ti-6Al-4V and a) quenched, b) air cooled and c) furnace cooled. [31]

Improved properties during fully reversed cyclic loading in air can be attained through processing below the β-transus to yield a "bi-modal" microstructure [53]. An example of a "bi-modal" type microstructure is shown in figure 2.14 [54] and a schematic diagram showing the processing route to obtain a bi-modal microstructure in Ti-6Al-4V is shown in figure 2.15 [15]. Substantial deformation of the α phase occurs during step II prior to a recrystallisation step in III.

The primary α phase remains untransformed during heat treatment in the α + β phase and the volume fraction of primary α is inversely controlled by the heat treatment temperature (Lever rule for phase proportionality). Heat treating high in the α + β phase leads to a low volume fraction of primary α, whilst a lower temperature results in a higher volume fraction. It should be mentioned that whilst the volume fraction of primary α is controlled by treatment temperature, the average primary α grain size is influenced by the width of α lamellae obtained following cooling from step I [15]. A fully equiaxed α microstructure can be obtained by either slow cooling from the re-crystallisation step to promote primary α grain growth or to perform the stage III processing operation very low in the α + β phase. During the deformation in step II, texture is developed in the α and β phases and a schematic diagram showing the effect of deformation temperature on texture evolution for rolled Ti-6Al-4V plate is given in figure 2.16 [5].
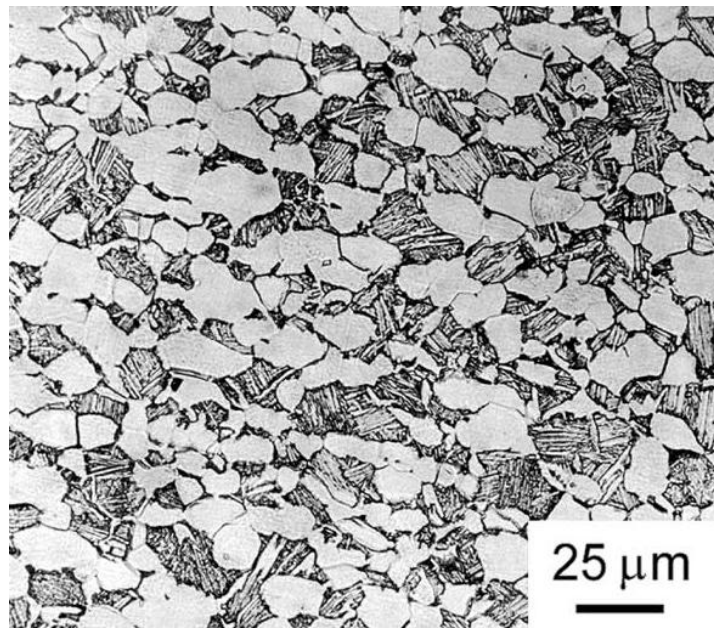
Figure 2.14: Example of a bi-modal type microstructure in Ti-6Al-4V. The bright contrast grains of primary α exist in a matrix of α lamellae (transformed β phase). From Peters and Ritchie [54]

For good overall combination of properties such as formability, moderate strength and improved fatigue and fracture properties, α + β can be processed to yield a mill annealed microstructure [5][15][50]. Here, the recrystallisation step in figure 2.15 is removed from the thermo-mechanical processing route and the alloy is annealed in the rolled or forged condition. The final heat treatment is typically above the Ti_3Al solvus, such that hardening does not occur and the purpose of the heat treatment being to fully anneal out any residual stresses that may exist in the mill product.
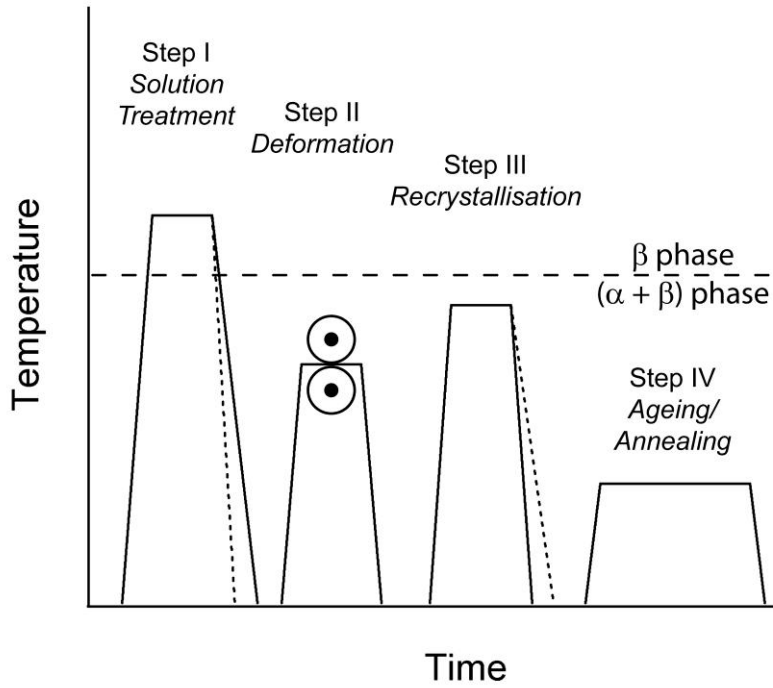
Figure 2.15: Schematic of the processing route to obtain a bi-modal microstructure in Ti-6Al-4V. Re-drawn from refs. [5][15]
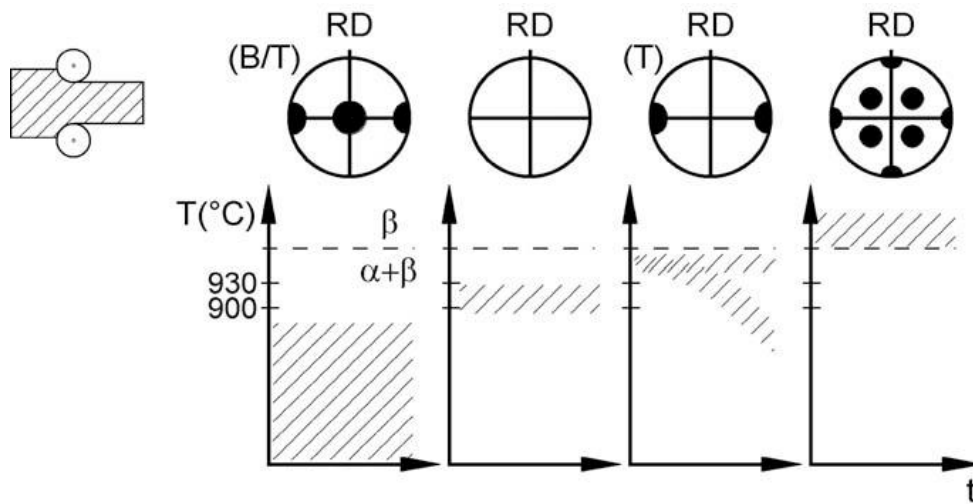
Figure 2.16: Schematic illustration of typical (0002) textures generated during rolling of Ti-6Al-4V. RD is the rolling direction and TD is the (long) transverse direction. From Williams and Lütjering [5].

2.3.2 *The near-α alloy Ti-834*

Developed by IMI Metals Corporation in the 1980's, Ti-834 is a creep and fatigue tolerant near-α titanium alloy with microstructural stability up to 600°C [55][56]. The compositional range of Ti-834 is shown in table 2.3 [57]. Ti-834 was designed for the aerospace industry and supersedes the creep resistant Ti-829 and Ti-685 alloys for application in the "hot-end" compressor stages of gas turbine engines. The development of Ti-834 arose from a requirement to improve the fatigue strength of high temperature near-α titanium alloys such as Ti-829. Despite possessing a high creep strength and resistance to oxidation [3][5][58], the coarse lamellar microstructure of the β-processed alloys are less resistant to the initiation of fatigue cracks. Whilst modest improvements in high cycle fatigue strength can be attained by limiting the duration of the β-recrystallisation step to prevent excessive grain growth and fast cooling to minimise α colony size, significant grain refinement is necessary to achieve comparable fatigue crack initiation properties to α + β alloys.

Table 2.3: Compositional range (in wt. %) of Ti-834 [57]

	Al	Sn	Zr	Nb	Mo	Si	C	Fe	O	Ti
Min.	5.50	3.00	3.00	0.70	0.25	0.20	0.04	-	0.08	Bal.
Max.	6.10	5.00	5.00	1.00	0.75	0.60	0.08	0.05	0.15	Bal.

Microstructural refinement of near-α alloys may be obtained through processing in the α + β phase to bi-modal microstructure (an example of which is shown in figure 2.14). The primary α grains that form during sub-transus processing pin the β grains thus preventing excessive growth. Due to the steep β-approach curve in alloys such as Ti-829, effective processing in the small α + β window is difficult to achieve in practice. The β approach curve for Ti-834 is shallowed by the addition of carbon and a marginal increase in the concentration of β stabilising elements, and hot working in the α + β phase can be practically achieved [56]. A comparison of the β-transus approach curve for Ti-6Al-4V, Ti-829 and Ti-834 is shown in figure 2.17.

Similarly to the processing of Ti-6Al-4V and in reference to figure 2.15, the volume fraction of primary α is controlled by the recrystallisation temperature. Typically, Ti-834 is heat treated high in the α + β phase to produce a target microstructure consisting of 10% − 15% primary α, although the primary forging step will be performed lower in the α + β field. In addition to the development of macro-texture during deformation, sharp texture heterogeneities can develop in Ti-834 billet at this stage. An EBSD map illustrating the size and form of regions of strong microtexture is given in figure 2.18 [59]. The regions of strong microtexture are referred to as "macrozones" and can behave as one structural unit that may lead to premature fatigue crack initiation if they are unfavourably orientated with respect to the stress axis. The effective structural unit size cannot be readily determined from light optical microscopy, and EBSD investigations have also been employed by Sackett *et al* [60] to study the fatigue crack initiation mechanisms in heavily microtextured near-α titanium alloys.
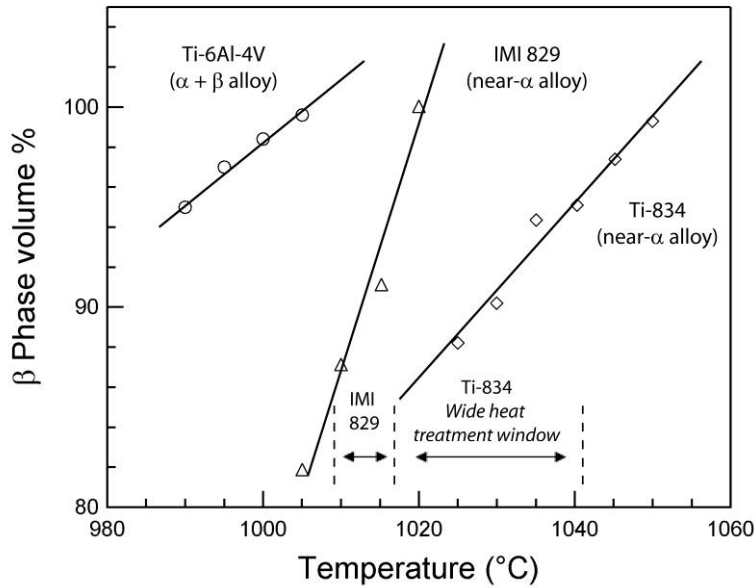
Figure 2.17: β-transus approach curves for Ti-6Al-4V, Ti-829 and Ti-834. Re-drawn from Neal [56]

The final stage of the processing route for Ti-834 is the ageing treatment. Here, the alloy is treated for 2 hrs at 700°C following rapid cooling from the solution heat treatment to enhance both creep and fatigue properties, through the respective precipitation of $(Ti,Zr)_x Si_y$ silicides and the Ti_3Al phase.

Alloying of silicon with titanium leads to a lowering of the high temperature creep rate and the effect of silicon concentration on the creep rate for Ti-Al-Zr-Si alloys is shown in figure 2.19. [61]. In a comprehensive study by Paton and Mahoney [61], the mechanism for the improved creep properties of silicon containing titanium alloys was ascribed to the clustering of Si atoms around mobile dislocations, which subsequently pin their movement by the precipitation of $(Ti, Zr)_x Si_y$ silicides. Maximising the amount of silicon in solid solution therefore equates to an improved creep life and the precipitation of silicides with the matrix during ageing would lead to a reduction in overall creep performance in near-α alloys. In the case of Ti-834 however, the optimum creep properties are obtained following ageing at 700°C, which is not consistent with the typical behaviour of near-α titanium alloys.
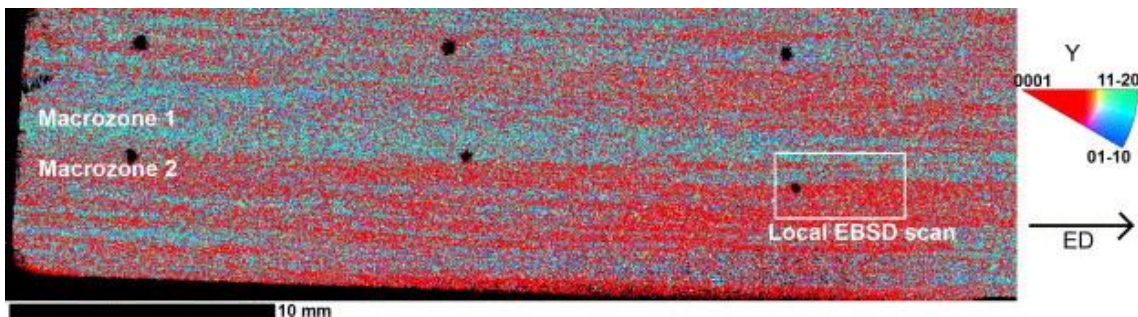
Figure 2.18: EBSD map with inverse pole figure colouring showing regions of sharp microtexture in Ti-834 billet. The red regions show primary and secondary α grains with basal planes closely aligned with the specimen surface. From Germain *et al* [59].
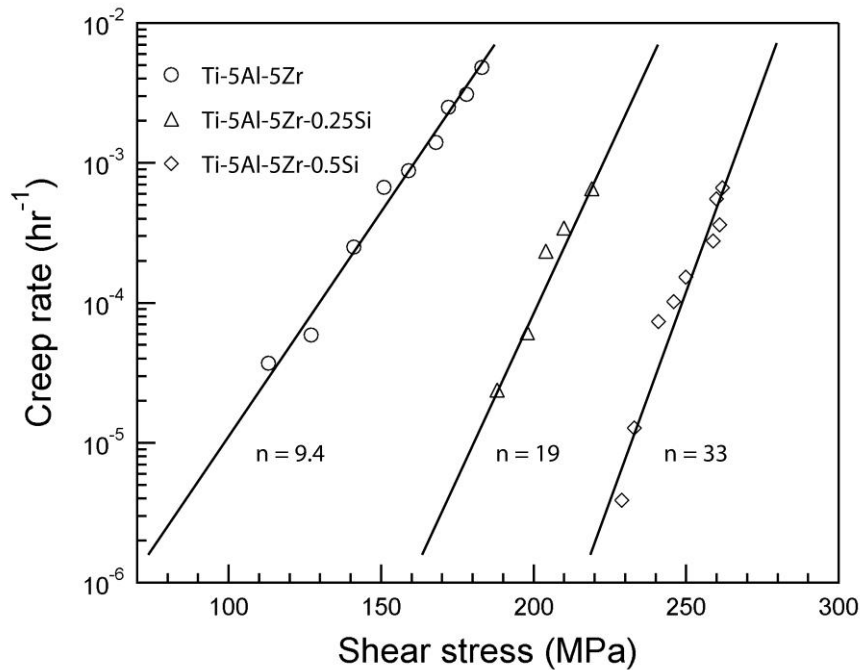
Figure 2.19: The effect of silicon content on creep rate of Ti-Al-Zr-Si alloys tested at ~540°C showing the stress exponent (n). Re-drawn from Paton and Mahoney. [61]

This may be due to the mechanisms governing creep deformation during high temperature testing. In the case of Paton's work [61], grain boundary sliding accounted for less than 10% of the total creep strain, with the rate controlling mechanism proposed to be solute drag. i.e. the pinning of mobile dislocations lowers the creep rate. Creep testing of Ti-834 by Andres *et al* [62] and Kestler *et al* [63] has highlighted however, the contribution of α lath boundary deterioration during deformation. In these circumstances, the prior ageing step was deemed beneficial to the creep properties due silicide precipitation along the α lath boundaries and the precipitation of Ti_3Al phase in the matrix. Over ageing of the alloy however, leads to a decrease in creep performance due to the depletion of silicon from the matrix, and the 2 hr ageing step recommended for Ti-834 achieves a balance between lath boundary strengthening whilst maintaining sufficient silicon in solid solution.

2.4 Machining and surface finishing

2.4.1 *Machining*

Following the primary and secondary processing steps, titanium forgings are typically machined to a condition of supply (COS) close to the forging supplier. The purpose of this initial step is to remove the oxide scale and prepare the forging for further roughing and finishing operations. Examples of machining processes include milling, turning and boring, and an introduction to the principles of machining is given in refs. [64][65]. Regardless of the type of machining process, material removal is achieved by chip formation resulting from the interaction of the tool with the surface of the material. The formation of a chip involves high rates of strain and large plastic deformations, and a schematic illustration of the chip formation during orthogonal cutting is shown in figure 2.20.
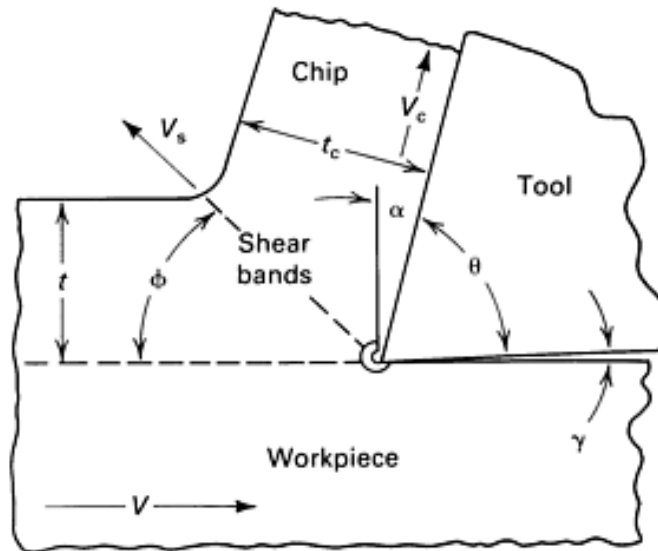
Figure 2.20: Schematic of the chip formation process during orthogonal cutting showing the rake angle (γ), and clearance angle (α). The uncut chip thickness is labelled t and the thickness of the chip following the formation of a shear band is labelled t_c. From ref. [65].

Important process variables during machining operations include the feed rate, cutting (or surface) speed and the depth of cut. The cutting speed is the relative velocity between the surface of workpiece and the tooling, whilst the feed rate is the relative axial movement of the tooling with respect to the cylindrical workpiece for turning operations. In milling, the feed rate is ordinarily quoted as the distance traversed across the workpiece by the spindle either per full revolution or per tooth. Two types of milling operation are possible; "climb milling" and "conventional milling". In conventional milling, the cutting direction is the same as the direction of movement of the spindle relative to the workpiece, whilst in climb milling the cutting direction is opposite to the direction of movement of the spindle.

Titanium alloys are typically classed as "difficult to machine" materials, [66] due to their low thermal conductivity and retention of strength at elevated temperatures. Both of these attributes can lead to excessive tool wear and result in a high cost of manufacturing. The term "machinability" is rather vague in nature and includes factors such as tool wear, surface finish and overall power consumption. An important parameter that governs the machinability of titanium alloys is the formation of adiabatic shear bands in the primary deformation zone (see figure 2.20). Here, the high strain rates, large strains and increased temperatures lead to flow softening within the chip and this results in the typical serrated chip morphology that is common to titanium alloys [67]. An example of the serrated chip morphology observed by Arrazola *et al* [67] during turning of Ti-6Al-4V is shown in figure 2.21. Attempts to model turning of titanium alloys have been made by Calamaz [68] and Sima [69] using constitutive laws modified to account for the flow softening at high strains and some success has been achieved in accurately predicting chip morphology.
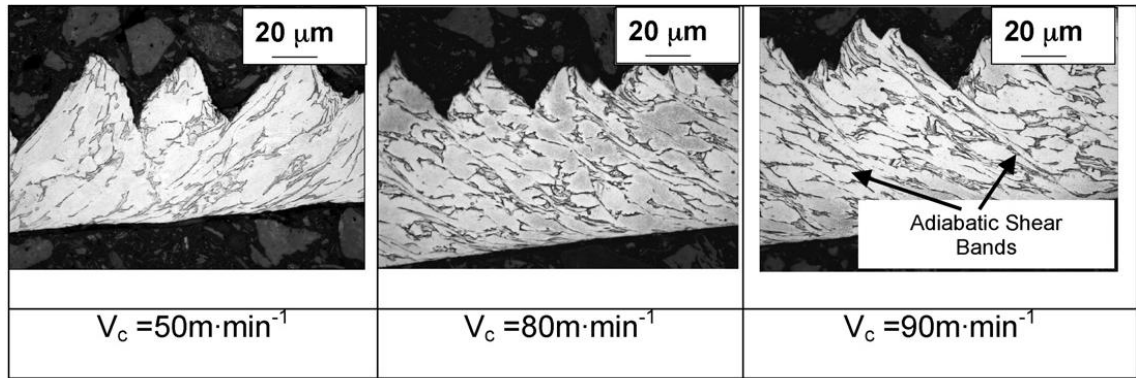
Figure 2.21: Light optical micrographs of chip morphology for machined (turned) Ti-6Al-4V as a function of surface cutting velocity (V_c). The location of adiabatic shear bands within the serrated chip is labelled. From Arrazola *et al* [67].

Aggressive turning strategies may result in a distorted microstructure below the machined surface. Typical metallurgical examination of machined titanium alloys by researchers is currently limited to light optical microscopy or comparatively low resolution secondary electron imaging [70][71]. In [71], Shankar *et al* performed a serried of experiments to investigate the effect of large strain machining on microstructure and deformation mechanism in CP-Ti. It was reported that significant microstructural refinement occurred within the fan-shape deformation zone that preceded the tool-chip interface. Shankar *et al* [71] also observed extensive mechanical twinning below the machined surface, and a light optical micrograph showing subsurface twinning to a depth of approximately 100 µm is shown in figure 2.22. Machining can be deleterious to the fatigue properties of titanium alloys due to poor surface finish or the introduction of residual stresses, with the introduction of residual stresses during milling of Ti-834 having been investigated by Sridhar *et al* [72]. In this study, the stresses were found to be compressive in nature, and although their relaxation during thermal annealing was measured, the effect of milling on surface damage was not investigated.
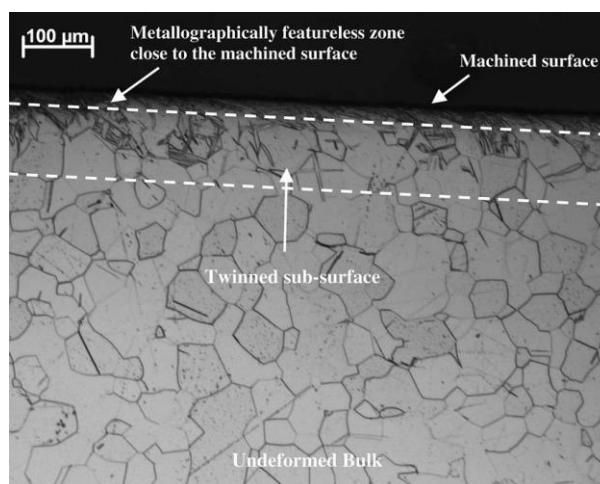
Figure 2.22: Light optical micrograph showing subsurface twinning of CP-Ti following large strain machining. From Shankar *et al* [71].

Outside the domain of titanium alloys, a more detailed analysis of deformation structures below a machined surface has been made by Guo *et al* [73][74] on Cu-30Zn brass, commercial purity Cu and CP-Ti. Through a combination of particle image velocimetry, TEM and EBSD to investigate both deformation levels and the deformed microstructures, Guo *et al* have elegantly presented their data in the form of a deformation map for the machining process (Fig. 2.23). The deformation structures resulting from high strain machining are plotted along with estimated strain rates and temperature as a function of cutting speed and shear strain. The deformation structures observed range from nano-twinned grains to micron-sized equiaxed grain that forms due to recrystallisation.
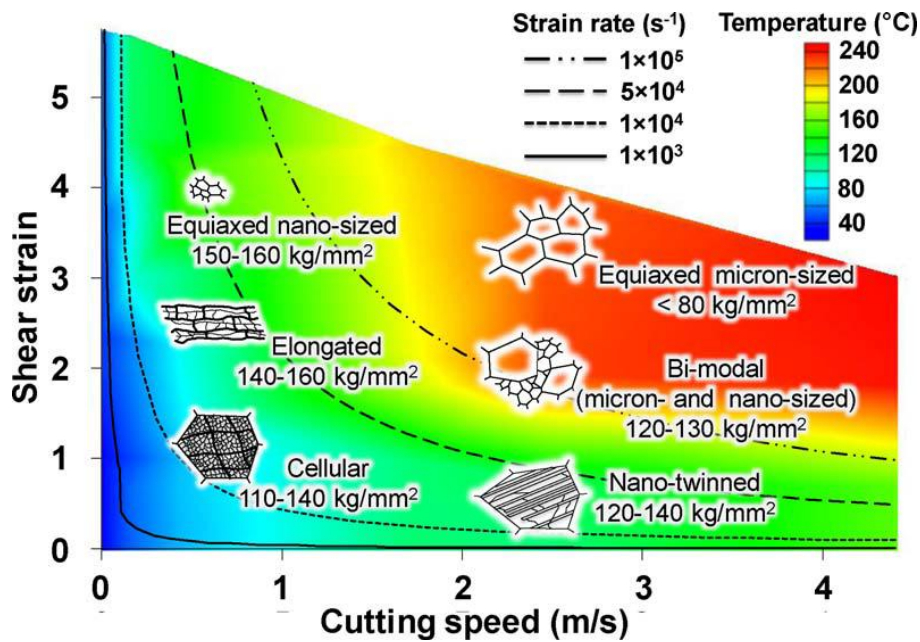
Figure 2.23: Deformation map for copper during high strain machining with the deformation microstructures as a function of shear strain and surface cutting speed characterised through transmission electron microscopy. From Guo *et al* [73][74].

Deformation maps such as the one presented in figure 2.23 are useful in engineering sub-surface microstructures during machining operations for the classical engineering materials and it is clear that the range in temperature, strain and strain rate strongly influence the mode of deformation as is the case during hot working operations. Little attention has been paid however, toward understanding the mode of deformation during industrial machining operations on advanced aerospace alloys.

2.4.2 *Shot peening*

Following final machining to net shape, surface treatments such as shot peening, deep rolling and low plasticity burnishing are often applied to components prior to assembly in order to improve their mechanical properties. In the case of shot peening, repeated impact of high velocity shot (typically either steel or glass) plastically deforms the material at the surface of a component, with the net effect being the introduction of an in-plane subsurface compressive residual stress [75]. An example of the residual stress profiles obtained following shot peening and subsequent thermal exposure of the α + β alloy Ti-6242 is shown in figure 2.24 [76]. From figure 2.24, it can be seen that the subsurface compressive residual stress penetrates to a depth of 100 μm, with a

balancing tensile stress toward the specimen bulk. According to Wagner [77], the surface plastic strain may either slightly improve fatigue crack initiation resistance, or have little effect; although it is well documented that the compressive residual stress retards the growth of fatigue cracks through closure [75-78].
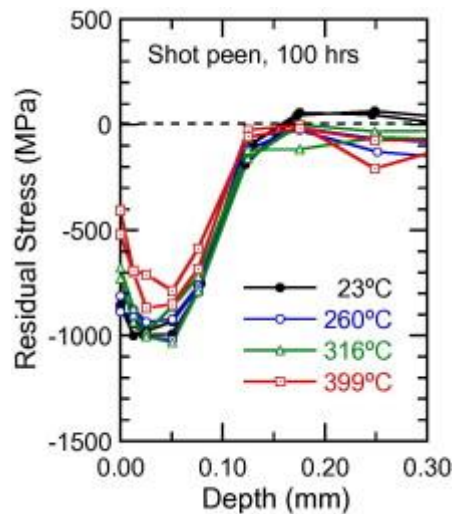
Figure 2.24: Effect of thermal exposure of up to 100 hours on the shot peened residual stress in Ti–6Al–2Sn–4Zr–6Mo. Shot peening intensity is 6A Almen with 100% coverage. From John *et al* [76].

Relaxation of the compressive residual stresses is reported to occur during cyclic loading according to Torres *et al* [79] however, with a reduction of approximately 50% in the peak compressive stress following 10^4 cycles in shot peened AISI 4340 steel. Similar observations have been made in the nickel alloy Udimet 720 following high temperature isothermal fatigue testing, where considerable stress relaxation occurred following one cycle [80], implying that the cold-worked surface layer may have a larger influence on fatigue properties than purported by Wagner [77]. Shot peening is also reported to improve the fretting fatigue performance of titanium alloys such as Ti-6Al-4V [81] in addition to plane fatigue properties [82].
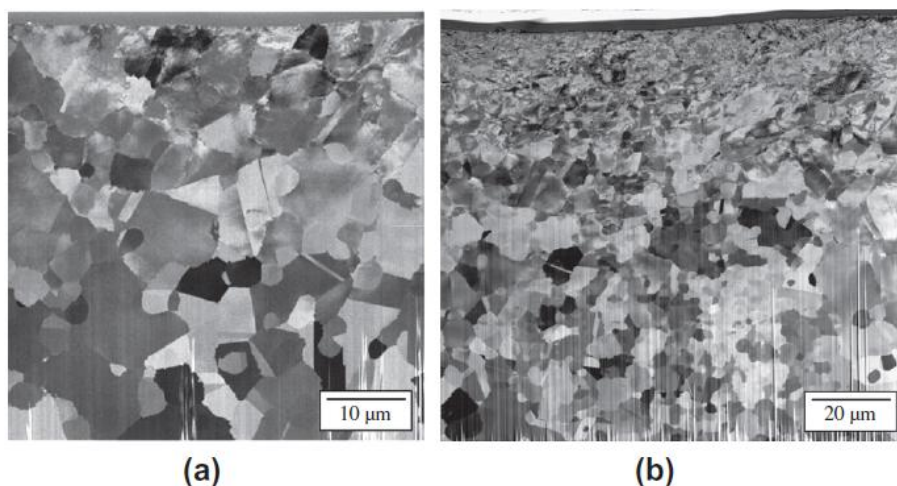
Figure 2.25: Ion beam induced secondary electron images of a Ni-based alloy cross-section with a shot-peened surface exposed to (a) 4–6 A and (b) 8–10 A intensity, with 110H steel shot at 200% coverage. From Child *et al* [83].

The microstructural response of an alloy to shot peening has not been extensively studied, with research efforts mainly centred on the residual stress profile and resulting surface roughness following shot peening e.g. [83]. Some microstructural investigations have been performed however, with Lindemann *et al* [84] reporting extensive mechanical twinning and kinking of lamellae following shot peening of a Ti-Al intermetallic material. The degree of strain hardening during shot peening of a Ni-based alloy has been recently investigated by Child *et al* [85] through EBSD analysis. Here, it was observed that the strain hardened region extends deeper into the alloy with increasing shot peening intensity and an example of the deformed subsurface microstructures, characterised through ion-beam microscopy, is shown in figure 2.25.

An increase in the high cycle fatigue strength does not always result from shot peening however. Recent work by Zay *et al* [86] has shown the HCF limit for Ti-6Al-4V with an equiaxed microstructure actually decreased following shot peening to an Almen intensity of 0.2 mmA. Fatigue testing was also performed on the α + β alloy Ti-54M and S-N curves from [84] are shown in figure 2.26. Both alloys were uni-directionally rolled at 800°C and test specimen blanks were machined form the plate in the transverse direction. Although both alloys in this investigation were hot rolled and heat treated in a similar manner, the Ti-54M specimens had a much finer microstructure, and concomitantly possessed higher fatigue strength at 10^7 cycles in the electro-polished (EP) condition.

According to Zey *et al*, the loss in HCF strength in shot peened Ti-6Al-4V was explained by the insensitivity of the coarse grained microstructure to the applied stress ratio (R), where little variation in HCF limit was observed between testing at stress ratios of R = -1 and R = 0.1. It was therefore proposed that the Ti-6Al-4V alloy was sensitive the superposition of the balancing tensile residual stresses from the shot peening process.
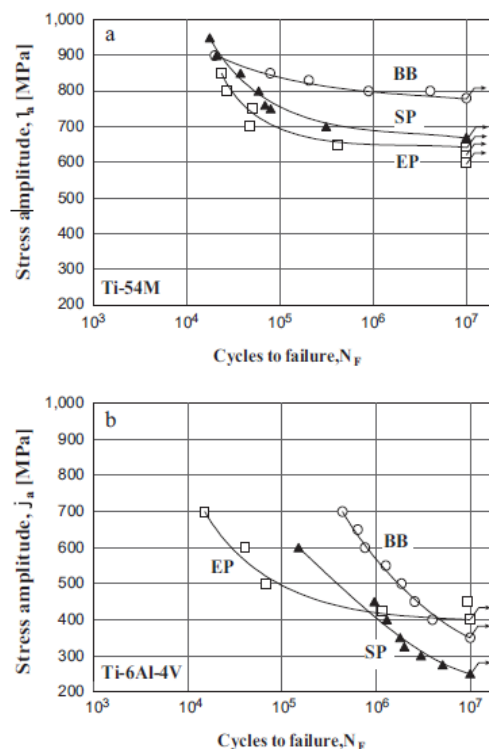
Figure 2.26: S-N curves for a) Ti-54M and b) Ti-6Al-4V illustrating the effect of shot peening (SP), ball burnishing (BB) and electro-polishing on the rotating beam fatigue life at R = -1. From ref [84].

References

[1] M. Jackson and K. Dring, Materials Science and Technology 22 (2006) 881 – 887

[2] I. J. Polmear, Light Alloys, Third edition, Arnold, London, 1995

[3] H. M. Flower, Materials Science and Technology 6 (1990) 1082 – 1092

[4] P. G. Partridge, Metallurgical Reviews 12 (1967) 169 – 194

[5] G. Lütjering, J. C. Williams, Titanium, First edition, Springer-Verlag, New York, 2003

[6] W. G. Burgers, Physica 1 (1934) 561 – 586

[7] N. Gey, M. Humbert, M. J. Phillipe *et al*, Materials Science and Engineering A 219 (1996) 80 – 88

[8] N. Gey and M. Humbert, Acta Materialia 50 (2002) 277 – 287

[9] N. Stanford and P. S. Bate, Acta Materialia 52 (2004) 5215 – 5224

[10] J. Romero, M. Preuss, J. Quinta da Fonseca, Acta Materialia 57 (2009) 5501 – 5511

[11] M. R. Daymond, R. A. Holt, S. Cai *et al*, Acta Materialia 58 (2010) 4053 – 4066

[12] H. Margolin and P. Farrar, Ocean Engineering 1 (1969) 329 – 345

[13] R. Boyer, Materials Science and Engineering A 213 (1996) 103 – 114

[14] I. Weiss and S. L. Semiatin, Materials Science and Engineering A 263 (1999) 243 – 256

[15] G. Lütjering, Materials Science and Engineering A 243 (1998) 32 – 45

[16] H. J. Rack, J. I. Qazi, Materials Science and Engineering C 26 (2006) 1269 – 1277

[17] M. Long and H. J. Rack, Biomaterials 19 (1998) 1621 – 1639

[18] I. Weiss, S. L. Semiatin, Materials Science and Engineering A 243 (1998) 46 – 65

[19] H. Conrad, M. Doner, B. De Meester, in: R. L. Jaffee and H. M. Burte (Eds.), Titanium: Science and Technology, Plenum Press, 1973, pp: 969 – 1005

[20] H. R. Ogden, R. I. Jaffe, TML Report No.20, October 19th 1955

[21] M. F. Savage, J. Tatalovich, M. J. Mills, Philosophical Magazine, 84 (2004) 1127 – 1154

[22] N. E. Paton J. C. Williams, G P. Rauscher, in: R. L. Jaffee and H. M. Burte (Eds.), Titanium: Science and Technology, Plenum Press, 1973, pp: 1049 – 1069

[23] M. Battaini, E. V. Pereloma, C. H. J. Davies, Metallurgical and Materials Transactions A 38 (2007) 276 – 285

[24] A. A. Salem, S. R. Kalidindi, R. D. Doherty, Acta Materialia 51 (2003) 4225 – 4237

[25] H. S. Rosenbaum, in: R. E. Reed-Hill, J. P. Hirth and H. C. Rogers (Eds.), Deformation Twinning, Gorden and Breach Science Publishers, New York, 1964, pp: 43 – 76

[26] J. C. Williams, R. G. Baggerly, N. E. Paton, Metallurgical and Materials Transactions A 33 (2002) 837 – 850

[27] M. Peters, J. Hemptenmacher. J. Kumpfery *et al*, in: C. Leyens and M. Peters (Eds.), Titanium and Titanium Alloys, Wiley-VCY Verlag GmbH & Co, Weinheim, 2003, pp: 1 – 36

[28] T. R. Cass, in: R. I. Jaffe and N. Promisel (Eds.), The Science, Technology and Application of Titanium, Pergamon Press, London, 1970, pp 733 – 739

[29] E. O. Hall, Twinning and Diffusionless Transformations in Metals, Butterworths Scientific Publications, London, 1954.

[30] D. R. Chichili, K. T. Ramesh, K. J. Hemker, Acta Materialia 46 (1998) 1025 – 1043

[31] J. W. Christian, S. Mahajan, Progress in Materials Science 39 (1995) 1 – 157

[32] S. L. Semiatin, T. R. Bieler, Acta Materialia 49 (2001) 3565 – 3573

[33] G. E. Dieter, Mechanical Metallurgy, Second edition, McGraw-Hill, United States, 1976

[34] S. G. Song, G. T. Gray III, Metallurgical and Materials Transactions A 26 (1995) 2665 - 2675

[35] S. R. Kalidindi, A. A. Salem, R. D. Doherty, Advanced Engineering Materials 5 (2003) 229 – 232

[36] P. G. Partridge, C. J. Peel, in: R. I. Jaffee and N. Promisel (Eds.), The Science, Technology and Application of Titanium, Pergamon Press, London, 1970, pp 517

[37] E. Cerreta, G. T. Gray III, Metallurgical and Materials Transactions A 35 (2004) 1999 – 2011

[38] L. Addessio, E. Cerreta, G. T. Gray III, Metallurgical and Materials Transactions A 36 (2005) 2893 – 2903

[39] R. W. Armstrong, in: R. E. Reed-Hill, J. P. Hirth and H. C. Rogers (Eds.), Deformation Twinning, Gorden and Breach Science Publishers, New York, 1964, pp: 356 – 377

[40] B. C. Ng, B. A. Simkin, M. A. Crimp *et al*, Intermetallics, 12 (2004) 1317 – 1323

[41] T. R. Bieler, A. Fallahi, B. C. Ng *et al*, Intermetallics, 13 (2005) 979 – 984

[42] R. W. Cahn, in: R. E. Reed-Hill, J. P. Hirth and H. C. Rogers (Eds.), Deformation Twinning, Gorden and Breach Science Publishers, New York, 1964, pp: 1 – 28

[43] T. A. Mason, J. F. Bingert, G. C. Kaschner *et al*, Metallurgical and Materials Transactions A 33 (2002) 949 – 954

[44] F. Bridier, P. Villechaise, J. Mendez, Acta Materialia 53 (2005) 555 – 567

[45] Z. Keshavarz, M. R. Barnett, Scripta Materialia 55 (2006) 915 – 918

[46] M. D. Nave, M. R. Barnett, Scripta Materialia 52 (2004) 881 – 885

[47] L. Jiang, J. J. Jonas, A. A. Luo *et al*, Materials Science and Engineering A 445 – 446 (2007) 302 – 309

[48] L. Wang, Y. Yang, P. Eisenlohr et al, Metallurgical and Materials Transactions A 41 (2010) 421 – 430

[49] J. R. Bingert, T. A. Mason, G. C. Kaschner et al, Metallurgical and Materials Transactions A 33 (2002) 955 – 963

[50] R. R. Boyer, in: R. Blockley and W. Shyy (Eds.), Encyclopedia of Aerospace Engineering, John Wiley & Sons, Chapter 175

[51] S. L. Semiatin, V. Seetharaman, I Weiss, Materials Science and Engineering A 243 (1998) 1 – 24

[52] B. Kad, S. E. Schoenfeld, M. S. Burkins, Materials Science and Engineering A 322 (2002) 241 – 251

[53] G. Lütjering, A, Gysler, in: G. Lütjering, U. Zwicker, W. Bunk (Eds.), Titanium Science and Technology, Deutsche Gesellschaft fur Metallkunde, Oberursel, 1984, pp: 2065 – 2083

[54] J. O. Peters, R. O. Ritchie, International Journal of Fatigue 23 (2001) S413 – S421

[55] D. F. Neal, in: G. Lütjering, U. Zwicker, W. Bunk (Eds.), Titanium: Science and Technology, Deutsche Gesellschaft fur Metallkunde, Oberursel, 1984, pp: 2419 – 2424

[56] D. F. Neal, in: P. Lacombe, R. Tricot, G. Beranger (Eds.), Proceeding of the 6th World Conference on Titanium, Cannes, France, 1988, Societé Francaise de Metallurgie, 1989, pp: 265 – 268

[57] Technical Brochure, Titanium Metals Corporation (TIMET)

[58] M. Leyens, M. Peters, W. Kaysser, Materials Science and Technology 12 (1996) 213 – 218

[59] L. Germain, N. Gey, M. Humbert *et al*, Acta Materialia 53 (2005) 3535 – 3543

[60] E. E. Sacket, L. Germain, M. R. Bache, International Journal of Fatigue 29 (2007) 2015 – 2021

[61] N. E. Paton, M. W. Mahoney, Metallurgical Transactions A 7 (1976) 1685 – 1694

[62] C. Andres, A. Gysler, G. Lütjering, in: F. H. Froes, I. L. Caplan (Eds.), Titanium '92: Science and Technology, TMS, Warredale, PA, 1993, pp: 311 – 318

[63] H. Kestler, H. Mughrabi, H. Renner, in: P. A. Blenkinsop, W. J. Evans and H. M. Flower (Eds.), Titanium: Science and Technology, The Institute of Materials, London, 1996, pp: 1171 – 1178

[64] M. C. Shaw, Metal Cutting Principles, Clarendon Press, Oxford, 1996.

[65] ASM Handbook, Volume 16, "Machining", ASM International, 1989

[66] N. Zlatin, M. Field, in: R.I. Jaffe, H. M. Burke (Eds.), Titanium Science and Technology, Plenum Press, New York, 1973, pp. 489-503.

[67] P. –J. Arrazola, A. Garay, L.-M. Iriarte et al, Journal of Materials Processing Technology 209 (2009) 2223 – 2230

[68] M. Calamaz, D. Coupard, F. Girot, International Journal of Machine Tools & Manufacture 48 (2008) 275-288

[69] M. Sima, T. Özel, International Journal of Machine Tools & Manufacture 50 (2010) 943-960

[70] J. I. Hughes, A. R. C Sharman, K. Ridgway, Proceeding of the Institute of Mechanical Engineers, part B: Journal of Engineering Manufacture 218 (2004) 1113

[71] M. R. Shankar, B. C. Rao, S. Lee et al, Acta Materialia 54 (2006) 3691 – 3700

[72] B. R. Sridhar, G. Devananda, K. Ramachandra *et al*, Journal of Materials Processing Technology 139 (2003) 628 – 634

[73] Y. Guo, C. Saldana, W. Dale Compton *et al*, Acta Materialia 59 (2011) 4538 – 4547

[74] Y. Guo, R. M'Saoubi, S. Chandrasekar, CIRP Annals – Manufacturing Technology 60 (2011) 137 – 140

[75] P. J. Withers, Reports on Progress in Physics, 70 (2007) 2211 – 2264

[76] R. John, D. J. Buchanan, S. K. Jha *et al*, Scripta Materialia 61 (2009) 343 – 346

[77] L. Wagner, Mater. Sci. Eng. A (1999) 210 – 216

[78] N. Barry, S. V. Hainsworth. M. E. Fitzpatrick, Materials Science and Engineering A 507 (2009) 50 – 57

[79] M. A. S. Torres, H. J. C. Voorwald, International Journal of Fatigue 24 (2002) 877 – 886

[80] A. Evans, S-B. Kim, J. Shackleton et al, International Journal of Fatigue 27 (2005) 1530 – 1534

[81] K. Liu, M. R. Hill, Tribology International 42 (2009) 1250 – 1263

[82] L. Wagner, C. Gerdes, G. Lütjering, in: G. Lütjering, U. Zwicker, W. Bunks (Eds.), Titanium Science and Technology, Deutsche Gesellschaft fur Metallkunde, Oberursel, 1984, pp:2147 – 2154

[83] M. Guagliano, Journal of Materials Processing Technology, 110 (2001) 277 – 286

[84] J. Lindemann, C. Buque, F. Appel, Acta Materialia 54 (2006) 1155 – 1164

[85] D. J. Child, G. D. West, R. C. Thompson, Acta Materialia 59 (2011) 4825 – 4834

[86] K. Zay, E. Maawad, H. –G. Brokmeier et al, Materials Science and Engineering A 528 (2011) 2554 – 2558

Chapter 3

An investigation into the microstructure and properties of shot peened Ti-834

3.1   Introduction

An effective measure to improve the fatigue properties of an engineering component is to introduce an in-plane compressive residual stress below its surface [1]. Whilst modern techniques such as deep-rolling and laser shock peening have amply demonstrated their effectiveness in achieving this result [2], a more mature method still widely employed for introducing the necessary plastic strain to place the sub-surface material in in-plane compression is shot peening [1][3-5]. During the peening process, the surface of a treated component is subjected to multiple impacts of hard steel spheres (termed 'shot'), which plastically deforms the material within the surface region. The resulting net compressive residual stress can retard the growth of surface nucleated cracks, leading to improved fatigue strengths in treated material [6]. With regard to titanium alloys, studies reporting the effects of shot peening on fatigue behavior under different loading conditions are available in the literature [7][8].

In addition to the introduction of compressive residual stresses, shot peening leads to alterations of the sub-surface microstructure, dislocation density and material hardness [9][10], and of particular concern to the engineering community is the stability of residual stresses following exposure to thermal energy [10-12]. It is pertinent to also consider however, the thermal and environmental stability of the plastically deformed region immediately below the shot peened surface. This is of significant importance to high temperature near-α titanium alloys, where service requirements dictate that the alloys not only possess a balance between bulk fatigue and creep properties, but maintain their resistance to oxygen uptake and microstructural stability up to temperatures of approximately 600°C.

During exposure to elevated temperature, near-α titanium alloys are susceptible to several mechanisms that reduce their post-exposure room temperature tensile ductility and fatigue properties; and the area has been the subject of extensive research over recent decades. First is the embrittlement of the near-surface region by oxygen uptake [13-16] and secondly, microstructural changes occur within the bulk that lead to enhanced planarity of slip, and concomitant loss of ductility [17-20].

Due to titanium's high affinity to oxygen, inward diffusion from the exposed surface occurs at elevated temperatures and the effect of surface oxygen contamination on the

room temperature tensile properties of near-α titanium alloys was reported by Shamblen and Redden [13], who concluded that ductility loss was proportional to the thickness of the oxygen-rich layer. It was postulated in [13] however, that although oxygen contamination was the dominant mechanism for ductility loss following thermal exposure in air, metallurgical instabilities in the bulk may contribute to a further loss in ductility. This was verified by Leyens [15], by comparing the room temperature tensile ductility (% R.A) of Ti-1100 following isothermal exposure of the alloy to air and in vacuum at circa 600°C. Although the most dramatic embrittlement occurred in material exposed to laboratory air, some degradation in the tensile ductility was measured in vacuum heat treated samples. The reported loss in tensile ductility of Ti-1100 without surface oxygen contamination following prolonged thermal exposure aligns with studies by Woodfield [18] and Ramachandra [19] who measured a four-fold decrease in % RA of Ti-829 and Ti-685 following thermal exposure at 575°C for 1000 hrs and 800°C for 24 hrs respectively.

In both cases, the proposed mechanism for bulk ductility loss was the precipitation of silicide particles of type $(Ti, Zr)_x Si_y$ along <c>-component dislocations, secondary α lath and martensitic α' plate boundaries, which were subsequently fractured during tensile straining leading to the formation of intense planar slip bands. The precipitation of silicides in the comparable near-α titanium alloy Ti-834 is also reported to occur along martensitic α' plate boundaries and between primary α grains and adjacent secondary α colonies during the ageing step at 700°C following solution heat treatment [20][21]. Whilst there has been some ambiguity over the precise mechanism for bulk embrittlement caused by high temperature exposure (short range ordering of aluminium to form fine dispersions of Ti_3Al, or $α_2$ formation, has also been discussed as a mechanism for embrittlement during prolonged ageing in ref. [22]), the microstructural and mechanical sensitivity of near-α titanium alloys to prolonged exposure is evident in the scientific literature.

What is perhaps quite not so evident is the effect surface treatments, such as shot peening, may have on the localized microstructural stability of the plastically deformed surface region following exposure to heat. Furthermore, recent studies investigating the effect of surface cold-working processes, namely shot peening and a surface mechanical attrition treatment, have reported enhanced diffusion rates of aluminium [23] and nitrogen [24] within the deformed surface region of pure iron. The increased diffusivity of solute elements was accounted for by the formation of a "nanostructured" surface layer containing a large density of non-equilibrium grain boundaries and dislocations. Based on this assertion, it can be anticipated that shot peening may also increase in the inward diffusion kinetics of oxygen in α-titanium during prolonged thermal exposure in air, through the introduction of short-circuit diffusion pathways within the cold-worked sub-surface region. The net result of this would be increased levels of sub-surface oxygen content, which may lead to the premature formation of surface micro-cracks during cyclic loading.

The creep resistant near-alpha titanium alloy Ti-834 is an advanced aero-structural material employed in the intermediate and high pressure compressor stages of gas turbine aero-engines. Due to its use in the "hot end" of aero gas turbine engines for the manufacture of compressor discs, rings and blades; Ti-834 possesses a good combination of creep and fatigue properties (in addition to oxidation resistance) up to its service temperature of 600°C [25]. Regions of the compressor assembly, such as the compressor discs and blade roots, are often shot peened prior to assembly in order to improve service fatigue performance and handling properties during assembly.

The aim of this chapter is to therefore investigate the effect of prior shot peening on the microstructural stability of a near-α titanium alloy during prolonged exposure at elevated temperatures. The study is divided into three components: First is to investigate the deformation mechanisms that occur during the shot peening process. Secondly, the microstructural response of Ti-834 within the plastically deformed surface region during long-term high temperature exposure is investigated. The third objective of the study is to measure oxygen uptake kinetics in both shot peened and non-peened material following prolonged exposure.

Finally, in order to compliment the microstructural analysis that has been performed on Ti-834 this research aims to identify whether the high-cycle fatigue properties following high temperature exposure are adversely affected by the peening process. Furthermore, the fatigue testing programme is intended to provide the design engineer with preliminary data to construct Haigh diagrams [26] and mapping the acceptable/unacceptable fatigue loading conditions for machined and shot peened material. In order to benchmark results against the traditional 'worse case' scenario for surface condition, shot peened material is compared with specimens tested in the as-machined condition. The fatigue testing programme is also supplemented by fractography and microstructural analysis to examine the mechanisms that control high cycle fatigue life in machined and shot peened surface conditions.

3.2   Experimental methods

Forged Ti-834 billet was supplied by TIMET UK and the chemical composition of the material is given in table 3.1. The billet was slowly cooled following hot working low in the (α+β) phase field and was not subject to any further thermomechanical processing or heat treatment. It should be noted that the microstructural condition of the supplied billet is not typical of that used in service[1], and as such, is a model microstructure for the purposes of this investigation.

Table 3.1: The chemical composition (in wt. %) of the Ti-834 billet supplied by TIMET UK. Analysis was performed at INCO Test, UK.

Al	Sn	Zr	Nb	Mo	Si	C	Ti
5.5	4	3.5	0.8	0.5	0.3	<0.1	Bal.

The billet was serial sectioned into coupons of approximately 10 mm thickness by electro-discharge machining (EDM) prior to shot peening. Material was shot peened to 9A Almen intensity using R32 steel shot at Metal Improvement Company, Derby, United Kingdom. No surface modification (e.g. grinding or polishing) was performed between EDM of the serial sectioned coupons and the shot peening process. Specimens were shot peened to 200% and 1200% coverage in order to investigate the effect of increasing the number of peening passes on deformation mechanisms and microstructural stability during thermal exposure.

---

[1] The Ti-834 billet is in the condition that would ordinarily be supplied to secondary wrought manufactures (e.g. Wyman-Gorman or Firth Rixson) for final forging into condition of supply disks and rings. A final solution heat treatment and ageing step is employed to attain the service specification microstructure.

Shot peened and EDM coupons were subsequently heat treated in laboratory air at temperatures of 650°C and 700°C for durations of 1272 hours and 1800 hours respectively, and air cooled following removal from the furnace. These temperature time combinations were selected in order to evaluate the thermal stability of the modified surface rather than provide a specific match to service conditions. However, the regimes chosen are sufficiently close to service conditions that trends concerning treated versus untreated surfaces should be reasonably valid. Furnace temperature during the heat treatments was monitored by a thermocouple placed close to the specimens in the furnace.

Coupons were sectioned along a plane parallel to the peening direction (direction of the shot stream) and were prepared for metallography using water lubricated silicon carbide grinding papers to achieve a planar finish. Preliminary polishing performed using 9 μm diamond suspension and final polishing with a 0.06 μm colloidal silica suspension. Microstructural characterization was performed using an Olympus BX-51 light microscope and an FEI Sirion field emission gun scanning electron microscope. Quantitative crystallographic data was acquired using electron backscatter diffraction (EBSD) with a 15 kV accelerating voltage, 10 nA probe current and a step size of 0.06 μm. Automated indexing and post-processing of the diffraction data was performed using Oxford Instruments HKL Channel 5 software.
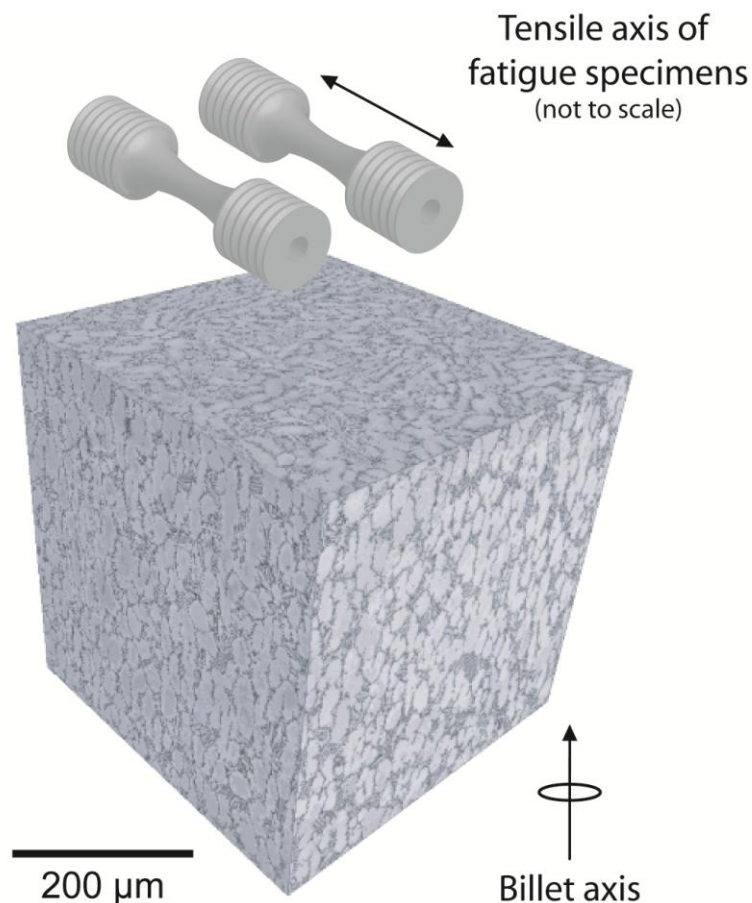
Figure 3.1: Schematic orientation of the Amsler M8 fatigue specimens with respect to the billet axis of the supplied Ti-834 material.

Following prolonged thermal exposure in air, secondary ion mass spectrometry (SIMS) was performed on shot peened and electro-discharge machined specimens to measure the effect of peening on the near surface oxygen diffusion profile. Following metallographic sectioning, SIMS analysis was performed at individual sites of increasing distance from the shot peened or electro-discharge machined edge using a Ga^+ primary ion beam. As a thin layer of stable TiO_2 immediately forms on an exposed surface of titanium, collecting secondary ^{16}O ion counts from the sectioned surface would not yield reliable data. Therefore, the secondary ion ^{16}O count at a depth of approximately 0.5 μm beneath the sectioned surface was taken to be indicative of the oxygen concentration at a given distance from the peened or machined edge. In order to obtain semi-quantitative oxygen concentration data of thermally exposed Ti-834, the secondary ion oxygen count of an oxygen-free silicon wafer was measured in the ion beam chamber to determine the background levels of ^{16}O. The SIMS oxygen count within the bulk of the as-received Ti-834 billet was measured and adjusted to account for background oxygen levels. SIMS data was subsequently normalized against the measured residual oxygen levels in the billet, which were obtained by chemical analysis at INCO test.

In order to compare the deformation response of Ti-834 at low strain rates with the higher strain rates associated with shot peening, flat tensile specimens were also wire EDM from the supplied billet and polished to a metallographic mirror finish using the methodology discussed above. Tensile testing was performed on an Instron testing rig at a strain rate of approximately 10^{-3} s^{-1}. The pre-polished surfaces of the tensile specimens were examined using light microscopy following tensile deformation.

Fatigue testing was performed using Amsler M8 specimens. The test specimen configuration results in a gauge diameter of 2.5 mm and a 25 mm gauge length. An advantage of employing this type of test specimen design is that the surface to volume ratio is maximised, thus the surface effects on fatigue life are more pronounced. A disadvantage however, is that the small cross-sectional area of the test specimen lends itself to interference from the large regions of microtexture (termed *macrozones*), which exist in this alloy and have been thoroughly characterised by electron backscatter diffraction [27].

Amsler M8 fatigue specimens were machined from the received billet of Ti-834 such that the stress axis was perpendicular to the billet axis as shown in figure 3.1. A number of fatigue specimens were shot peened to 200% coverage at 9A Almen intensity using R32 steel shot at Metal Improvement Company, Derby, UK. The specimen thread was protected during the shot peening process and only the gauge length was treated. Specimens were tested in the as-machined and shot peened conditions both prior to, and following thermal exposure at 650°C in laboratory air. Due to the limited number of available fatigue specimens and the large number of experimental variables, a staircase loading method [26] was chosen to assess the high cycle fatigue limit of the shot peened and machined specimens. The fatigue tests were performed at a frequency of 66 Hz in laboratory air and at a stress ratio of 0.1. A mean positive tensile stress for the fatigue testing was employed to preserve the fracture surfaces following failure for examination. The constant life fatigue endurance limit ($\Delta\sigma_{ES}$) was then calculated using the following equation [26]:

$$\Delta\sigma_{ES} = \Delta\sigma_{PS} + (\Delta\sigma_F - \Delta\sigma_{PS}).\left(\frac{N_f}{N_{RO}}\right) \qquad\qquad \text{Eqn. 2.1}$$

Where $\Delta\sigma_{PS}$ is the stress range of the penultimate loading step, $\Delta\sigma_F$ the stress range of the loading step required for failure, N_f the number of cycles to failure in the final loading step and N_{RO} the number of cycle considered a run out, which was 10^7 cycles in this study. Analysis of the fracture surfaces was performed on the failed specimens using an FEI Sirion field emission gun scanning electron microscope. To assess whether microcracking occurred within the surface oxygen diffusion layer (commonly referred to as the α-case), a selected number of fractured fatigue specimens were sectioned parallel to the tensile loading axis and prepared for metallography using the same method as the shot peened coupons.

3.3   Results and discussion

3.3.1   *Metallography and tensile properties of the received billet*

The starting microstructure of the received material is shown in figure 3.2. The microstructure is comprised of a large volume fraction (~80%) of elongated primary α grains with an average aspect ratio of approximately 2:1. Transformed β grains with coarse single-colony secondary α laths are visible at triple-point boundaries between the primary α grains. Polarized light microscopy showed the billet to contain regions of strong microtexture (Fig. 2b) and the backscatter electron micrograph shown in figure 2c) shows the primary α grains to be delineated with retained β. The microstructure of the alloy is consistent with the thermo-mechanical processing route applied to it; differing to the more typical bi-modal microstructure normally observed in solution heat treated and aged (SHT + A) Ti-834.
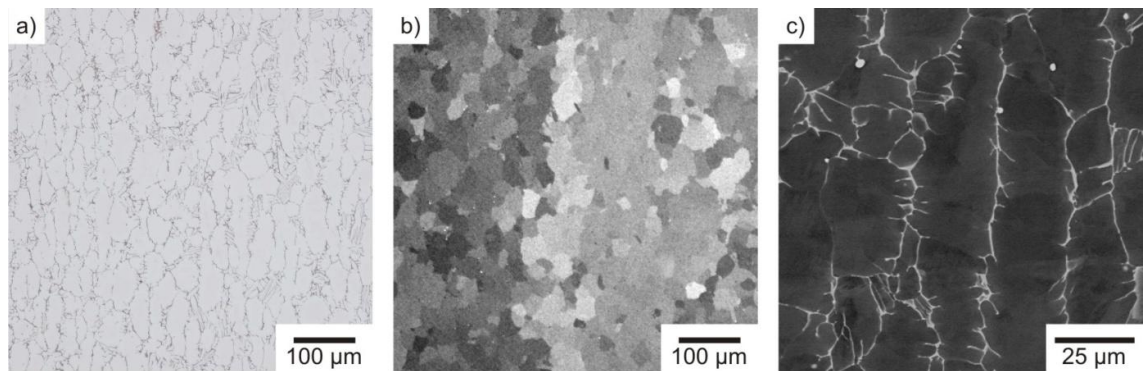
Figure 3.2: Starting microstructure of the Ti-834 billet supplied by TIMET UK. The etched microstructure is provided in a) and a polarized light micrograph is shown in b). A higher magnification backscatter electron micrograph is shown in c).
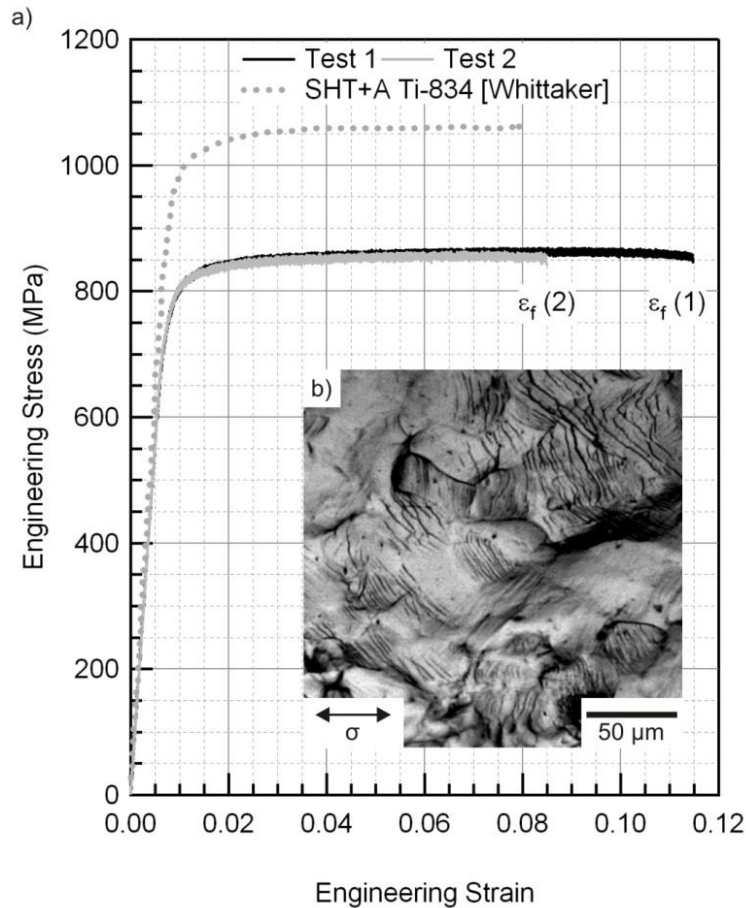
Figure 3.3: a) Tensile properties of the received Ti-834 billet. The tensile behavior of solution heat treated and aged (SHT + A) Ti-834 from Whittaker [28] is shown for comparison. A light micrograph showing the intersection of slip bands with the pre-polished surface of a tensile specimen is given in the inset b). The micrograph in b) was obtained at an engineering strain of 0.10 (Test 1) and σ indicates the stress axis.

The tensile properties of Ti-834 are shown in figure 3.3a). The 0.2% offset yield strength calculated from both tensile tests was 790 MPa with the two specimens failing at strains of 8.5% and 11.5%. Tensile properties of Ti-834 in the solution heat treated and aged condition from Whittaker [28] are shown for comparison. The material tested in the as-forged condition shows an offset yield strength of approximately 20% less than that of fully heat treated material, which is likely to arise from the lack of strengthening modes such as α_2 and bulk silicide precipitation along the α/β lath interfaces that occurs during the final ageing step at 700°C in fully heat treated material.

Figure 3.3b) is a light micrograph showing the intersection of slip bands with the pre-polished surface of a Ti-834 tensile specimen following straining to fracture. Slip bands can be observed in the majority of the α grains and no evidence of mechanical twinning was found through light optical microscopy. This aligns with the results of other studies [29], in which twinning was not found to be an active deformation mode during quasi-static tensile testing of Ti-834 at room temperature.

3.3.2 *Microstructural analysis of shot peened Ti-834*

The microstructural response of Ti-834 to shot peening is shown in figure 3.4 and figure 3.5. Cross-sectional polarized light micrographs showing the microstructural damage

that occurs immediately below the shot peened surface in Ti-834 are given in figure 3.4. Low magnification micrographs are given in figure 3.4a) and 3.4b) and increased magnification micrographs representative of the regions delineated by white dashed lines are shown in c) and d). Mechanical twins of approximately 1-2 μm width and possessing a low radius of curvature boundary with the matrix can be observed within α grains in material peened to both 200% and 1200% coverage. The observation of mechanical twinning in Ti-834 is in contrast to the microstructural observations of quasi-statically loaded Ti-834 where no evidence of mechanical twinning was found.

When viewed under polarized light, the twins are of opposite contrast to the parent grain and EBSD analysis identified the twins to be characterized by a misorientation of ~85° about the [12-10] crystal axis (Fig. 3.5b), which corresponds to the {10-12} twin mode in hexagonal metals. [30] The {10-12} type mechanical twins are delineated by black boundaries in the all-Euler EBSD map in figure 3.5a) and a schematic illustration of the {10-12} twin mode showing the twinning planes and directions is given in figure 3.5c). As α-titanium has a c/a ratio of less than √3, operation of the {10-12} twin mode leads to an extension along the *c*-axis of the HCP crystal and are thus often referred to as tensile twins.

The maximum depth to which twinning was observed in material peened 200% and 1200% coverage was approximately 50 μm, although there is a marked increase in twin density with increasing peening coverage and the twin density data as a function of depth and peening coverage is presented in figure 3.6. In the case of material peened to 200% coverage, a maximum twin linear fraction of 0.08 has been measured below the shot peened surface whilst peened to 1200% coverage results in a maximum twin linear fraction of 0.17. The increase in twin fraction aligns with the concept that increasing peening coverage introduces a larger amount of total plastic strain below the treated surface. It can also be observed from figures 3.4-3.6 that the density of twinning is not uniform below the shot peened surface, with certain regions showing an increased prevalence for mechanical twinning. It may therefore be anticipated that the plastic strain introduced during the shot peening process is also accommodated by dislocation glide.

Due to the limited number of active slip systems at room temperature, twinning plays an important role in accommodating homogeneous plastic deformation in unalloyed α-titanium [31-34]. Alloying with aluminium is reported to suppress mechanical twinning however, [35][36] and no evidence of twinning was observed during quasi-static tensile testing of Ti-834 [29]. The observation of mechanical twins in shot peened Ti-834 is therefore unexpected based on current understanding of deformation of titanium. The precise mechanism in which the propensity for twinning decreases with increasing aluminium content is unclear. Paton and Williams [35] postulated that the measured reduction in critical resolved shear stress for non-<*a*> type slip more readily permits deformation by dislocation motion parallel to the *c*-axis, therefore eliminating the need for extension or contraction of the crystal along the *c*-axis to be accommodated by mechanical twinning. The effect of aluminium on the stacking fault energy of titanium has also been investigated by Metzbower [37] and it was reported that increasing aluminium content leads to a decrease in the stacking fault probability. As increasing stacking fault energy is documented to raise the twinning stress for FCC metals such as copper as reported by Meyers [38], it is likely that a similar effect may be realised when increasing aluminium content in titanium. Regardless of mechanism, the microstructural observations strongly suggest that increasing aluminium concentration lowers a titanium alloy's propensity to deform by mechanical twinning.
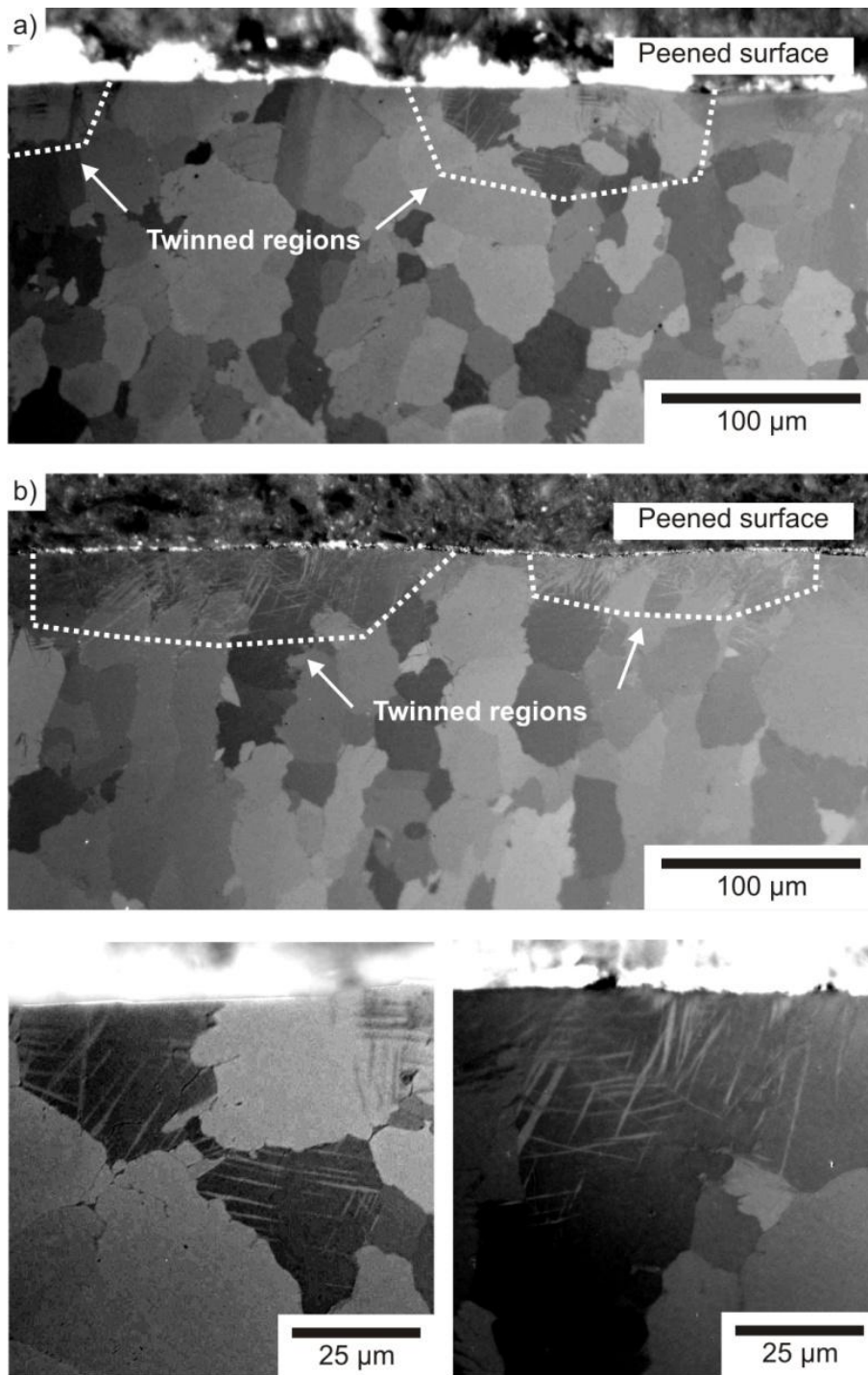
Figure 3.4: Cross-sectional polarized light micrographs of Ti-834 shot peened to a) 200% and b) 1200% peening coverage. The peening direction (direction of the shot stream) is approximately vertical.
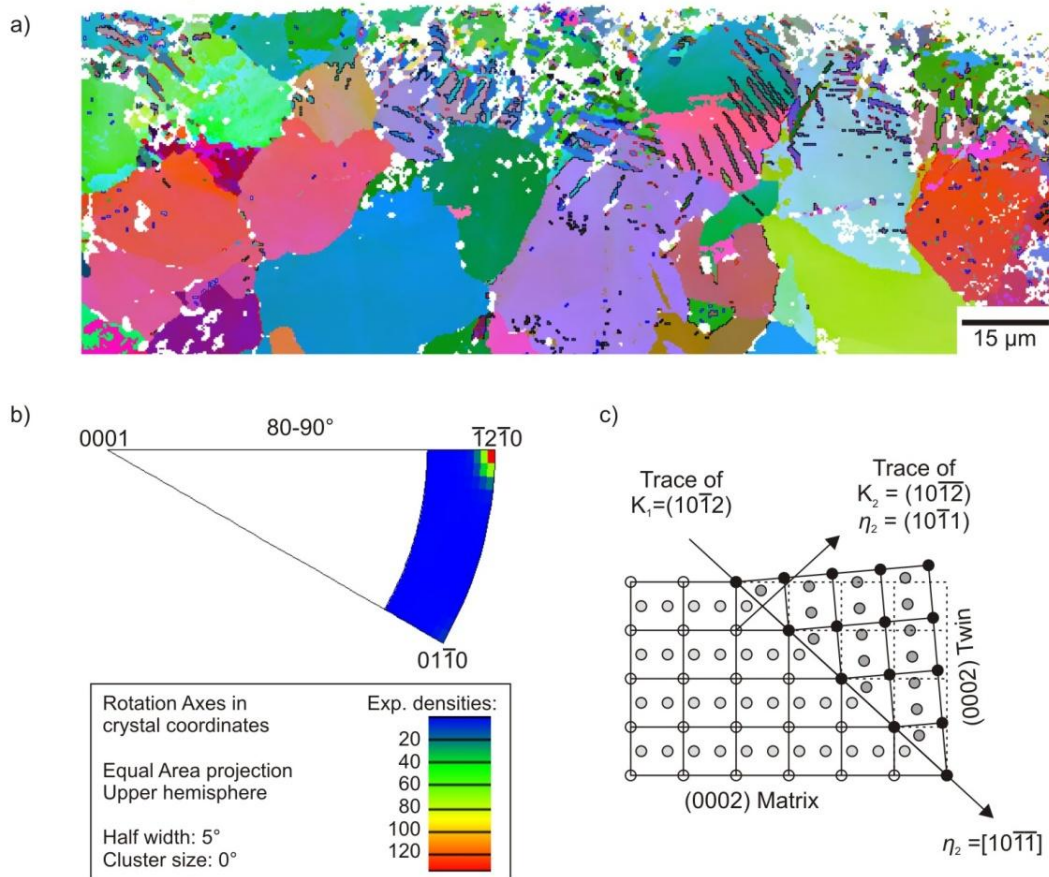
Figure 3.5: A cross-section EBSD map of Ti-834 shot peened to 1200% peening coverage is given in a). The top of the map corresponds to the shot peened edge. The corresponding misorientation axis plot of an α grain containing mechanical twins is shown in b) and a schematic {1-210} projection of the HCP lattice illustrating {10-12} mechanical twinning is provided in c).

In order to account for the observation of mechanical twins in shot peened Ti-834, it is pertinent to now consider both the average grains size of the alloy and the strain rates associated with shot peening. During a study on the dynamic testing of high-purity titanium, Gray reported a higher incidence of twinning in a coarse grained structure [39]. The grain size of the Ti-834 alloy investigated in this study (circa $60 - 100$ μm) however, is not largely dissimilar to the typical primary-α grain and transformed β colony packet size observed in solution heat treated and aged Ti-834. As mechanical twinning has not previously been observed in Ti-834 during low strain rate testing, it is likely that the average grains size is not key factor promoting deformation by twinning.

The mechanical response of metallic materials is highly sensitive to strain rate and the high deformation rates arising from the shot peening process are likely to strongly control the mode of plastic deformation. Mechanical twinning has been reported during shock loading of Ti-6Al-4V [40] and the effect of strain-rate on the twinning shear stress has been thoroughly reviewed by Meyers [38] and Christian [41]. In the latter two, it is discussed that the twinning shear stress is largely independent of strain-rate (and temperature), and the work of Chichilli [34], which demonstrated that the twin volume fraction in CP titanium increases with shearing stress only, is presented as an example by Meyers [38].
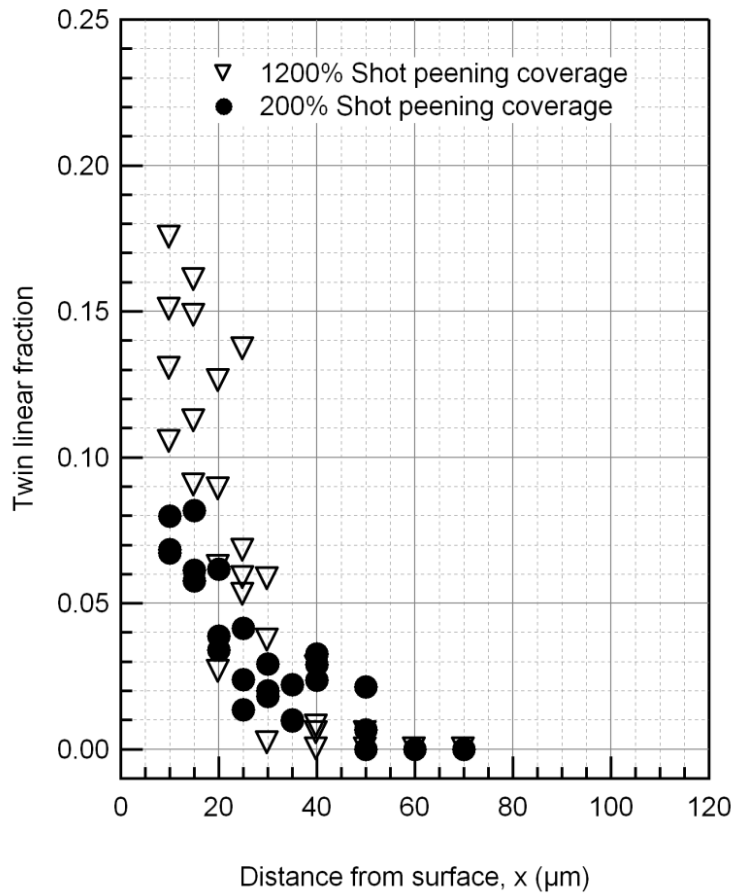
Figure 3.6: Twin line fraction as a function of distance from the shot peened surface for Ti-834 shot peened to 200% and 1200% peening coverage. Peening intensity was 9A Almen. Line fraction measurements were measured in at least three different areas imaged using polarized light microscopy.

Whilst the twinning shear is considered to be independent of strain-rate, the shearing stress required to activate dislocation glide is not. With increasing strain-rate, a commensurate increase in resolved shear stress to activate slip is required. Based on this assertion, it is hypothesized that the resolved shear stress for slip on certain slip systems (such as on the {10-11} and {11-22} planes) rises above the twinning shear stress for Ti-834 at the strain rates associated with shot peening, whilst at quasi-static rates, the resolved shear for all slip modes is falls below that of twinning. This concept, illustrated schematically in figure 3.7, provides an initial explanation for observation of mechanical twins in shot peened Ti-834. Irrespective of deformation mode, it is evident that shot peening heavily distorts the crystal structure within the first 50 – 60 μm from the workpiece surface and it can be readily anticipated that the distorted microstructure will be sensitive to subsequent thermal exposure.
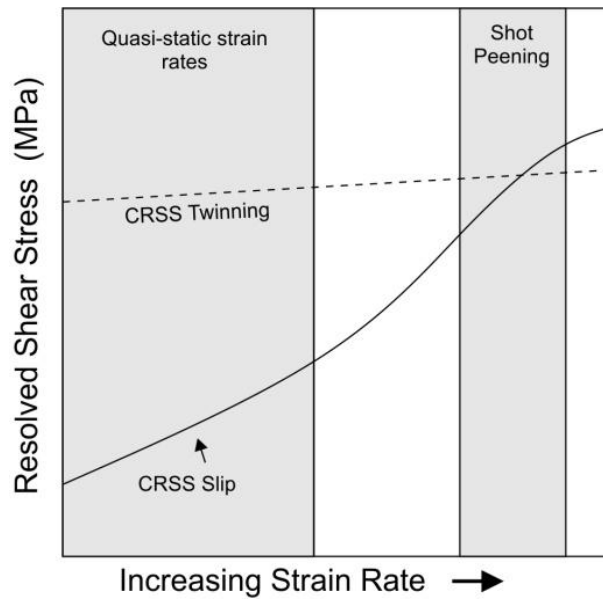
Figure 3.7: Schematic illustration showing the proposed relationship between the resolved shear stress for slip and twinning in Ti-834. At quasi-static rates, the shear stress for slip is significantly lower than that of twinning, whilst the strain rates associated with shot peening lead to the resolved shear stresses for slip approaching that of twinning.

3.3.3 *The microstructural response of shot peened Ti-834 to thermal exposure*

Backscatter electron micrographs of shot peened Ti-834 following prolonged thermal exposure in laboratory air at 600°C and 700°C for 1272 hrs and 1800 hrs respectively are presented in figure 3.8. In material peened to 200% and 1200% coverage, bright-contrast precipitates can be observed within the first 50 μm below the shot peened surface. Such precipitation is not observed below the EDM surface, or within the bulk material following identical thermal exposure time and temperatures and it is therefore clear that precipitation is restricted to within the plastically deformed region of shot peened material.

X-EDS analysis was performed on regions containing the larger precipitates in the peened material exposed to 700°C and although it was not possible to accurately determine their composition due to the large interaction volume of the electron beam with respect to the precipitate size, the local concentration of Zr in the vicinity of the precipitates was measured to be much greater than the residual Zr content of the alloy. Transmission electron microscopy has not been performed in this study to accurately characterize the nature of the precipitates, but it is inferred that they are of composition $(Ti,Zr)_6Si_3$ (S_2 Silicides), which are reported to form along martensitic α' and secondary α lath boundaries during ageing of Ti-834 at 700°C [20][21] and other near-α titanium alloys based on the Ti-Al-Zr-Si system [19][42]. The size of the precipitates increases with increasing thermal exposure time and temperature, and figure 3.8c) shows the onset of silicides precipitation following exposure at 650°C for 1272 hrs.
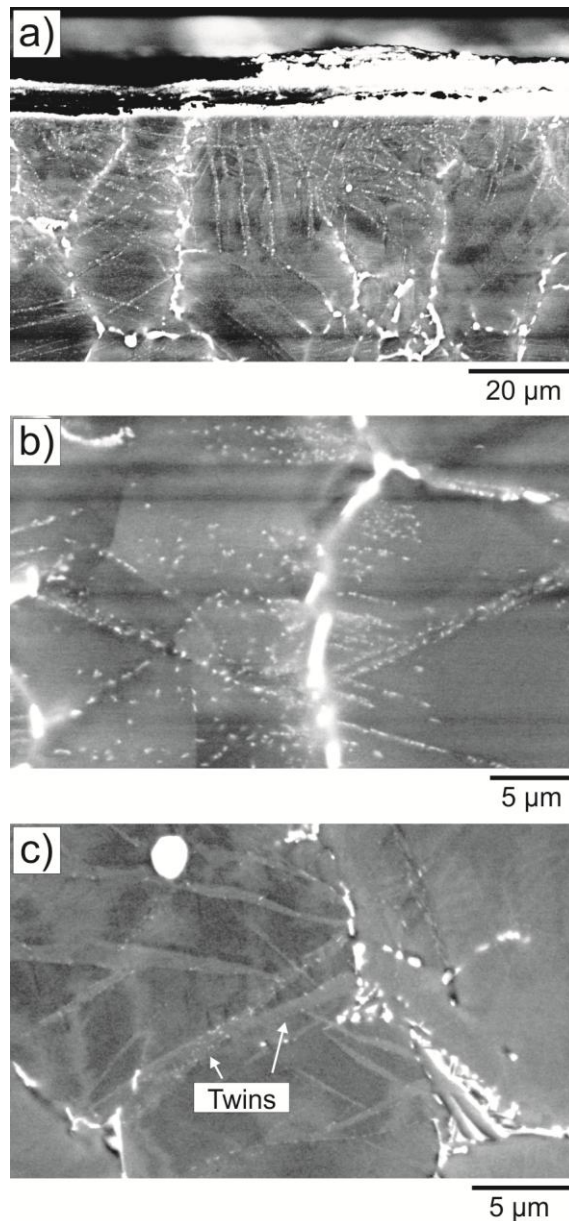
Figure 3.8: Cross-sectional backscatter electron micrographs of shot peened Ti-834 following thermal exposure at 700°C for 1800 hrs a) and b), and 600°C for 1272 hrs c). Micrographs b) and c) are high magnification images of a region within the first 50 μm of the shot peened edge.

Closer examination of the backscatter electron micrographs showed that silicides precipitated along, or very close to, the mechanical twin boundaries. The mechanical twins are visible under backscatter electron imaging as a result of electron channeling contrast and are labeled in figure 3.8c). In the deformed surface layer, twinning is not observed in every grain and it is anticipated that silicide precipitation has also occurred along slip bands (regions of high dislocation density localized to a particular slip plane).

Two possible explanations are proposed for the precipitation of silicides along twin boundaries and within regions of high dislocation density. The first is drawn from the mechanism proposed by Paton and Mahoney [43] for the increased creep resistance to Ti-Zr-Si alloys. Here, the improved creep resistance in Si bearing Ti alloys is attributed to the pinning of mobile dislocations during stage II creep by the precipitation of titanium silicides. In this study however, silicide precipitation was not observed in

tensile pre-strained samples that were subsequently exposed to elevated temperatures (circa 540°C) and it was suggested that it was necessary for a mobile dislocation to sweep through the titanium matrix and in doing so collect a Si atmosphere; rather than for diffusion of Si to a stationary dislocation to occur. i.e. the precipitation is strongly stress assisted.

Similar observations were made by Assadi whilst investigating the influence of Si and Mo on the high temperature strength of α-titanium alloys [44]. As the large amount of plastic strain introduced during shot peened may result in a driving force for metallurgical recovery during thermal exposure through a mechanism such as climb and annihilation of dislocations, it is conceivable that dislocations do become mobile and that subsequent Si clustering and ultimate silicide precipitation occurs. Whilst this assertion does not align with the observations of Paton and Mahoney [43], the greater strain imparted on the workpiece (and the slightly higher temperatures investigated) may account for observed precipitation during static exposure to elevated temperatures.

A second proposed mechanism is drawn from established theory on the heterogeneous precipitation of secondary phases in metals. As discussed previously, Ramachandra [21] reported silicides to precipitate along α' martensitc platelet boundaries during static ageing of solution heat treated and quenched Ti-834. In addition to precipitation of silicides along α' plate boundaries, Flower [42] reported the precipitation of Ti-Si silicides on <c>[0002] dislocations during ageing of Ti-1Si alloys; in contrast to the work of Paton and Mahoney [43] who showed that during subsequent ageing, Si clustering did not occur on <a>-type dislocations that were introduced through tensile pre-straining of the material. As <c+a> dislocations possess a larger burgers vector than that of <a>-type dislocations, it can be anticipated that the driving force for nucleation will be higher. It is possible that during shot peening of Ti-834, plastic strain is accommodated by <c>-component dislocations such as dislocation glide along the {10-11} plane in the <11-23> direction, resulting in an increase in available nucleation sites for silicide precipitation under static ageing conditions.

Although both mechanisms are plausible in accounting for the precipitation of silicides within the heavily cold-worked surface layer, their presence confirms that the crystal structure in Ti-834 is heavily distorted by the shot peening process; implying that diffusional processes will be accelerated during subsequent annealing.

3.3.4 *Oxygen profiles of shot peened and thermally exposed Ti-834*

The effect of surface finish on the sub-surface oxygen content is shown in the form of oxygen profiles obtained by secondary ion mass spectrometry (SIMS) in figure 3.9. Data were obtained for two surface finishes: Wire electro-discharge machined (EDM) and shot peened to 200% and 1200% coverage. Wire EDM and specimens peened to 200% coverage were exposure to laboratory air at 700°C for 1800 hrs, whilst the specimen shot peened to 1200% coverage was exposed to a temperature of 650°C for 1272 hrs.

The oxygen concentration is presented in normalized quantities, i.e. the ratio of oxygen content at a given distance from the exposed surface to the residual oxygen content of the alloy, as measure from chemical analysis at INCO test. From the oxygen profile data, it can observed that shot peening leads to an increase in the measured levels of sub-surface oxygen when compared with the wire EDM surface and increasing the shot peening coverage to 1200% further promotes the ingress of oxygen during elevated temperature exposure in Ti-834. It can also be noted that whilst the relationship between oxygen content and distance from the exposed surface may by expressed by a solution to Fick's second law for the wire EDM and 200% peening coverage samples exposed to

laboratory air at 700°C, the oxygen concentration profile for the specimen shot peened to 1200% peening coverage is close to linearity within the first 50 μm below the exposed surface, suggesting that the diffusion of oxygen within the first 50 μm has deviated from a mechanism of bulk interstitial diffusion.

Figure 3.10 shows SIMS oxygen diffusion data for shot peened and EDM Ti-834 normalized against a silicon wafer of known oxygen concentration. From this data, a semi-quantitative measurement of oxygen concentration can be made for both un-peened and peened material. Compared with the wire EDM surface finish, a 20% increase in oxygen content is observed in shot peened Ti-834. As atomic diffusion along such short circuit diffusion pathways is significantly faster than that of bulk diffusion [45], the increased sub-surface oxygen content in shot peened material can be attributed to rapid diffusion along the mechanical twin boundaries and dislocation slip bands within the plastically deformed surface layer. Enhanced diffusion kinetics of interstitial elements within a heavily cold worked surface region have also been reported by Tong *et al*, who measured accelerated nitrogen diffusion in surface mechanical attrition treated α-iron [24].

Although the results of the secondary ion mass spectrometry investigation align well with other studies [24][25], two further points of discussion that should be addressed. Firstly, it may be argued that the temperature rise during the shot peening process itself might be responsible for increased sub-surface oxygen content. Whilst adiabatic heating is likely to occur during successive impact of the shot media with the work-piece, an investigation into the shot peening of a 304L stainless steel suggested that the maximum temperature rise did not exceed 100°C [46]. Further to this, even if the low thermal conductivity of titanium lends itself to significant temperature rises during the shot peening process; it can be argued that the lack of silicide precipitation in the shot peened material prior to thermal exposure suggests that any rise in temperature is of insufficient duration to allow significant diffusion processes to occur.

A second discussion point is centered on the role of the twin boundaries in accelerating oxygen diffusion during prolonged thermal exposure. Whilst is it conceivable that pipe-diffusion oxygen will readily occur along slip bands, a theoretical twin boundary is fully coherent with its parent crystal as rotational and/or tilt symmetry exists across the mirror (K_1) plane [30][45]. In a poly-crystalline aggregate however, the shear displacement of atoms is geometrically constrained by the adjacent grains and the twin is of lenticular form to accommodate the resulting lattice strain around the mechanical twin boundary [30],.with increasing boundary curvature reducing the subsequent local lattice strain.

The mechanical twins observed in shot peened Ti-834 possess a low boundary curvature radius when compared with the twinning observed during quasi-static deformation of CP-Ti [47]. As discussed in chapter 2 , this suggests that a large degree of localized lattice strain may be present within the vicinity of the twin boundary, with the resulting lattice strain likely to be accommodated by dislocation arrays along the boundary (similar to low-angle grain boundaries). An early review of dislocations at twin interfaces has been performed by Cahn [48], where two types of twinning dislocations at twin/matrix boundaries, namely "Frank" and "Bullough" dislocations are discussed. Further to this, as the interfaces of deformation twins can present obstacles to dislocation glide [49], the multiple impact nature of the shot peening process implies that dislocation pile-up at twin interfaces will occur should the mechanical twins form early on in the peening process.
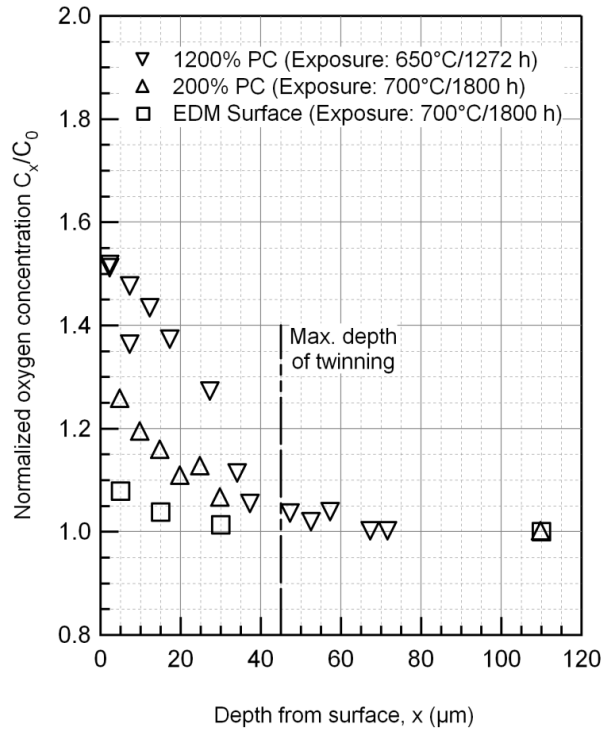
Figure 3.9: Normalized oxygen concentration profiles measured using secondary ion mass spectrometry of thermally exposed Ti-834. The influence of surface condition (EDM – electro-discharge machined; 200% PC – 200% shot peening coverage; and 1200% PC – 1200% shot peening coverage) on oxygen uptake following isothermal exposure in laboratory air is shown.
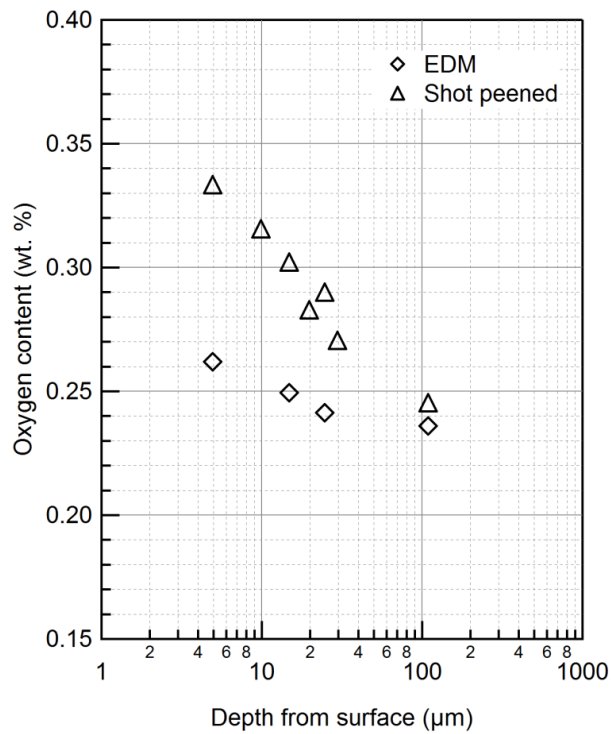
Figure 3.10: Quantitative oxygen concentration profiles of Ti-834 thermally exposed in the wire EDM and shot peened (1200% coverage) conditions at 700°C for 1800 hrs in laboratory air.

This aligns well with the work of Paton *et al* [36] who observed a high density of dislocations within {10-12} type twins during compression testing of Ti-Al binary alloys. In this case, the local rotation of the crystal structure within a twin leads to an orientation which is favourable for dislocation slip, thus leading to slip within the twinned medium and subsequent pile-up at the twin/parent interface.

Although insufficient experimental evidence has been collected to ascertain whether a high dislocation density exists adjacent to the twin interface as a result of the low boundary curvature; or whether the multiple shot impacts lead to high stress field from slip pile-up at twin boundaries, it is reasonable to argue that a high degree of lattice distortion is associated with the twin interface region. The net result of this is that the twin boundary regions are very likely to act as short circuit diffusion pathways for oxygen and their defective nature is further inferred from the concomitant precipitation of silicides during thermal exposure.

3.3.5 *High cycle fatigue results of shot peened and machined Ti-834*

Fatigue data for the Ti-834 material tested in the as-machined and shot peened conditions is presented in table 3.2 and figure 3.11 shows the constant life endurance limits for machined and shot peened Ti-834 following thermal exposure in air at 650°C. Data for the fatigue endurance limits were collected using the staircase loading method and calculated using equation 2.1 in section 3.2. For specimens tested in the as-machined and shot peened conditions, there is negligible difference in the constant life fatigue endurance limit, with the calculated endurance stress range being in the region of 270 MPa for the two surface conditions. Both the room temperature tensile yield strength and the high cycle fatigue endurance limit of Ti-834 as measured in this study are lower than those reported by other researchers [28] and the manufacturer's datasheet.

Table 3.2: High cycle fatigue properties of the Ti-834 specimens in the shot peened and as-machined conditions. The constant life fatigue endurance limit, $\Delta\sigma_{ES}$, was calculated from equation (1).

Specimen	Surface condition	$\Delta\sigma_{PS}$ (MPa)	$\Delta\sigma_{F}$ (MPa)	N_f	$\Delta\sigma_{ES}$ (MPa)
1	Machined	270	315	9.30E+04	270.04
2	Machined	270	315	3.50E+06	271.58
3	Machined	270	315	2.90E+06	271.31
4	Machined	270	315	9.40E+05	270.42
5	Peened 200%	270	315	2.60E+06	271.17
6	Peened 200%	270	315	3.20E+06	271.44
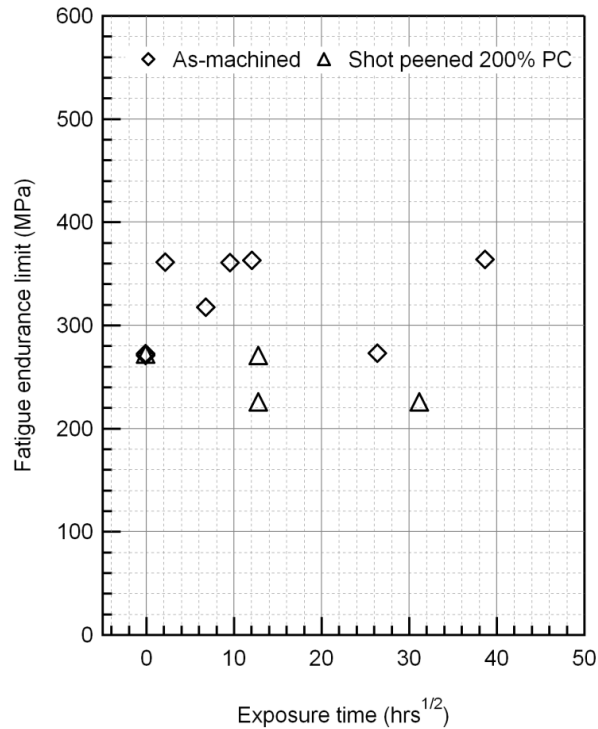
Figure 3.11: Graph showing the constant life fatigue endurance limits for machined and shot peened (200% Peening coverage) Ti-834 following thermal exposure in air at 650°C. The constant life endurance limit was calculated from equation (1) using a staircase loading method [29]. Fatigue testing was performed at a stress ratio of R = 0.1.

Figure 3.12 shows the fracture surface of a Ti-834 fatigue specimen tested in the as-machined condition. Three regions of distinct fracture surface morphologies were observed and these are labeled A, B and C. In region A, clusters of similarly orientated facets corresponding to the size and shape of the primary α grains are present both within the bulk of the material and may be observed to intersect with the specimen surface. Region B shows extensive river line markings illustrating the local direction of crack growth the ductile fracture area resulting from final overload failure is shown in region C.
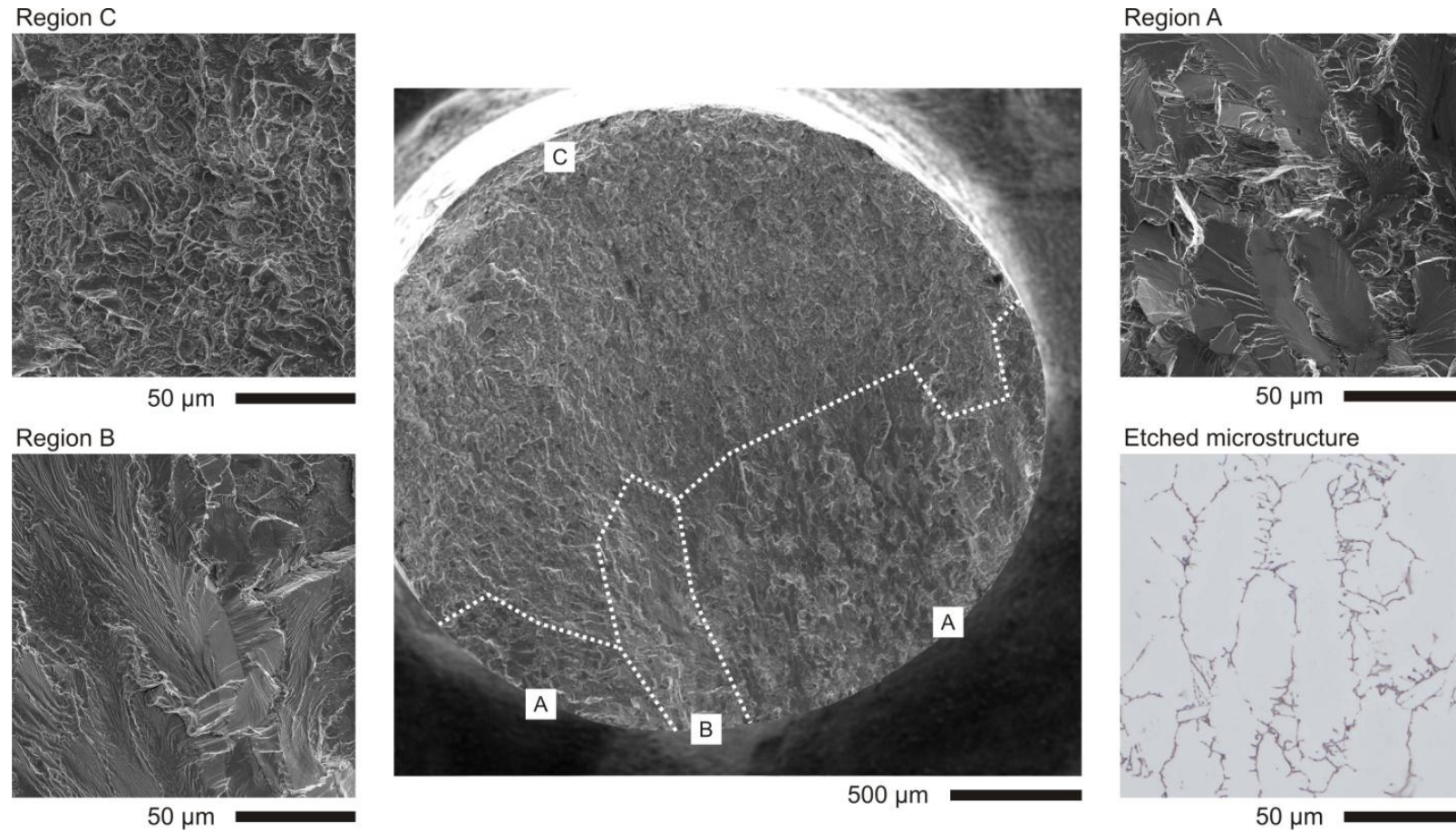
Figure 3.12: Fracture surface of Ti-834 fatigue specimen tested in the as-machined condition. Higher magnification secondary electron micrographs of three regions labeled A, B and C in which different fracture surface morphologies are observed are shown. The etched microstructure of the received Ti-834 material is shown for comparison of size of form of microstructural features.

Although no definitive fatigue crack initiation site could be indentified in the specimen tested in the as-machined condition, the presence of closely aligned facets in region A suggests that multiple subsurface crack initiation may have occurred within that area, with crack growth continuing along cleavage planes through adjacent α-grains that have a similar crystal orientation with respect to the tensile axis.

Interestingly, such faceting is normally associated with cold-dwell type fatigue failures in near-α alloys such as Ti-6242 [50], although similar faceting has been observed during high cycle fatigue testing of Ti-6Al-4V with R > 0 [51]. It is notable that the region of similarly aligned facets is relatively large when compared against the cross-sectional area of the fatigue specimen, with the heavily faceted area broadly corresponding in size to the regions of sharp microtextural heterogeneities that have been reported in Ti-834 by Germain et al [27] and in Ti-6Al-4V by Bantounas et al [52]. It is therefore plausible that the mechanism of fatigue failure in this case is strongly controlled by the multiple initiation of microcracks within a cluster of alpha crystals favourably orientated for slip along either the {0002} basal or {10-10} prismatic planes, thus resulting in a rapid reduction in effective cross-sectional area of the fatigue specimen. This, in conjunction with the lack of strengthening modes which occur during the 700°C ageing step in fully heat treated Ti-834 material, provides a reasonable explanation for the lower than reported high cycle fatigue endurance limit for the Ti-834 billet investigated in this study.

Whilst it may be rightly argued that the lower fatigue limits may be associated with surface condition, the identical endurance limits for both machined and shot peened specimens suggest that metallurgical factors, rather than surface effects are more prominent in controlling fatigue life in the non-thermally exposed test condition.

In the case of the machined specimens, short thermal exposure durations lead to an initial increase in the fatigue endurance limit. This trend is not anticipated based on the assertion that surface oxygen contamination is deleterious to the fatigue properties of titanium alloys [16][53]. It would be expected that even short exposure times to air would lower the fatigue limit of the alloy. This discrepancy may firstly be due to the relaxation of the residual stresses introduced during the machining operation [54]. Secondly, it is credible that for short exposure times, the limited diffusion of oxygen into the specimen surface leads to a local strengthening effect without a significant loss in ductility, therefore suppressing fatigue crack initiation at the surface. This has the effect of raising the high cycle fatigue endurance limit and effectively "flattening" the S-N curve.

Further support for this argument can be drawn from a recent study investigating the effect of oxygen boost diffusion on the fatigue properties of Ti-6Al-4V [55]. In contrast to a study by Dong et al [53], who reported deterioration in high cycle fatigue life following oxygen boost diffusion treatment of Ti-6Al-4V, Omidbaksh et al [55] measured an increase in the rotary bending high cycle fatigue life of a Ti-4Al-2V alloy following boost diffusion treatment. In the same study, oxygen boost diffusion slightly reduced the number of cycles to failure at higher stresses, suggesting that an oxygen enriched surface layer is deleterious to fatigue properties when testing in the low-cycle regime. With increasing surface oxygen levels however, the fracture toughness is significantly lowered reduced defect sensitivity will lead to a lowering of fatigue initiation lives.
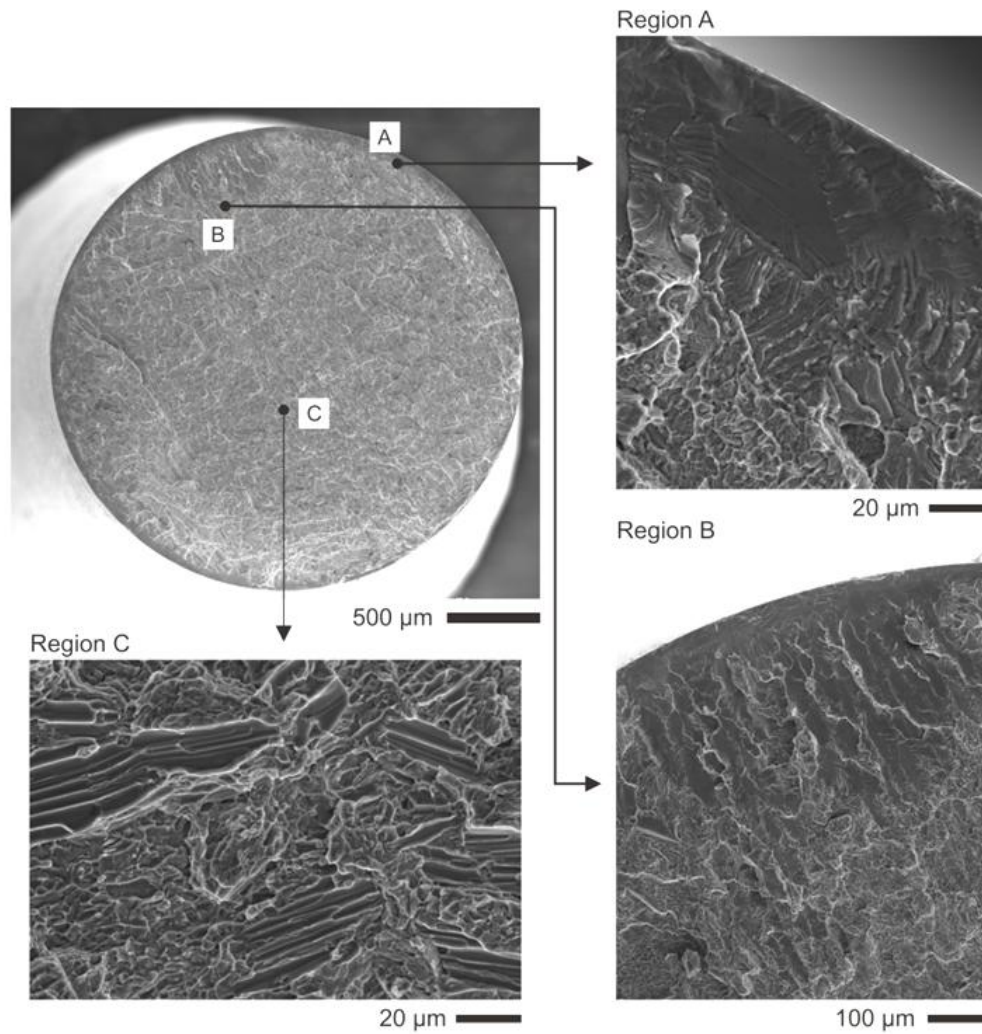
Figure 3.13: Fracture surface of a machined Ti-834 fatigue specimen tested following exposure to laboratory air for 1500 hrs at 650°C. Higher magnification micrographs of the areas labeled A, B and C are also shown.
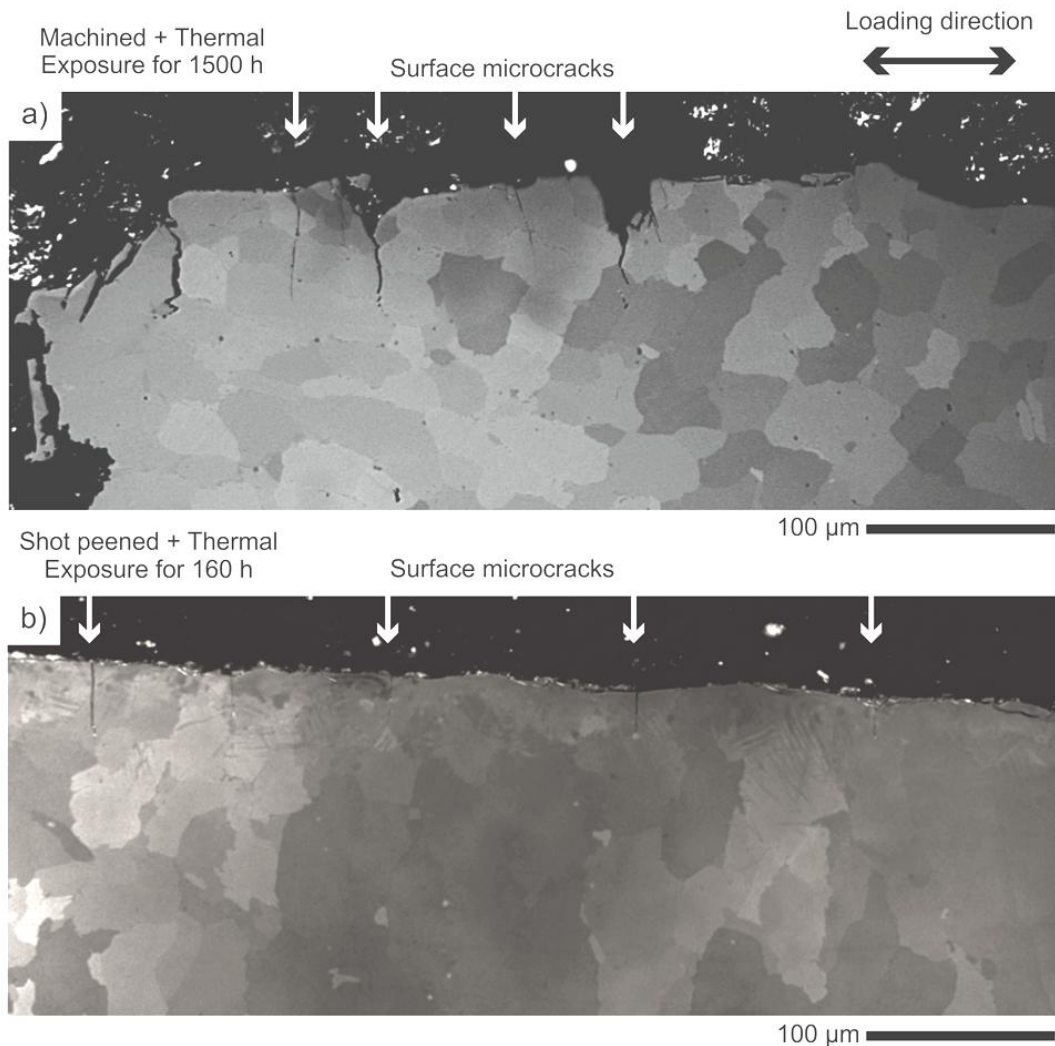
Figure 3.14: Cross-section polarised light micrographs of a) machined and b) shot peened fatigue specimens tested following thermal exposure at 650°C for 1500 h and 160 h respectively.

Fractography of the fatigue specimen tested following thermal exposure for 1500 hrs (figure 3.13) shows circumferential faceting to a depth of approximately 50 µm below the surface (Region A in figure 3.13). Whilst no definitive crack initiation site can be identified, evidence of crack penetration into the substrate in the form of closely aligned facets can be seen in regions B and B'. Evidence of extensive fluting within the ductile overload region can be seen in region C. The area density of flutes is greater in the thermally exposed specimen suggesting that slip has become more planar in nature within the specimen bulk. This is likely to be a resultant effect of short range ordering of aluminium to form α_2 precipitates during thermal exposure.

A further observation is that surface microcracks can be observed close to the fracture surface in the cross-sectional light micrograph shown in figure 3.14a). Surface microcracking within the specimen gauge was not observed in the machined fatigue specimens thermally exposed to air for shorter durations. It is therefore apparent that a threshold alternating or mean stress to initiate surface microcracks within the oxygen enriched zone exists, and that this stress decreases with increasing thermal exposure time in air.

Shot peening results in a lowering of the fatigue endurance limit following comparatively short thermal exposure times as is shown in figure 3.11. Figure 3.14b) is a cross-section light micrograph through the gauge length of the shot peened fatigue specimen following thermal exposure for 160 hrs at 650°C. Small microcracks can be observed within the surface region and penetrate to a depth of approximately 50 μm. The distribution of the surface microcracks is fairly uniform, with an average crack spacing of 50 μm. This result demonstrates that surface microcracks are able to form more readily in shot peened material during fatigue loading following thermal exposure in air.

Whether a relationship exists between the relative ease in which surface microcracks form during fatigue loading and the final failure mode are directly linked requires further investigation. The stress ratio of R = 0.1 employed in the course of this testing programme would encourage subsurface/microstructural mechanisms to control fatigue failure, whilst fully reversed loading (R = -1) would generally favour surface crack initiation [7]. Nevertheless, the experimental evidence suggests that peening promotes surface crack initiation in thermally exposed Ti-834 and it is therefore important to consider the effects of surface treatment on the fatigue properties of such high temperature titanium alloys.

3.4   Chapter conclusions

An investigation into the effect of shot peening on the microstructural response, oxygen uptake and high-cycle fatigue properties of the near-α titanium alloy Ti-834 has been undertaken. Microstructural characterisation of the deformation microstructures below the shot peened surface has been performed using light optical microscopy, backscatter scanning electron microscopy and electron backscatter diffraction. Secondary ion mass spectrometry has been employed to assess the effect of prior shot peening on the oxygen diffusion kinetics in Ti-834 following thermal exposure in air, and preliminary high cycle fatigue testing has been undertaken to investigate the role of shot peening on surface crack initiation. The results and key discussion points of this chapter are summarized as follows:

1. Deformation of Ti-834 during quasi-static tensile testing proceeds via dislocation glide along slip planes and directions, and no evidence of mechanical twinning could be identified. During shot peening, {10-12} tensile type mechanical twin are observed within the first 50 μm from the peened surface. The density of mechanical twins increases with increasing peening coverage, but increasing peening coverage does not lead to commensurate increase in depth to which mechanical twinning occurs.
2. The volume fraction of twinning below the shot peened surface of Ti-834 is heterogeneous; with certain regions showing and increased prevalence for deformation via mechanical twinning.
3. Secondary ion mass spectrometry has shown that shot peening leads to an increase in near-surface oxygen content following thermal exposure in air when compared with wire EDM specimens. The increased levels of oxygen content in shot peened material are accompanied by the precipitation of silicides (likely to by S_2 type) along the mechanical twin boundaries and in regions of high dislocation density. The proposed mechanism which accommodates increased

oxygen uptake in shot peened specimens is the introduction of short-circuit diffusion pathways through the cold working process.

4. Mechanical testing shows that shot peening does not increase the high cycle fatigue life of Ti-834. Evidence exists however, that a decrease in room temperature fatigue performance occurs in shot peened material following prolonged thermal exposure in air at 650°C and shot peening promotes surface microcracking of Ti-834 following long-term thermal exposure in air.

The observed phenomena reported in this chapter suggest that shot peening may be deleterious to the mechanical integrity of components manufactured from Ti-834, although whether such an effect is translated across other alloys of the near-α class such as Ti-6242Si requires further investigation. Nevertheless, these research finding have demonstrated that a metallographic approach can provide a mechanistic understanding into the effects of surface treatment on subsequent microstructural stability and mechanical properties of titanium alloys such as Ti-834.

References

[1] P. J. Withers, Reports on Progress in Physics 70 (2007) 2211 – 2264

[2] R. K. Nalla, I. Altenberger, U. Noster *et al*, Materials Science and Engineering A 355 (2003) 216 – 230

[3] R. Fathallah, G. Inglebert, L. Castex, Materials Science and Technology 14 (1998) 631 – 639

[4] A. M. Korsunsky, Journal of Strain. Analysis for Engineering Design 40 (2005) 817 – 834

[5] M. A. S. Torres, H. J. C. Voorwald, International Journal of Fatigue 24 (2002) 877 – 886

[6] H. Luong, M. R. Hill, Materials Science and Engineering A 527 (2010) 699 – 707

[7] L. Wagner, C. Gerdes, G. Lütjering, in: G. Lütjering, U. Zwicker, W. Bunk (Eds.), Titanium: Science and Technology, Oberursel, Germany, 1984, pp.2147-2154.

[8] L. Wagner, Materials Science and Engineering A (1999) 210 – 216

[9] J. Lindemann, C. Buque, F. Appel, Acta Materialia 54 (2006) 1155 – 1164

[10] O. Vöhringer, in: H. Wohlfahrt, R. Kopp, O. Vöhringer (Eds.), Proceedings of the 3rd International Conference on Shot Peening (ICSP3), Garmish-Partenkirchen, Germany, DGM Informationsgesellschaft Verlag, Oberursel, pp. 185–204.

[11] R. C. McClung, Fatigue and Fracture of Engineering Materials and Structures 30 (2007) 173 – 205

[12] R. John, D. J. Buchanan, S. K. Jha *et al*, Scripta Materialia 61 (2009) 343 – 346

[13] C.E. Shamblen, T.K. Redden, in: R.I. Jaffe, N.E. Promisel (Eds.), The Science, Technology and Application of Titanium, London, UK, 1970, pp.199-208.

[14] S. Hardt, H. H. Maier, H. –J. Christ, International Journal of Fatigue 21 (1999) 779 – 789

[15] C. Leyens, M. Peters, D. Weinman *et al*, Metallurgical and Materials Transactions A 27 (1996) 1709 – 1717

[16] H. Fukai, H. Iizumi, K. Minakawa *et al*, ISIJ International 45 (2005) 133 – 141

[17] A. Madsen, E. Andrieu, H. Ghonem, Materials Science and Engineering A 171 (1993) 191 – 197

[18] A. P. Woodfield, P. J. Postans, M. H. Loretto *et al*, Acta Materialia 36 (1988) 507 – 515

[19] C. Ramachandra and V. Singh, Metallurgical Transactions A 16 (1985) 227 – 231

[20] P.S. Bate, P.L. Blackwell, J.W. Brooks, in: P. Lacomb, R. Tricot, G. Béranger (Eds.), Sixth World Conference on Titanium, Cannes, France, 1988, pp.287-292.

[21] C. Ramachandra, A. K. Singh, G. M. K. Sarma, Metallurgical Transactions A 24 (1993) 1273 – 1280

[22] D. Eylon, S. Fujishiro, P. J. Postans *et al*, Journal of Metals 36 (1984) 55 – 62

[23] C. Zhong, L. Liu, Y. Wu *et al*, Materials Letters 64 (2010) 1407 – 1409

[24] W. P. Tong, N. R. Tao, Z. B. Wang *et al*, Science 299 (2003) 686 – 688

[25] D. F. Neal, in: G. Lütjering, U. Zwicker, W. Bunk (Eds.), Titanium Science and Technology, Oberursel, Germany, pp. 2419-2424.

[26] R. S. Bellows, S. Muju and T. Nicholas, International Journal of Fatigue 21 (1999) 687 – 697

[27] L. Germain, N. Gey, M. Humbert *et al*, Acta Materialia 53 (2005) 3535 – 3543

[28] M. T. Whittaker, W. J. Evans, International Journal of Fatigue 31 (2009) 1751 – 1757

[29] J. R. Cho, D. Dye, K. T. Conlon *et al*, Acta Materialia 50 (2002) 4847 – 4864

[30] E. O. Hall, Twinning and Diffusionless Transformation in Metals and Alloys, (Butterworths Scientific Publications, London, 1954) pp.68-78

[31] P. G. Partridge, International Materials Reviews 12 (1969) 169 – 194

[32] A. A. Salem, S. R. Kalindini and R. D. Doherty, Acta Materialia 51 (2003) 4225 – 4237

[33] Y.B. Chun, S.H. Yu, S.L. Semiatin *et al*, Mater. Sci. Eng. A 398 (2005) 209 – 219

[34] D. R. Chichili, K. T. Ramesh, K. J. Hemker, Acta Materialia 46 (1998) 1025 – 1043

[35] N. E. Paton J. C. Williams, G P. Rauscher, in: R. I. Jaffee and H. M. Burte (Eds.), Titanium: Science and Technology, Plenum Press, 1973, pp.1049-1069

[36] J. C. Williams, R. G. Baggerly and N. E. Paton, Metallurgical and Materials Transactions A 53 (2002) 837 - 850

[37] E. Metzbower, Metallurgical Transactions 2 (1971) 3099 – 3103

[38] M. A. Meyers, O. Vöhringer, V. A. Lubarda, Acta Materialia 49 (2001) 4025 – 4039

[39] G. T Gray III, Journal de Physique IV 7 (1997) C3–423 – C3–428

[40] G. T Gray III, P. S. Follansbee, in: P. Lacomb, R. Tricot, G. Béranger (Eds.), Sixth World Conference on Titanium, Cannes, France, 1988, pp.117-127.

[41] J.W. Christian, S. Mahajan, Progress in Materials Science 39 (1995) 1 – 157

[42] H. M. Flower, P. R. Swann, D. R. F. West, Metall. Trans. 2 (1971) 3289 – 3297

[43] N.E. Paton, M.W. Mahoney, Metallurgical Transactions A 7 (1976) 1685 – 1694

[44] A. T. K. Assadi (1977) *The Influence of Silicon and Molybdenum on the High Temperature Strength of some Titanium Alloys based on the Alpha Phase*, PhD Thesis, Imperial College of Science and Technology

[45] D. Porter and K. Easterling, Phase Transformations in Metals and Alloys, 2nd Edition, Taylor and Francis Group, FL, 1992.

[46] S. Rouquette, E. Rouhaud, H. Pron *et al*, Proceedings of the 9th International Conference on Shot Peening, ICSP9, Paris, France, 6th -9th September 2005, pp.113-118

[47] A. A. Salem, S. R. Kalidindi, R. Doherty, Scripta Materialia 46 (2002) 419 – 423

[48] R. W. Cahn, in: R. E. Reed-Hill, J. P. Hirth, H. C. Rogers (Eds.), Deformation Twinning, Gordan and Breach Science Publishers, New York, 1964, pp.1-28

[49] R. W. Armstrong, in: R. E. Reed-Hill, J. P. Hirth, H. C. Rogers (Eds.), Deformation Twinning, Gordan and Breach Science Publishers, New York, 1964, pp.356-377

[50] V. Sinha, M. J. Mills, J. C. Williams, Metallurgical and Materials Transactions A 35 (2004) 3141 – 3248

[51] I. Bantounas, D. Dye, T. C. Lindley, Acta Materialia 58 (2010) 3908 – 3918

[52] I. Bantounas, T. C. Lindley, D. Rugg, D. Dye, Acta Materialia 55 (2007) 5655 – 5665

[53] H. Dong, X. Y. Li, Materials Science and Engineering A 280 (2000) 303 – 310

[54] B. R. Sridhar, G. Devananda, K. Ramachandra *et al*, Journal of Materials Processing Technology 139 (2003) 628 – 634

[55] F. Omidbakhsha, A.R. Ebrahimia, S.H. Mousavia *et al,* Surf. Coat. Technol. 205 (2011) 2954 – 1963

Chapter 4

Deformation mechanisms during shot peening: The role of chemistry, temperature and microtexture

4.1   Introduction

The general effect of shot peening on the microstructural stability and fatigue endurance limit of Ti-834 following prolonged thermal exposure has been addressed in chapter three; with little overall emphasis placed on explaining the metallurgical mechanisms through which subsurface plastic strain is accommodated. Whilst the study of deformation mode in titanium alloys as a function of temperature and alloy chemistry [1], texture [2][3] and strain rate [4][5] under controlled loading conditions has been the subject of extensive research, it is pertinent to investigate whether the well established fundamentals of plastic deformation are applicable to industrial surface engineering processes such as shot peening.

In chapter three, it was observed that spatial distribution of mechanical twins in shot peening Ti-834 was heterogeneous, suggesting that competing processes are in operation to accommodate plastic strain within the deformed surface layer. The competing mechanisms of twinning versus slip in alpha-titanium have been extensively studied and advances in electron backscatter diffraction techniques have facilitated attempts to predict deformation mode during loading using Schmid factor analysis. For example, during room temperature plane strain compression testing of CP-Ti, Battaini *et al* [2] have shown that a strong crystal orientation effect exists on the mode of deformation, with the activity of {11-22} twinning controlled by the frequency of *c*-axis close to the compression direction. The orientation dependency on deformation mode is not limited to commercial purity titanium alloys, as amply demonstrated by Semiatin and Bieler [3][6]. During hot compression testing of hot-rolled Ti-6Al-4V plate, with peak flow stress being controlled by the direction of compression test with respect to the rolling direction. Subsequent, electron backscatter diffraction analysis showed that where high Schmid factors for prism-<*a*> and basal-<*a*> slip exist, macro shear bands developed during sub-transus hot working of Ti-6Al-4V [6]. More recently, Prakash *et al* [7] have hypothesized that "whole grain" twinning can occur in Ti-6Al-4V during room temperature compression testing.

The role of testing temperature and alloy chemistry is also reported to have a pronounced effect on the deformation mode of alpha titanium. Through investigating the deformation behaviour of Ti-Al single crystals under simple compression, Williams *et al* [1] observed that the propensity for mechanical twinning in single crystals loaded parallel to the *c*-axis decreased with increasing aluminium content, with pyramidal-$<c+a>$ becoming the dominant deformation mode at higher aluminium concentrations. In the same study, it was found that increasing the temperature of compression testing led to a decrease in the critical resolved shear stress (CRSS) for basal-$<a>$ and prism-$<a>$ slip, whilst increasing aluminium content lead to a concomitant rise in the respective CRSS values for the two slip modes.

The importance of alloy chemistry, strain-rate and temperature on deformation mode is not limited to titanium and its alloys. During testing of high and low purity Zirconium, Kaschner and Gray [8] observed an increased incidence for mechanical twinning in samples tested at high strain-rates (3.5×10^3 s^{-1}) at room temperatures and quasi-statically at -196°C. Similar observations have been made for rolled Hafnium plate by Cerrata and Gray [9] and the importance of loading direction with respect to the average *c*-axis orientation was highlighted. Variations in both the yield point and the strain hardening behaviour were observed in specimens loaded parallel to the plate normal (through thickness) and perpendicular to the plate normal (in-plane). The predominance for twinning also increased at lower temperatures. The effect of compression testing temperature also has a pronounced effect of deformation mode in Magnesium alloys [10]. Barnett *et al* [10] observed a transition from twinning to slip dominated plastic flow in an Mg-3Al-1Zn alloy during compression testing in the temperature range ambient to 200°C.

As experimental studies have provided strong evidence pertaining to the role of temperature, chemistry and microtexture on deformation mode during controlled deformation testing such as uni-axial compression and plane-strain compression, the aim of this chapter is to investigate whether such variables control deformation mode during an industrial process. In order to determine the effects of alloy chemistry and temperature on deformation mode during shot peening, trials were undertake at Metal Improvement Company, Derby, UK on commercial purity titanium (CP-Ti), Ti-834 and Ti-6Al-4V. Coupons of the respective alloys were either cooled to cryogenic temperatures or heated in a furnace prior to shot peening. Reference material was also shot peened at room temperature. To supplement the shot peening trials and investigate the dependency of deformation mode of microtexture, rolled plate of Ti-6Al-4V was also shot peened to similar process conditions at room temperature.

The analysis provided in this chapter is therefore divided into two sections; the first considers the effect of alloy chemistry and temperature on deformation mode, whilst the second focuses on the effect of underlying microtexture in Ti-6Al-4V. It may seem convenient to treat the crystal orientation effects as independent from temperature and chemistry, but as the Ti-834 billet investigated in the peening trials study possesses a large degree of microtexture it is anticipated that fully separating the competing factors would be extremely difficult. In view of this the analysis of results is divided into two parts, but the discussion will attempt to address the preponderance for mechanical twinning during shot peening of titanium as a whole.

4.2 Experimental methods

4.2.1 *Materials*

For the shot peening trials to investigate the effect of temperature and chemistry on the mechanical response of titanium alloys, rod-rolled CP-Ti (ASTM-II) and forged billet of Ti-834 and Ti-6Al-4V were supplied by TIMET UK. Testing was performed on the same billet of Ti-834 that was investigated in chapter three and the chemical composition is provided in section 3.2.1. Chemical analysis was not performed on the CP-Ti or Ti-6Al-4V material. The rolled Ti-6Al-4V plate used in the second part of this study was supplied by Rolls-Royce, Derby, UK. Information pertaining to the specific processing route of the material was not provided.
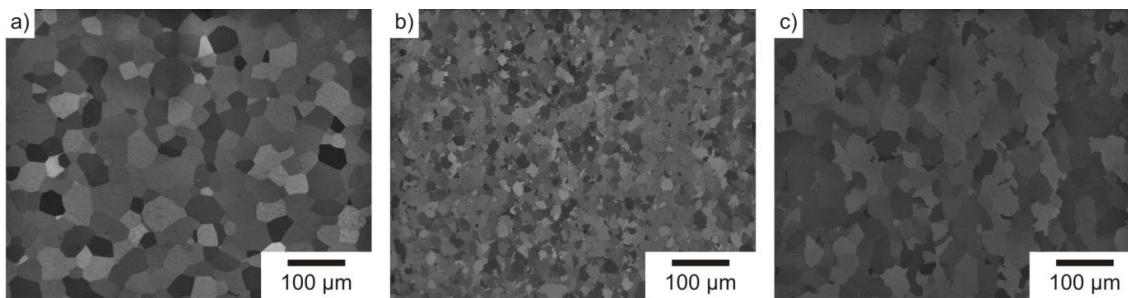
Figure 4.1: Starting microstructures of the CP-Ti a), Ti-6Al-4V b) and Ti-834 c) alloys studied during the shot peening trials (polarized light).

The starting microstructures of the three alloys used for the shot peening trials are shown in figure 4.1. The CP-Ti alloy was processed below the beta-transus and the microstructure is therefore comprised of equiaxed alpha grains that result from the recrystallisation step. The grain size of the Ti-834 material is comparable to that of CP-Ti, although the primary alpha grains are somewhat elongated and posses an aspect ratio slightly higher than 1. Nevertheless, the respective microstructures are of sufficient similarity to obtain a meaningful comparison between chemistry and the mechanical response of the two titanium alloys during shot peening. A finer grain size was present in the forged Ti-6Al-4V material when compared with CP-Ti and Ti-834 however, with an equiaxed grain size of approximately 20 μm. To prepare the test material for shot peening, 10 mm thick coupons of Ti-834 and Ti-6Al-4V were electro-discharged machined from the wrought product. In the case of rod-rolled CP-Ti bar, 10 mm thick coupons were sectioned from the using a silicon carbide cut-off wheel.

The Ti-6Al-4V plate material used to investigate crystal orientation effects on deformation mode and strain localisation during shot peening was processed above the beta-transus. Following super-transus processing, the material was slow cooled to yield a fully transformed microstructure consisting of coarse secondary alpha laths. The starting microstructure is shown in figure 4.2 and regions of sharp textural heterogeneities (or macrozones) can be observed under polarized light (figure 4.2a)).
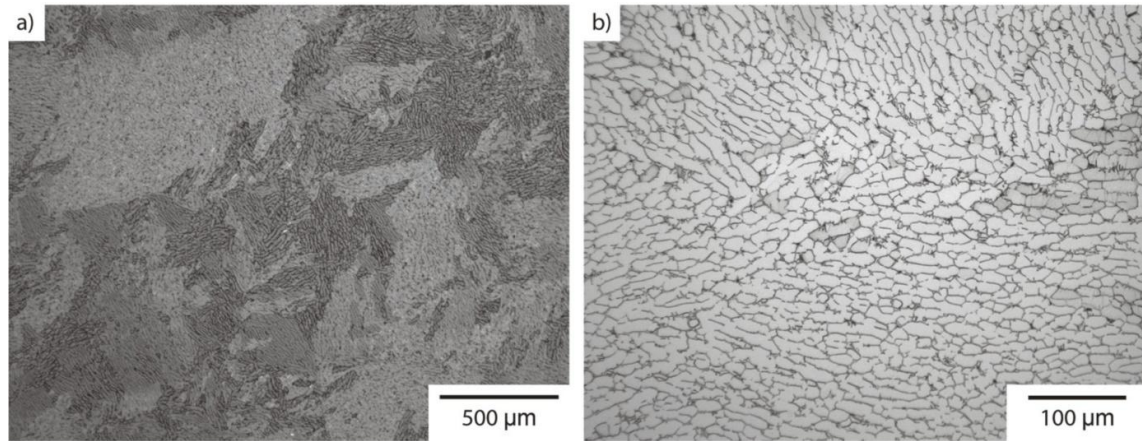
Figure 4.2: Starting microstructures of the rolled Ti-6Al-4V plate used to investigate the effect of microtexture on deformation mode and strain localisation during shot peening. A low magnification polarized light micrograph showing regions of sharp microtexture is given in a) and a high magnification micrograph of the etched microstructure is shown in b)

4.2.2 *Shot peening*

Trials to investigate the effect of workpiece temperature on deformation mode during shot peening were performed at Metal Improvement Company, Derby, UK. Coupons of Ti-834 and CP-Ti were shot peened to 200% coverage to 9A Almen target intensity at cryogenic temperature, room temperature and 270°C. To achieve cryogenic temperatures, coupons were soaked in liquid nitrogen for 15 minutes prior to the shot peening process. Following removal from the liquid nitrogen bath, specimens were clamped in a holding fixture and shot peened. Precise control of temperatures was not achieved and therefore it can only be estimated that peening occurred at a workpiece temperature in the region of -196°C.

More control of temperature was achieved in the heated samples however. Specimens were heated for 30 minutes at 270°C ($\pm$ 5°C) in a small chamber furnace that was located on-site and the temperature inside the furnace at the same elevation as the shot peening coupon was monitored using a k-type thermocouple. Figure 3 a) is an engineering drawing of the specialist fixture designed to clamp the heated titanium coupons during the peening process and figure 4.3b) is a photograph of the specimen holding fixture and clamp. The assembly was designed such that both the workpiece coupons and holding fixture could be placed in a chamber furnace and heated to required temperature. This was necessary in order to minimise the time delay between removal from the furnace and the start of the shot peening process. The time between furnace removal and start of the peening operation was approximately 15 seconds. As peening was only performed to 200% coverage, the duration of the process was less than 20 seconds. It is anticipated however, that some heating or cooling of the workpiece coupons occurred during the whole operation and the target peening temperatures are therefore referred to as approximate ones during the subsequent analysis.

Rolled Ti-6Al-4V plate was shot peened to 1200% coverage at 9A Almen intensity at Metal Improvement Company using R32 steel shot. The peening process for the Ti-6Al-4V plate was performed separately to the peening trials, which investigated the effect of allow chemistry and work-piece temperature. In regard to the wrought processing condition of the Ti-6Al-4V plate, the peening direction (direction of the shot stream) was parallel to the through thickness direction.

4.2.3 *Microstructural characterisation*

Following shot peening, all specimens were sectioned parallel to the peening direction in order to examine the near-surface microstructure in cross-section. Metallography specimens were ground using water lubricated SiC papers with 9 μm diamond suspension employed for the fine grinding step. Final polishing of the specimens was performed using colloidal silica suspension. Microstructural analysis was performed through light optical microscopy and quantitative crystallographic data was acquired using electron backscatter diffraction. Post-processing of the EBSD data was undertaken using HKL Channel-5 software. To investigate the subsurface hardening resulting from shot peening, microhardness data was collected using a load range 0.05 – 0.2 Kg and a dwell of 15 seconds.
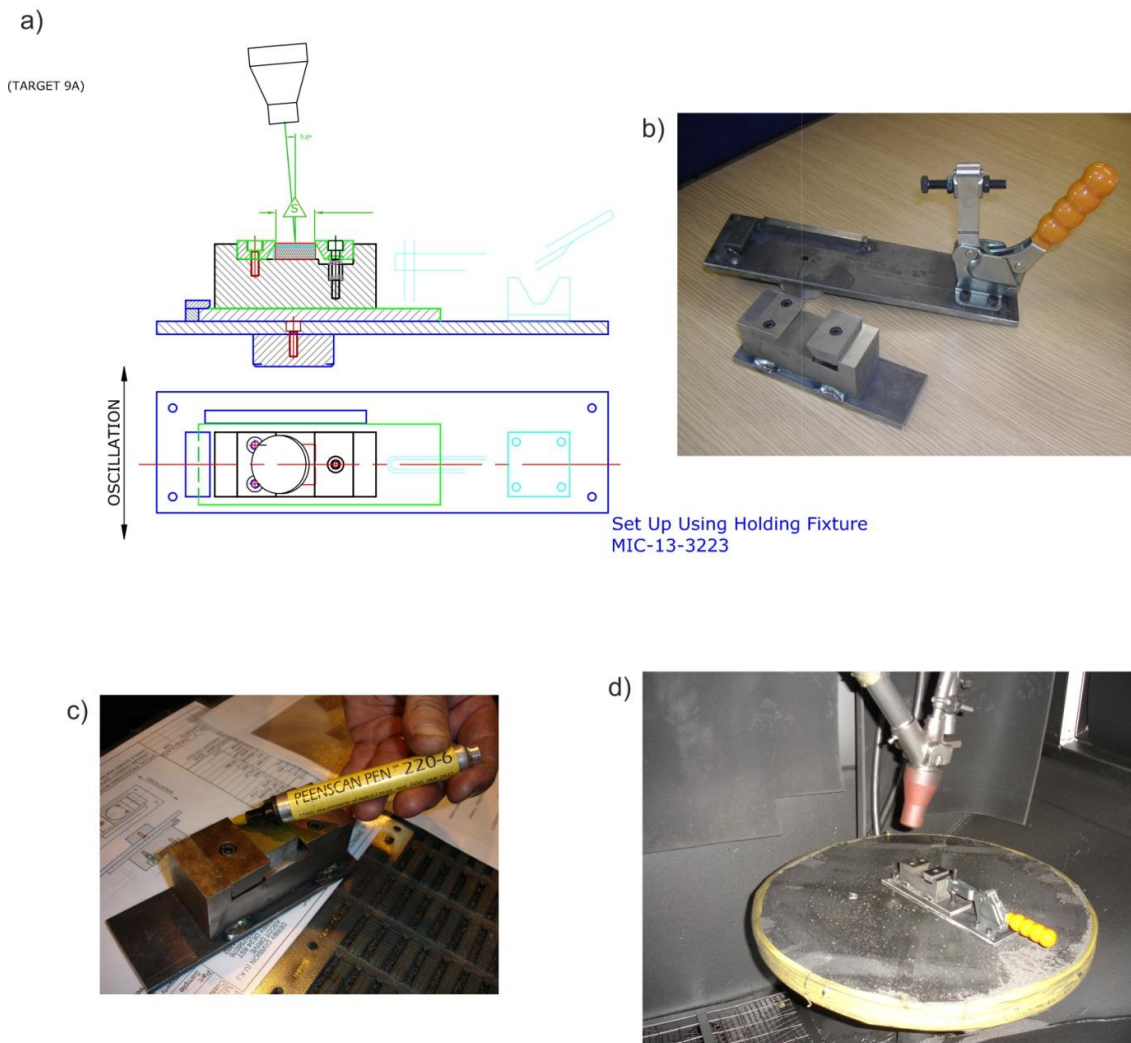
Figure 4.3: a) Engineering drawing of the specimen holding fixture and clamp assembly employed in the shot peening trials to investigate the effect of workpiece temperature. The corresponding photograph of the two assembly components is shown in b). Photographs of the workpiece within the clamping assembly and within the shot peening chamber are given in c) and d) respectively.

4.3 Results section 1: The effect of alloy chemistry and workpiece temperature

Cross-sectional polarized light micrographs of CP-Ti, Ti-6Al-4V and Ti-834 are shown in figures 4.4 and 4.5. Lower magnification photo-micrographs are given in figure 4 and higher magnifications are presented in figure 5. Mechanical twins can be observed in all specimens although their presence is considerably more pronounced in CP-Ti and figure 4.6 shows microhardness data and twin density measurements for the three alloys. In the case of CP-Ti, a strong microstructural gradient exists below the shot peened surface and this is reflected in the variation in microhardness profiles. Microhardness profiles were obtained at three individual locations and the whole dataset is presented in figure 4.6.

The largest degree of subsurface hardening occurs during shot peening of CP-Ti at 280°C, whilst the least occurs following shot peening at cryogenic temperatures. An increase in the depth of subsurface hardening is accompanied by a measured increase in twin linear fraction, with the maximum depth to which twinning occurs increasing with workpiece temperature. In reference to figures 4.4 and 4.5, shot peening of CP-Ti leads to an extremely fine grain structure immediately below the peened surface, followed by transition region where the twin density decreases with increasing distance. Such a microstructural gradient (i.e. twin density gradient) has been observed by Shaw *et al* [11] in nickel alloys following similar severe surface deformation processes.

The light micrographs in figures 4.4 and 4.5 and the microhardness data (figure 4.6) suggest that the effect of the workpiece temperature on the subsurface deformation microstructures is far less pronounced in Ti-6Al-4V and Ti-834. From the microhardness data, it is apparent that negligible subsurface hardening has occurred in both Ti-6Al-4V and Ti-834 at the temperatures investigated. This is likely to result from the limitations in spatial resolution that is attainable using the microhardness technique. Mechanical twinning can be observed in both Ti-6Al-4V and Ti-834 from the polarized light micrographs in figure 4.5, although the maximum depth to which twinning occurs is approximately 50 μm, which is somewhat less than in CP-Ti.

The spatial resolution of the microhardness equipment employed in this study is within the region of 30-50 μm and it would therefore prove difficult to detect any appreciable surface hardening. In addition to this, a large fluctuation in bulk hardness can be observed in both Ti-6Al-4V and Ti-834, when compared with the more stable bulk hardness profile measure in CP-Ti. It is therefore possible that any surface hardening resulting from the shot peening process is lost within the noise. Whilst no evidence has been sought in this study, it is plausible that the noise in the bulk hardness is attributable to localised microtextural gradients within the Ti-834 and Ti-6Al-4V material, and some evidence of microtexture in the supplied Ti-6Al-4V can be seen from the polarized light micrograph in figure 4.1b). Further to this, as discussed in chapter 3, sharp texture heterogeneities have been reported in Ti-834 [12].
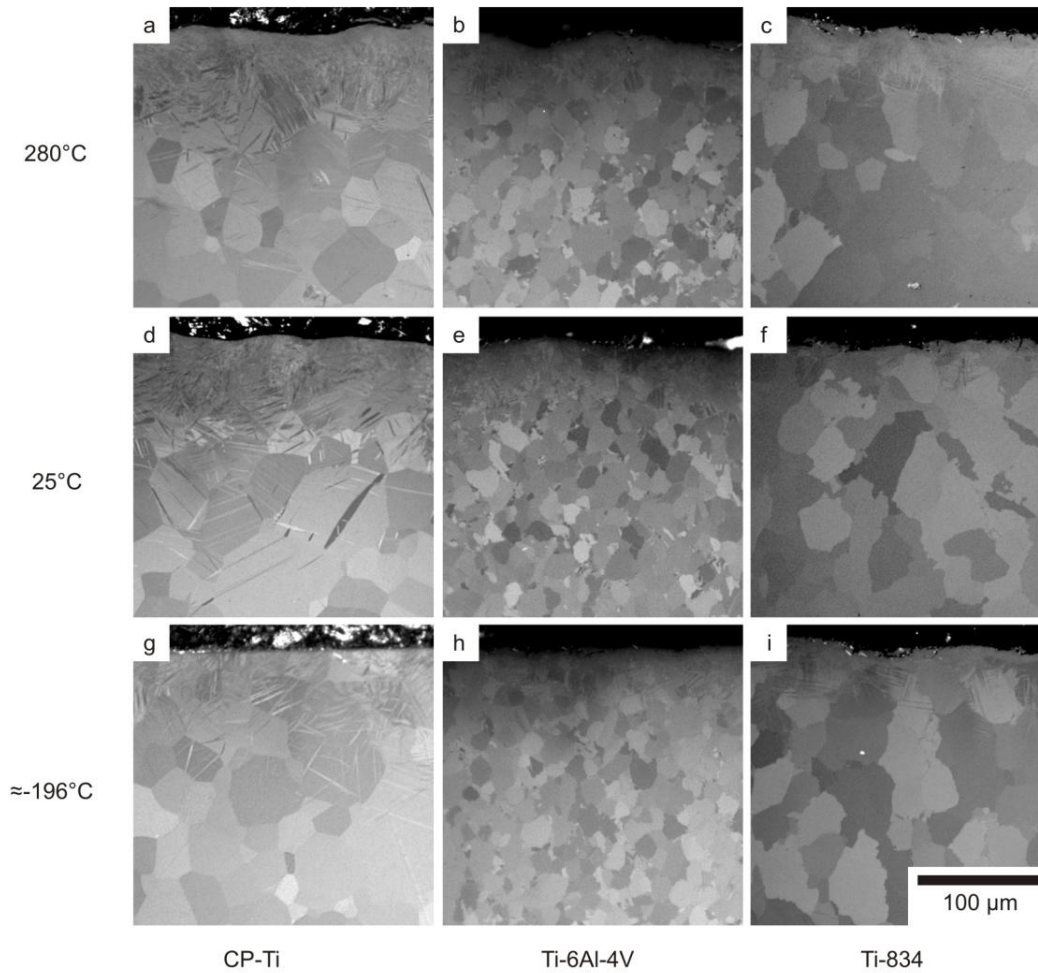
Figure 4.4: Low magnification polarized light micrographs showing the deformed surface region of CP-Ti, Ti-6Al-4V and Ti-834. Specimens were shot peened at cryogenic temperatures, room temperature and 280°C.
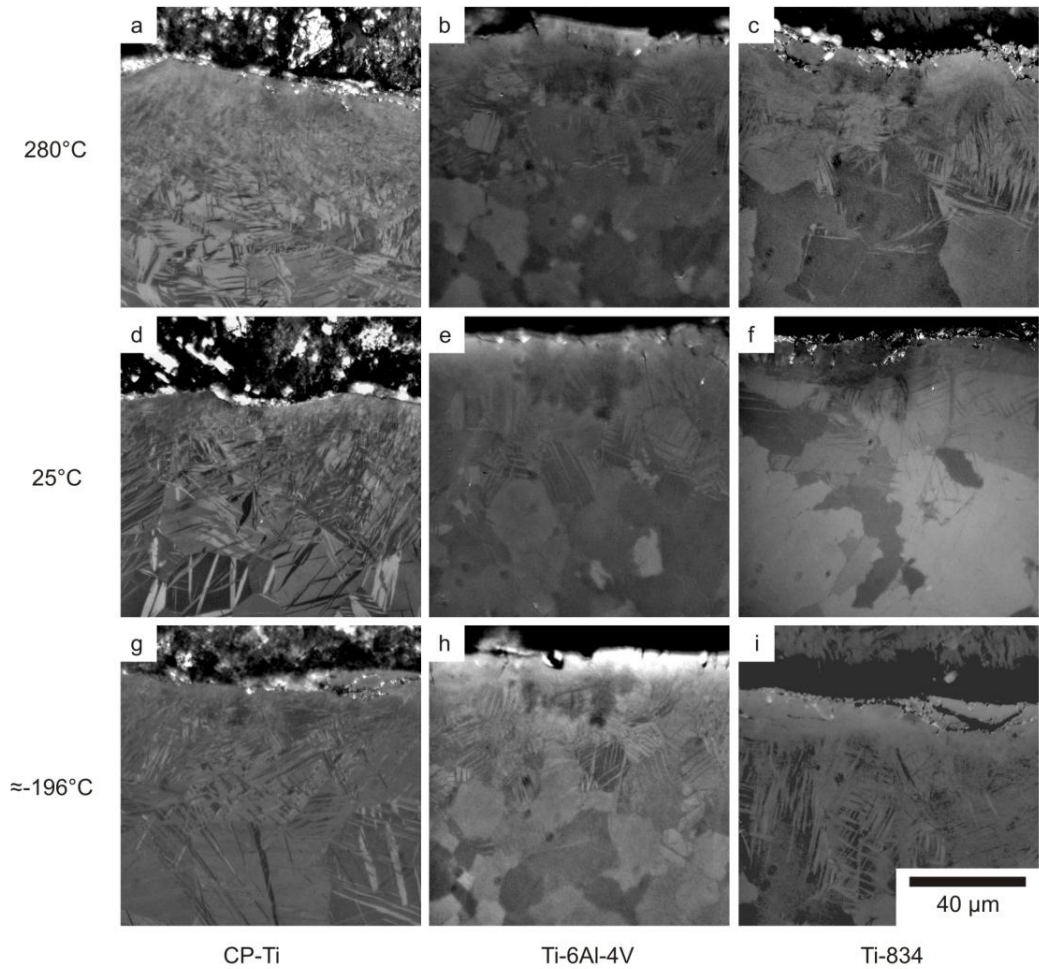
Figure 4.5: High magnification polarized light micrographs showing the deformed surface region of CP-Ti, Ti-6Al-4V and Ti-834. Specimens were shot peened at cryogenic temperatures, room temperature and 280°C.

In view of the limitations of light microscopy in determining the effect of workpiece temperature on deformation mode in Ti-834, EBSD analysis was performed on samples shot peened at cryogenic and elevated temperatures. Figure 4.7 is an EBSD map with pattern quality (band contrast) colouring of Ti-834 shot peened at -196°C. In reference to figure 4.7, the direction of the shot stream is labelled as the peening direction (PD), whilst the normal to the peening direction is referred to as the in-plane (IP) direction. From the pattern quality map, the plastically deformed subsurface region is represented by pixel data with low Kikuchi band contrast. The band contrast of the electron backscatter diffraction pattern improves with increasing distance from the shot peened surface and the bulk microstructure of Ti-834 becomes clearer. From the EBSD data, the depth of the plastically deformed surface region extend to approximately 50 µm below the shot peened surface; corresponding to the results of the polarized light microscopy.

Crystal plane trace analysis has been performed on a number of grains in order to identify whether the microstructural features evident from the pattern quality map correspond to a particular crystal plane in the hexagonal close packed lattice. Trace analysis has been used by Keshavarz *et al* [13] and Zhou *et al* [14] in conjunction with Schmid factor analysis to determine the slip mode in magnesium alloys and a lead-free solder. Slip trace analysis on Ti-6Al-4V deformed in tension has also been performed by Bridier *et al* [15] using a combination of SEM and EBSD analysis. In the latter study, it was proposed that Schmid's law was useful in predicting the nature of slip systems, but was unable to predict whether a given slip system would be activated. Trace analysis has also been performed by Barnett [16] to assist with the analysis of deformation twinning and dislocation slip in magnesium alloys.

The technique can provide qualitative information on whether a microstructural features identified from a pattern quality map lies on (or close to) a crystal plane, although as with many metallographic techniques, EBSD data is a two dimensional projection of a three dimensional system. Crystallographic traces of the higher order planes will therefore lie close together in a two dimensional projection and it would be necessary to serial section a sample in order to gain more confidence in identifying planes. Nevertheless, trace analysis is widely employed in the literature to study deformation systems in crystalline materials.
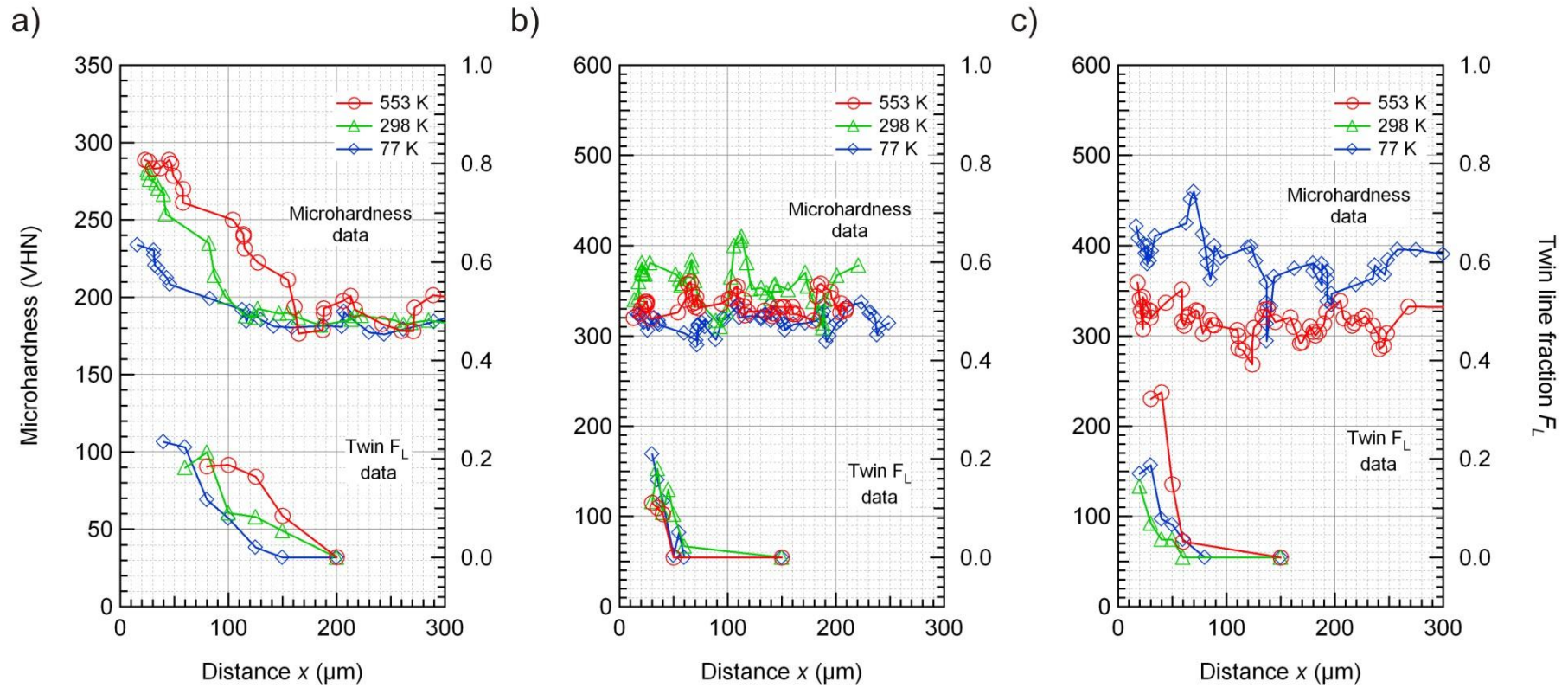
Figure 4.6: Microhardness and twin density data as a function of depth from the shot peened surface and temperature for a) CP-Ti, b) Ti-6Al-4V and Ti-834 c). The twin density data is presented as the linear fraction of twinned volume at a given distance from the peened surface.
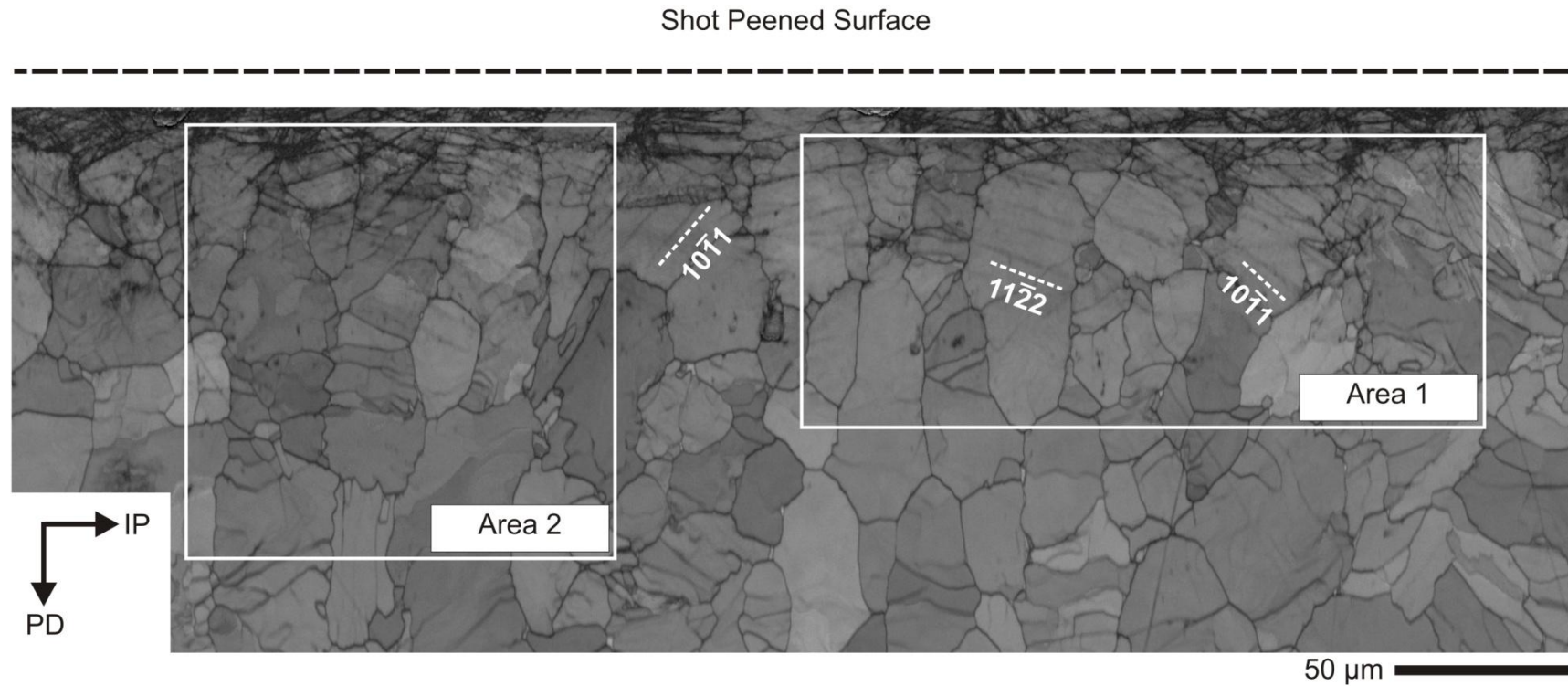
Figure 4.7: Electron backscatter diffraction map with pattern quality colouring of Ti-834 shot peened at -196°C. The region analysed is immediately below the show peened surface using a step size of 0.25µm. Increased magnification images of area 1 and area 2 are presented in figures 4.8 and 4.9 respectively. The direction of the shot stream, or peening direction (PD) is vertical. The radial or in-plane (IP) direction is normal to the peening direction and represents the net direction of plastic deformation arising from the shot peening process.
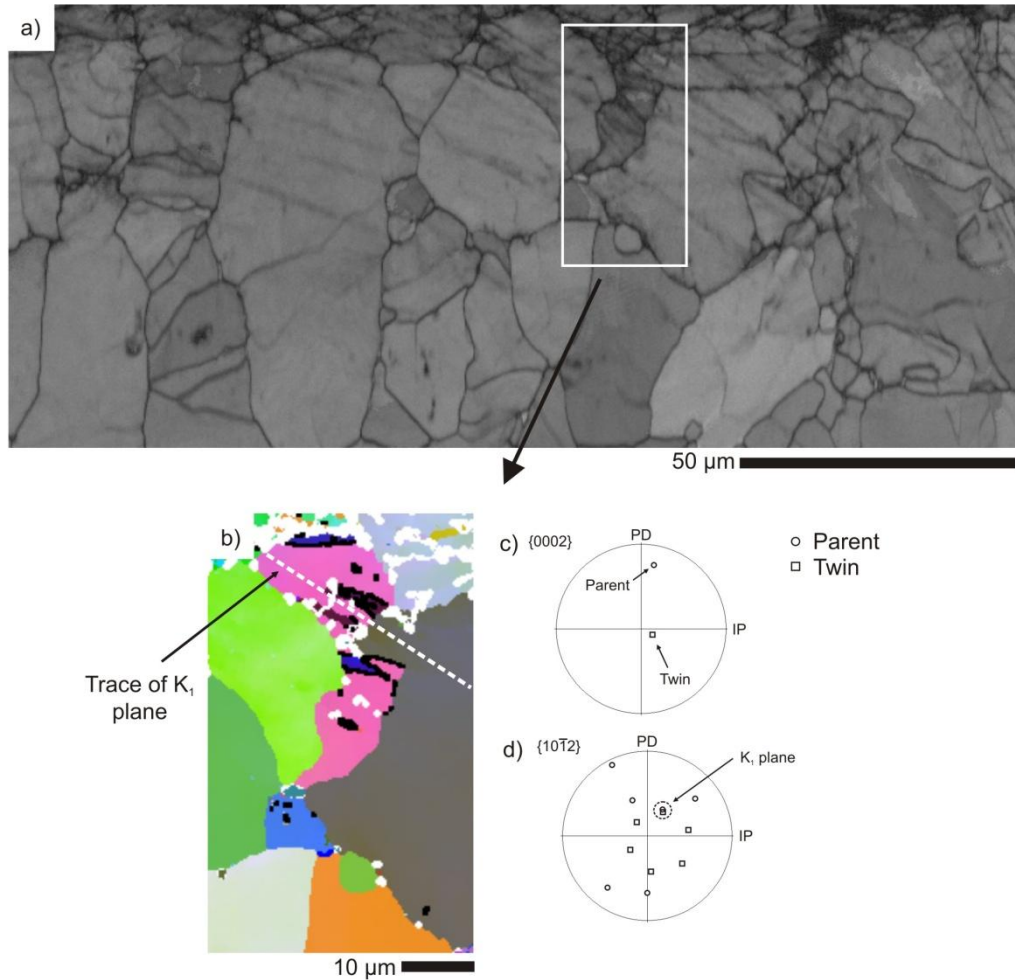
Figure 4.8: Electron backscatter diffraction maps of "Area 1" in figure 4.7. A pattern quality map of the whole area is given in a) and an enlarged all-Euler map of the twinned region is shown in b). Corresponding {0002} and {1-12} projections of the twinned grain are shown in c) and d). The trace of the {10-12} K_1 twinning plane is delineated by a dashed white line in b).

Figure 4.8 shows the region marked "Area 1" in figure 4.7. The corresponding EBSD data is presented in the form of a pattern quality map in figure 4.8a) and figure 4.8b) is an all-Euler coloured map of the region demarked by the white box. In figure 4.8b), boundaries corresponding to a rotation of 85° (± 5°) about the <1-210> axis) are delineated in black. As discussed previously in chapter 3, a crystal boundary of such misorientation corresponds to the {10-12} twin mode and figures 4.8c) and 4.8d) show examples of the {0002} and {10-12} stereographic projections for a twinned grain. The K_1 twinning plane lies on the {10-12} crystal plane and the coincident poles of the parent grain and twinned volume are illustrated in figure 4.8d).

The trace of the K_1 plane is marked on figure 4.8b) and lies close to the orientation of the twin boundaries. The EBSD data were interrogated for the presence of other twin modes such as the {10-11} <1012> and {11-23} <-1-122> systems as reported to occur in CP-Ti and Ti-6Al-4V by Hu and Randle [17], but no evidence of their existence was found using the angle-axis misorientation criteria within this data. Mechanical twinning is also accompanied by dislocation slip within the alpha grains and slip bands (represented by planar arrays of low band contrast pixel data) can be observed in the pattern quality map shown in figure 4.7.
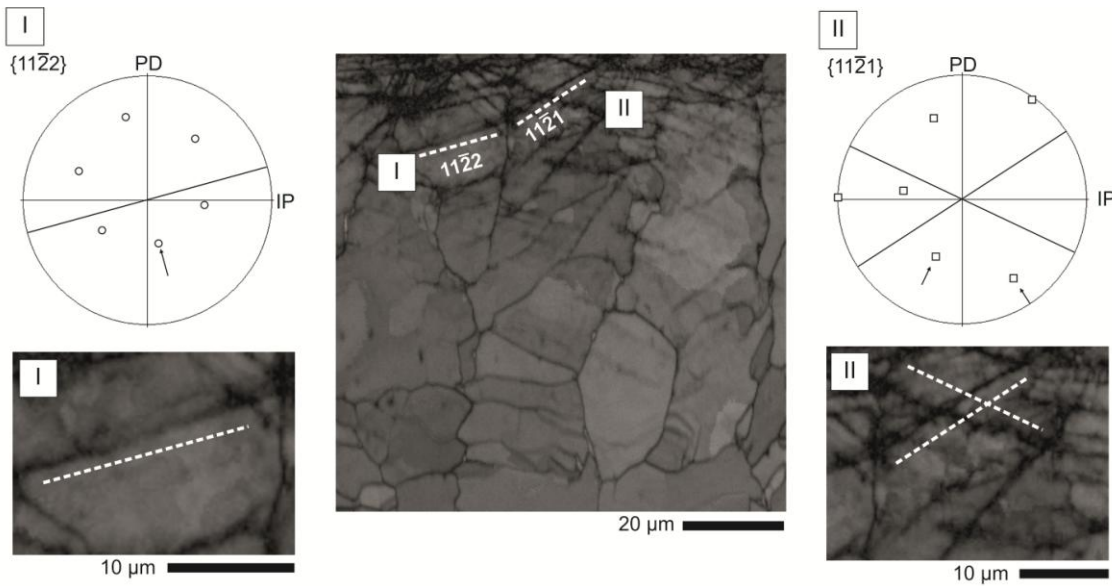
Figure 4.9: Electron backscatter diffraction maps of Ti-834 shot peened at -196°C with pattern quality colouring for the region labelled "Area 2" in figure 4.7. Traces of the {1122} and {1121} planes are shown by white dashed lines. Enlarged maps of the microstructural features marked I and II are shown along with the corresponding {1122} and {1121} stereographic projections.

Figure 4.9 is a pattern quality map of "Area 2" from figure 4.7. Trace analysis has been performed on the microstructural features marked I and II, and the corresponding {11-21} and {11-22} stereographic projections are shown. In this region, no evidence for mechanical twinning was found through interrogating the ESBD data for angle-axis pairs corresponding to the reported twin modes in CP-Ti.

From the enlarged pattern quality map of region II (Fig. 4.9) however, poor pattern quality (band contrast) along {11-21} can be observed. This suggests that atomic activity has occurred along crystal planes within the {11-21} family. This would correspond to the {11-21}<-1-126> twin system as indexed by Mironov *et al* [18] during warm forging of CP-Ti and reported Battaini *et al* [2] during plane strain compression of CP-Ti, but no further evidence to confirm its existence was obatained. As the region analysed is close to the shot peened surface, the indexing rate of the electron backscatter diffraction patterns is low and it is possible that distortion (and crystal rotation) in the twinned volume was sufficiently large to prevent indexing of the diffraction pattern.

To investigate whether a dependency of deformation mode on crystallographic orientation exists during peening at cryogenic temperatures, the orientation of alpha crystals that exhibit {10-12} twinning with respect to the peening direction are plotted on the {0002} projections shown in figure 4.10. The orientations of alpha grains that do not show mechanical twinning and are inferred to deform solely by dislocation glide are also marked. From the dataset analysed, grains with their *c*-axis closely aligned with the peening direction (PD) deform by {10-12} mechanical twinning, whilst those with a *c*-axis lying "in-plane" tend to deform by dislocation movement rather than mechanical twinning.
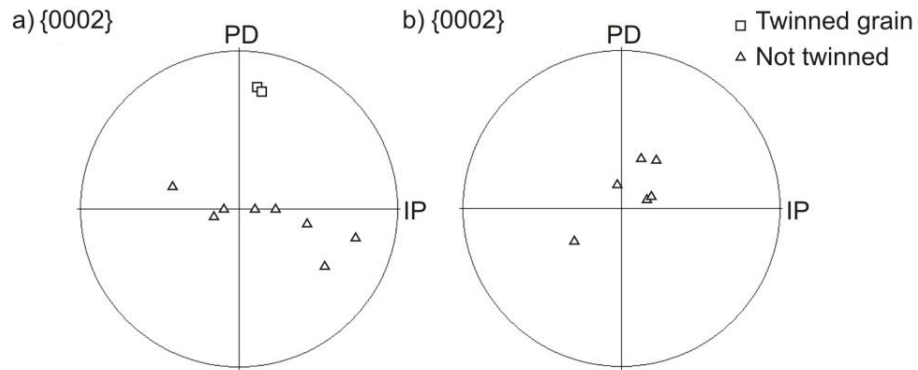
Figure 4.10: {0002} projections showing the orientation of twinned grains (open squares) and non-twinned grains (open triangles) in Ti-834 shot peened at cryogenic temperatures (196°C). The data from regions labelled "Area 1" and "Area 2" in figure 4.7 are shown in a) and b) respectively.

Figure 4.11 is a pattern quality map of Ti-834 shot peened at 280°C. Trace analysis has been performed on a selection of the microstructural features observed in the pattern quality map and the corresponding stereographic projections for the site marker I through the IV are presented above the EBSD map. In line with the analysis of Ti-834 peened at cryogenic temperatures, the region analysis is immediately below the shot peened surface and the direction of the shot stream, or peening direction (PD), is vertical.
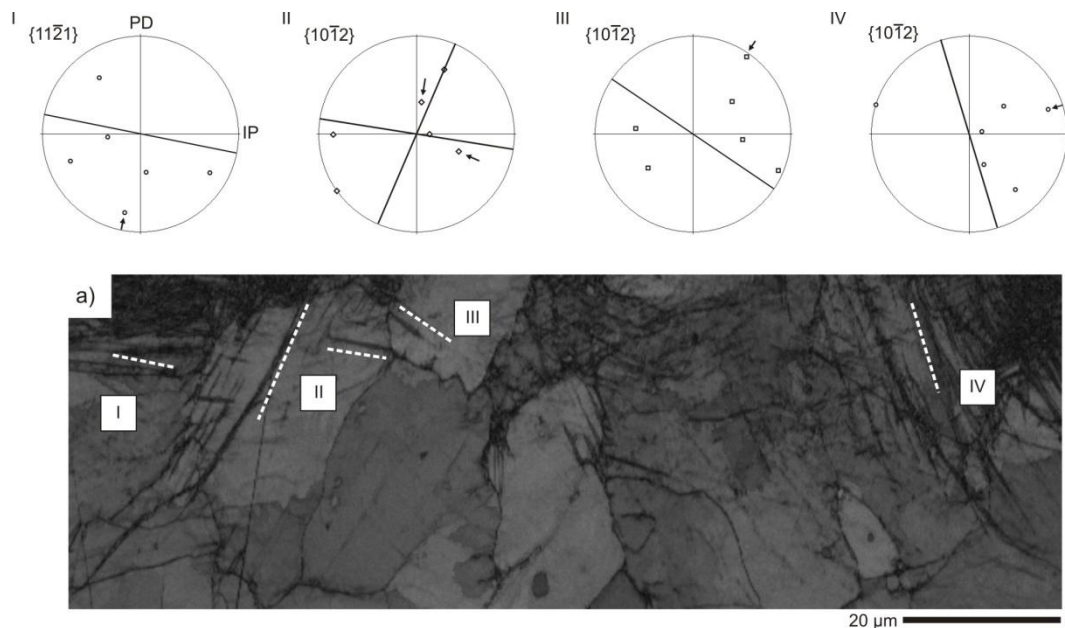
Figure 4.11: Electron backscatter diffraction map with pattern quality colouring of Ti-834 shot peened at 280°C. The region analysed is immediately below the show peened surface using a step size of 0.25µm. Crystal traces indicating the possible twin modes are given for the regions labelled I through to IV.

The EBSD data for Ti-834 peened at 280°C (Fig. 4.11) is of lower quality than that obtained for the Ti-834 sample peened at cryogenic temperatures. The metallographic preparation methodology was identical to the material shot peened at low temperature and it possible that the increased strain introduced following peening at elevated temperatures is at least in-part responsible for the lower rate of indexing and poorer diffraction pattern quality.
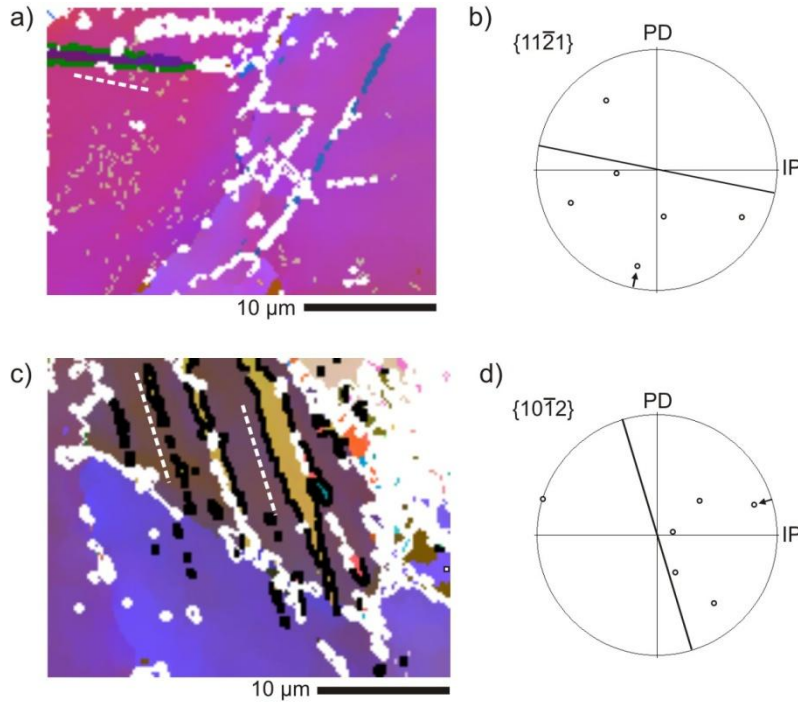
Figure 4.12: All-Euler coloured maps of the regions labelled I and IV in figure 4.12 are shown in a) and c) respectively. Traces of the {11-21} and {10-12} planes are delineated by dashed white lines, with the corresponding stereographic projections shown in c) and d).
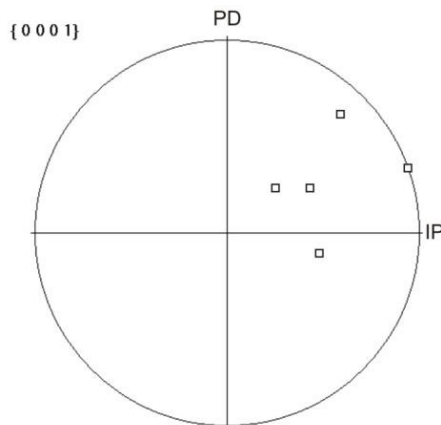
Figure 4.13: Basal pole figure showing the orientations of the twinned grains in the Ti-834 sample shot peened at 280°C (open squares). The peening direction (PD) is vertical and the in-plane direction (IP) is horizontal.

Lenticular features lying close to {11-21} and {10-12} can be observed in the pattern quality map and the corresponding all-Euler coloured maps of regions I and IV are shown in figures 4.12 a) and c). In figure 4.12a), {11-21}<-1-126> twin boundaries are delineated in green and {10-12}<10-1-1> twin boundaries by black in figure 4.12b). Traces of the respective K_1 planes are also shown by dashed white lines. The twin boundaries align closely to the trace of the {10-12} K_1 twinning plane in the case of figure 4.12b) although some deviation between the {11-21} K_1 plane and the respective

twin boundary can be observed in figure 4.12a). A possible explanation for the discrepancy is that the orientations of the parent and twinned volumes are based on grain average orientations, rather than the local orientation of the crystals at the twin-matrix interface.

Figure 4.13 shows the orientations of the twinned grains with respect to the peening direction in T-834 peened at 280°C. Dissimilarly to the observations in Ti-834 peened at cryogenic temperatures, the *c*-axis of the twinned grains are not closely aligned with the shot peening direction (PD) and crystal orientations that do not exhibit twinning during peening at low temperatures appear to readily twin at 280°C.

4.4 Results section 2: Microstructural analysis of shot peened Ti-6Al-4V plate product form

Figure 4.14 is a polarized light micrograph of Ti-6Al-4V shot peened to 1200% peening coverage at an Almen intensity of 9A. Evidence of mechanical twinning can be observed within the first 50 μm from the peened edge. Although the micrograph lacks resolution and clarity, it can be noticed that the depth to which twinning occurs is somewhat non-uniform. The bright contrast region on the right hand side of the micrograph appears to have a lower twin density than the central region of the micrograph.
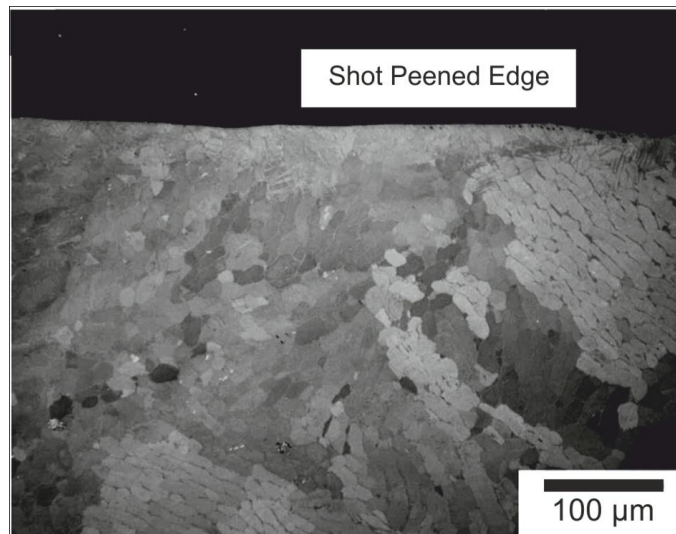
Figure 4.14: Polarised light micrograph of Ti-6Al-4V plate shot peened to 1200% peening coverage.

As with the microstructural analysis of peening trials material presented in the previous section, full analysis of heterogeneities of deformation mode is challenging with light microscopy and EBSD analysis of a representative region below the shot peened surface is shown in figure 4.15. Figure 4.15a) is an all-Euler coloured map of an area immediately below the shot peened surface of Ti-6Al-4V peened to 1200% coverage. Similarly to Ti-834 and CP-Ti, EBSD analysis confirmed the presence of {10-12}-type mechanical twins up to a depth of 50 – 60 μm. Two regions (demarked "Zone 1" and "Zone 2") are highlighted in figure 4.15a); with the first region showing a higher twin density. Diffraction data sub-sets for the respective zones were extracted from EBSD map and the local orientations of the alpha phase in zone 1 and zone 2 are presented in

figure 4.15c). The {0002} pole figures in figure 4.15c) are orientated such the peening direction (PD) is normal to the plane of the page and the X and Y axis correspond to the in the in-plane (IP) direction.
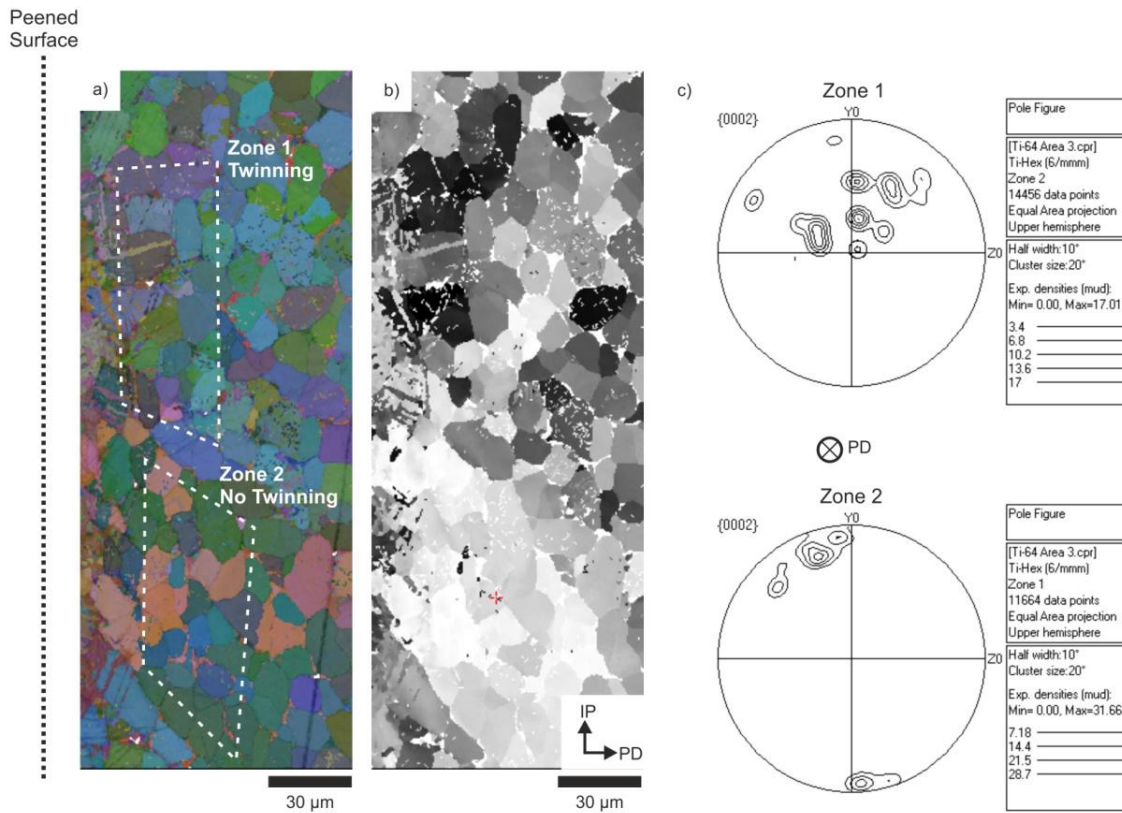
Figure 4.15: Electron backscatter diffraction analysis of shot peened Ti-6Al-4V plate. The in-plane direction (IP) is vertical and the peening direction (PD) is horizontal. An all-Euler colouring map is given in figure a) and the Schmid factor map for {10-10} prismatic slip with the direction of loading assumed to be parallel to the peening direction is given in b). Figure c) shows {0002} basal plane projections for the sub-set areas labelled "Zone 1" and "Zone 2". In figure c), the peening direction is normal to the plane of the page. Electron diffraction data was collected with a beam step size of 0.25 μm.

In the case of zone 1, where both the existence of mechanical twins occurs to a greater depth and the overall density is higher, the alpha grains are orientated with their *c*-axis close to the peening direction. This aligns with the analysis of diffraction data obtained from Ti-834 shot peened at cryogenic temperatures and considerably less twinning occurred in zone 2 where the *c*-axis of the alpha grains lies close to the in-plane direction (Fig. 4.16c)). Illustrating the effect of local average crystal orientation on deformation mode can be achieved with the aid of Schmid factor mapping as shown in figure 4.16b). Here, the Schmid factors for {10-10} <11-20> prism slip are automatically calculated by the HKL Channel 5 software; assuming a loading direction parallel to the direction of the shot stream (PD). The alpha-grains in zone 2 are favourably orientated for {10-10}<11-20> prismatic slip with Schmid factors approaching 0.5, whilst in zone 1, the <11-20> direction and {10-10} plane are respectively perpendicular and normal to the peening direction and therefore posses low Schmid factors for prismatic and basal slip.

4.5   Discussion

The observation of extensive mechanical twinning in CP-Ti when compared with Ti-6Al-4V and Ti-834 is unsurprising. Twinning has been identified by EBSD to readily occur in CP-Ti by Battaini *et al* [2] and through X-ray diffraction by Ungár *et al* [19]. Experiments into the high strain-rate response of CP-Ti by Chichili *et al* [4], also reported mechanical twinning to be an active deformation mode, with an increase in strain rate leading to a commensurate increase in twin density. Although twinning is considered to be favoured by higher strain rates and lower temperatures, raising the temperature of the workpiece increases the density of mechanical twins in CP-Ti. This is likely to result from an increase in the total amount of plastic work imparted into the workpiece during peening at 280°C. At lower temperatures, the flow stress of CP-Ti is higher and as the kinetic energy of the shot remained constant throughout the trials, a lower proportion of the shot energy is converted into plastic work (approximated by the area under the flow curve).
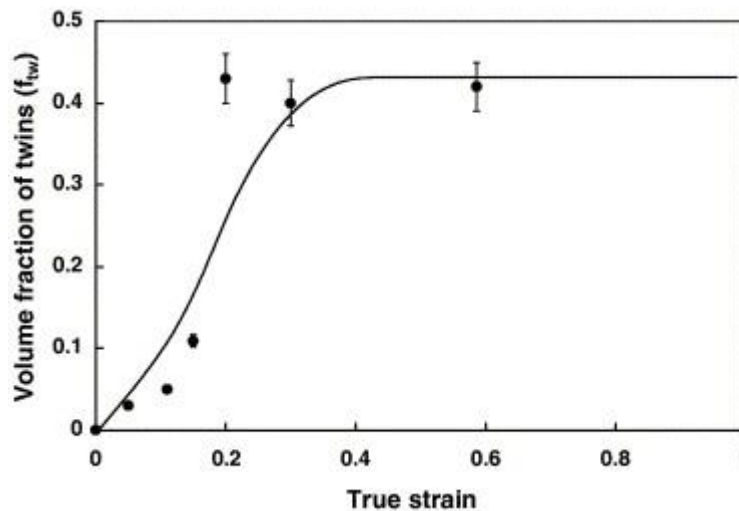
Figure 4.16: Twin volume fraction as a function of true strain during plane strain compression of CP-Ti. Closed circles are experimental data and the solid line shows the results of crystal plasticity modeling (figure from Salem *et al*. [20]).

The increase in subsurface hardening with higher peening temperatures can be explained by the interaction of dislocations with twin boundaries. The work of Salem *et al* [20][21] has shown strong evidence of strain hardening of CP-Ti due to deformation twinning, with Kalidindi *et al* [22] and Lee *et al* [23] discussing that the mechanism for strain hardening is due to both a reduction in effective slip length (Hall-Petch effect) and the conversion of glissile dislocations within the twinned volume into sessile dislocations as a result of the twinning shear transformation (Basinski mechanism).[1]

The decreased propensity for mechanical twinning in Ti-6Al-4V and Ti-834 aligns with the work of Paton *et al* [1] that suggests an increase in aluminium content promotes deformation by slip along the pyramidal {10-11} plane in the <11-23> direction. Although, twinning has been observed in Ti-6Al-4V tested in compression at

---

[1] It is worth highlighting at this point that twinning also contributes to a textural softening effect due to the reorientation of "hard" alpha-grains (*c*-axis parallel to the loading direction) to an orientation more favourable to prismatic dislocation glide. Whilst this mechanism for softening is well reported [18-21], such a hypothesis somewhat contradicts the Basinski mechanism. It is beyond the scope of this thesis however, to attempt to address the issue further.

strain rates of 10^3 [5], it is not generally considered to be an important deformation mode in the material under low strain-rate deformation. The nature of the shot peening experiment does facilitate a direction comparison across the three alloys however. As discussed above, the shot media is of constant kinetic energy and any variations in yield strength (and strain hardening behaviour) of the material will have a direct influence on the total plastic strain imparted into the surface of the workpiece. Ti-834 and Ti-6Al-4V have higher tensile strengths than CP-Ti and it is therefore arguable that less cold-work is introduced into the surfaces of the two alloys. As twinned volume fraction in alpha-titanium is a function of strain as shown in figure 4.16 [20][21], it is entirely plausible that the variation in twin density across the three alloys is controlled by the effective yield strength of the materials (itself a function of alloy chemistry), rather than competing modes of deformation based on changes in CRSS for $<c+a>$ slip or twinning.

An additional factor that appears to control deformation mode is the underlying microtexture of Ti-834 and Ti-6Al-4V during shot peening at low and ambient temperatures respectively. As can be seen in figures 4.7 – 4.9 (and in contradiction of conventional theory that twinning is favoured by lower temperature deformation [24]), only a limited amount of twinning occurred in Ti-834 during peening at cryogenic temperatures. Here, the majority of the alpha crystals are orientated such that the basal plane poles are normal to the peening direction. In this situation (and assuming loading parallel to the peening direction), the crystals are favourably orientated for prism slip, whilst the grains in which twinning occurred are "hard" orientations [6]. Although it appears that twinning is suppressed by low temperature shot peening, it is likely that the region selected for EBSD has captured a region where twinning is unlikely to occur based on the local crystallographic microtexture.

Further evidence pertaining to the role of microtexture on deformation mode at low and ambient temperatures, can be drawn from the analysis of shot peened Ti-6Al-4V plate in figure 16. Similarly to the results of shot peened Ti-834, twinning is favoured in regions where the average c-axis orientation of the alpha grains is parallel to the peening direction. If the loading direction is assumed to be parallel to the peening direction (PD), then it follows that the direction of maximum shear is at 45° to the PD with a resulting low Schmid factor for prism or basal slip. As reported by Song and Gray [25] during compression of zirconium alloys, grains where the twin plane was close to the maximum shear direction demonstrated increased preponderance for mechanical twinning.

The above analysis is based on the simplification that the stress axis is parallel to the peening direction and provides a convenient argument (not proof) to explain the propensity for twinning in alpha grains with a c-axis normal to shot peened surface. Whilst this simplification may form a basis to explain the observed microstructural response of Ti-834 and Ti-6Al-4V to shot peening at low and ambient temperatures, a number of limitations exist. The first is the obvious argument that an impact of a spherical body on a planar surface leads to a complex sub-surface state of stress and further work is required to fully understand the stress state during shot peening and relate it to deformation mode. A second limitation to assuming compressive loading parallel to the peening direction can be identified by examining the twin mode indexed by EBSD. As alpha titanium has a c/a ratio of less than $\sqrt{3}$, activation of the {10-12} twin mode leads to an extension of the crystal along the c-axis and is therefore termed a "tensile twin". Assuming a compressive loading parallel to the peening direction can therefore not explain the occurrence of {10-12} twinning in "hard" orientation crystals during shot peening. The observation of tensile twinning under loading conditions in which compression twinning should occur has also been observed in pure magnesium

by Nave and Barnett [26], who suggested that tensile twinning in grains with *c*-axis parallel to the compression axis resulted either from local stress-state anomalies caused by deformation of adjacent grains or that the twins occurred on unloading.

The discrepancy between the apparent orientation dependency of deformation mode during shot peening of Ti-834 at cryogenic temperatures (and Ti-6Al-4V plate at room temperature) with more random orientation of twinned crystals during warm peening of Ti-834 is an unexpected result. If current understanding of titanium deformation modes is applied, then twin propensity would decrease at higher temperatures and it could be argued that the orientation sensitivity of whether a grain twins or not would increase. That is, it might be expected that an increasingly high Schmid factor would be required to activate twinning on {10-12} with increasing workpiece material temperature.

Some explanation can be drawn from the nature of shot impact with the workpiece at different temperatures. It can be seen from the cross-sectional light micrographs of shot peened CP-Ti (Fig. 4.4a) d) and g) that the planarity (flatness) of the peened surface decreases with increasing peening temperature. As discussed earlier, this may be attributed to increased strain imparted into the surface regions of the workpiece. Increasing deviation of the peened surface from planarity with temperature suggests that the shot has penetrated further into the workpiece during impact. At lower temperatures, the contact area between the impacting shot and the workpiece is relatively low and this proposed concept is illustrated schematically in figure 4.17. With increasing temperatures, the workpiece material flows more readily and the contact area between shot and workpiece increases. It can be suggested that the increase in contact area between the shot and the workpiece leads to a more radial distribution in load during impact, leading to activation of twinning in crystals where the twin plane does not lie close to the peening direction.
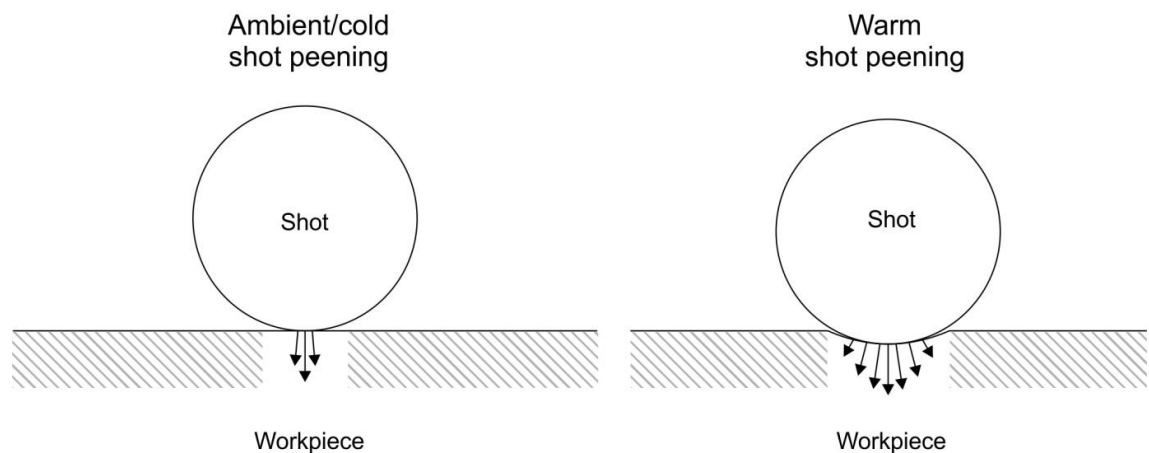
Figure 4.17: Schematic illustration showing the proposed effect of workpiece temperature on load distribution during peening at low and high temperatures.

The concept of a more radial load distribution during peening at higher temperatures is hypothetical and no experimental evidence other than the observed increase in surface roughness with peening temperature has been collected. Regardless, in conjunction with evidence for increased plastic strain, the increased preponderance for twinning at higher temperatures could be explained by the change in the mechanical stress state.

4.6   Chapter conclusions

Shot peening trials have been performed on a range of titanium alloys to investigate the role of chemistry, workpiece temperature and microtexture on deformation mode. The workpiece was cooled or heated prior to shot peening to obtain target temperatures of -196°C and 280°C. Specimens were also shot peened at ambient/room temperature.

In the case of CP-Ti, raising the temperature of the workpiece during peening increases the plastic strain imparted into the subsurface regions and this is manifested in an increase in twin fraction and subsurface hardening.

A more complex situation arises in the case of Ti-834. Electron backscatter diffraction analysis suggests that the underlying microtexture has some control of the mode of deformation (twinning versus slip) during low temperature peening. A similar observation has been made in rolled Ti-6Al-4V plate shot peened at ambient temperatures. In both cases, alpha grains with *c*-axis orientated parallel to the peening direction tended to deform by {10-12} mechanical twinning whilst those where the c-axis was normal to the peening direction did not undergo twinning.

At elevated peening temperatures, Ti-834 showed an increased propensity for twinning regardless of crystal orientation. Current understanding suggests that twinning would be more dominant as a deformation mode at low temperatures; with dislocation slip being favoured at higher temperatures. This anomaly observed during shot peening may be attributed to the changes in stress state during impact of the shot with the workpiece surface. The research suggests that deformation mode is sensitive to temperature, alloy chemistry and to a certain extent microtexture, and further work is required to fully understand the key variables controlling mode of deformation during shot peening.

References

[1] N. E. Paton, R. G. Baggerly, J.C Williams, Metallurgical and Materials Transactions A 33 (2002) 837 – 850

[2] M. Battaini, E. V. Pereloma, C. H. J. Davies, Metallurgical and Materials Transactions A 28 (2007) 276 – 285

[3] S. L. Semiatin, T. R. Bieler, Metallurgical and Materials Transactions A 32 (2001) 1787 – 1799

[4] D. R. Chichili, K. T. Ramesh, K. J. Hemker, Acta Materialia 46 (1998) 1025 – 1043

[5] A. J. Wagoner Johnson, C. W. Bull, K. S. Kumar *et al*, Metallurgical and Materials Transactions A 34 (2003) 295 – 306

[6] T. R. Bieler, S. L. Semiatin, International Journal of Plasticity 18 (2002) 1165-1189

[7] D.G. Leo Prakasha, R. Dingb, R.J. Moata *et al*, Materials Science and Engineering A 527 (2010) 5734 – 5744

[8] G. C. Kaschner, G. T. Gray III, Metallurgical and Materials Transactions A, 31 (2000) 1997 – 2003

[9] E. Cerreta, G. T. Gray III, Metallurgical and Materials Transactions A, 35 (2004) 1999 – 2011

[10] M. R. Barnett, Z. Keshavarz, A. G. Beer *et al*, Acta Materialia 52 (2004) 5093 – 5103

[11] L.L. Shaw, A.L. Ortiz, J.C. Villegas, Scripta Materialia 58 (2008) 951 – 954

[12] M Humbert, L. Germain, N. Gey *et al*, Materials Science and Engineering A 430 (2006) 157 – 164

[13] Z. Keshavarz, M. R. Barnett, Scripta Materilaia 55 (2006) 915

[14] B. Zhou, T. R. Bieler, T.-K. Lee, K.-C.Liu, J. Electron. Mater. DOI: 10.1007/s11664-009-0929-6

[15] F. Bridier, P. Villechaise, J. Mendez, Acta Materialia 53 (2005) 555 – 567

[16] M. R. Barnett, Materials Science and Engineering A 464 (2007) 8 – 16

[17] Y. Hu, V, Randle, Scripta Materialia 56 (2007) 1051 – 1054

[18] S. Y. Mironov, G. A. Salishchev, M. M Myshlvaey *et al*, Materials Science and Engineering A 418 (2006) 257 – 267

[19] T. Ungár, M. G. Glavicic, L. Balogh, *et al*, Materials Science and Engineering A 493 (2008) 79 – 85

[20] A. A. Salem, S. R. Kalidindi, S. L. Semiatin, Acta Materialia 53 (2005) 3495 – 3502

[21] A. A. Salem, S. R. Kalidindi, R. D. Doherty, Scripta Materialia 46 (2002) 419 – 423

[22] S. R. Kalidindi, A. A. Salem, R. D. Doherty, Advanced Engineering Materials 5 (2003) 229 – 232

[23] W. B. Lee, C. Y. Lee, W. S. Chang *et al*, Materials Letters 59 (2005) 3315 – 3318

[24] J. W. Christian and S. Mahajan, Progress in Materials Science, 39 (1995) 1 – 157

[25] S. G. Song, G. T. Gray III, Metallurgical and Materials Transactions A 26 (1995) 2655 – 2675

[26] M. D. Nave, M. R. Barnett, Scripta Materialia 51 (2004) 881 – 885

Chapter 5

Microstructural damage during high speed milling of Ti-834 and Ti-6Al-4V

5.1   Introduction

The next generation of civil aircraft platforms such as the Boeing 787 Dreamliner and Airbus A350-XWB will consist of a predominantly carbon fibre composite fuselage, empennage and wing structure, such aircraft will require an increase in titanium usage (approx. 20% by weight) for fasteners and high strength forgings, due to its superior galvanic corrosion resistance, linear thermal expansion coefficient and elastic modulus when coupled with graphite. The increased usage of titanium in the aerospace industry requires a commensurate increase in the productivity of downstream manufacturing processes such as machining. Unfortunately, the very properties that make titanium a popular engineering alloy also lead to difficulties during machining. The low thermal conductivity and high cutting forces due to retention of mechanical strength at high temperatures leads to excessive tool wear and prohibitive manufacturing costs [1] [2]. The vast majority of aerostructural titanium components require milling operations to take the product from forged, plate or cast condition to the often complex finished form.

Due to the difficulties in machining titanium at productive rates, there have been concerted efforts to advance the boundaries of high productivity milling and in particular high speed milling for finishing and semi-finishing applications. There is a growing trend within the aerospace industry for rough machining to be carried out close to the forging supplier, therefore most of the interest from aircraft manufacturers and tier 1 and 2 aerospace suppliers is on finishing and semi-finishing. Due to the intermittent nature of milling, much higher surface speeds can be achieved than in turning, as the periodic thermal loading and unloading cycle does not see temperatures rise to a maximum and plateau as in turning [3]. Maximum surface speeds for high speed titanium milling of Ti-6Al-4V can be up to 300 m.min^{-1} whereas turning is unlikely to exceed 80 m.min^{-1} [4]. Machinability is typically judged by the following four criteria [5]; chip formation, cutting force, tool life and surface condition. In achieving the higher surface speeds, quoted above, research has focussed particularly on observing and improving tool life, using chip formation and cutting forces as good indicators to the health of the process. Assessment of surface condition and optimisation of machining parameters is often limited to surface topography and for critical

applications would include relatively low magnification light microscopy. Current surface integrity practice applied by mechanical engineers characterises macroscopic features such as surface tearing, chip smearing and general deformation of grains in the direction of cutting [6]; with little emphasis placed on subsurface microstructural damage incurred during the high speed milling process.

Although machine finishing and semi-finishing processes are not considered to impart a comparable level of surface damage with processes such as peening or laser shock peening, research has suggested that machining operations lead to subsurface residual stresses in titanium alloys [7]. As in the case of shot peening, such residual stresses are likely to result from the introduction of residual plastic strain immediately below the surface of a machined component. In chapters 3 and 4, evidence has been presented that both the mode and magnitude of microstructural damage imparted during the shot peening process is not only sensitive to alloy chemistry, but also the underlying microtexture of the alloy. The aim of this final research strand is to firstly assess qualitatively the magnitude of subsurface damage imparted onto a component during a machining operation using high resolution electron microscopy. As microtexture has been shown to influence deformation mode during shot peening, a second aim is to investigate the sensitivity of microstructural damage to the local crystallographic orientation of the alpha-phase. The latter aim is addressed using a combination of finite element modelling of the machining process and post-mortem electron backscatter diffraction analysis of the machined titanium alloy.

A description of the finite element modeling procedure is given within the experimental methods section; providing information pertaining to the input variables and some details of orthogonal cutting simulations undertaken by other researchers.

5.2   Modeling and experimental methods

5.2.1   *Finite element modeling*

In order to understand the stress and strain field close to the tool/workpiece interface and aid microstructural studies, numerical modeling of the orthogonal cutting of Ti-6Al-4V has been performed using the finite element package DEFORM^{TM}-2D [8]. Orthogonal cutting is a simplified plane-strain model for a metal removal process and provides information on the material flow within the shear-zone ahead of the tool/workpiece interface (see figure 2.20 in chapter 2). Whilst orthogonal cutting differs from the milling process, milling is a more complex operation from a kinematic perspective, and therefore requires more detailed and time-consuming finite element simulations.

In the two dimensional plane-strain simulations, the tooling was modeled as an un-coated tungsten carbide elastic object with approximately 800 mesh elements. The tool geometry employed in the simulation provided a relief angle of 7° and a clearance angle of 7°, which is representative of a typical turning operation for titanium alloys [9]. The workpiece was modeled as a visco-plastic object and (machining-specific) tabulated flow data for the Ti-6Al-4V alloy employed in this simulation was provided with the DEFORM^{TM}-2D software.

Flow stress data for Ti-6Al-4V in the temperature range 20°C to 700°C as provided by Scientific Forming Technologies Corporation [8] are shown in figure 5.1. Above strains of ~1, the material flow softens, although in the tabulated data set the magnitude of flow softening is independent of temperature and strain rate. This is not necessarily an accurate representation of the mechanical behaviour of titanium alloys. A

study by Semiatin and Bieler [10] demonstrated that with increasing strain rate, the magnitude of flow softening in a β-processed Ti-6Al-4V alloy was sensitive to the prior alpha colony size during compression testing at ~800°C.

The workpiece was discretised into 2000 quadrilateral elements with a minimum element size of approximately 5 μm employed around the tool/workpiece contact region. At the start of the simulation, the number of elements through to uncut chip thickness of 0.1 mm was approximately 30. The simulation was run at a surface cutting speed of 180 m.min^{-1}, with a continuous re-meshing employed to achieve chip separation from the workpiece. The re-mesh criterion was set to an interference depth of 0.002 mm between the tool and workpiece to avoid excessive penetration of the mesh. A series of mesh windows were defined around the tool and workpiece to control the relative element size and ensure that during re-meshing, a fine mesh was maintained in the chip deformation zone and along the trailing edge of the tool. Figure 5.2 shows the meshing arrangement for the tooling and workpiece.

In order to account for heat transfer from workpiece to tool, a thermal boundary condition was defined along the interface between the chip and rake face of the tooling. Values for heat transfer coefficient quoted in the literature for machining of titanium alloys range from 20 kWm^{-2}K^{-1} [11] to 1000 kWm^{-2}K^{-1} [12] and in this study a constant heat transfer coefficient of 20 kWm^{-2}K^{-1} was selected. Similarly, some uncertainty exists around the appropriate friction model to use when simulating orthogonal cutting of titanium [11 - 14]. Calamaz *et al* [11] employed a Coulomb limited Tresca law to control the interface friction between the tool and the rake face whilst Sima and Özel [12] considered three contact and sticking regions at tool/chip interface. As the intention of the model is provide an *insight* into the state of stress and strain during chip formation in titanium alloys, the Coulomb limited Tresca friction law employed by Calamaz *et al* [11] in orthogonal cutting simulations using the finite element code FORGE2 was selected for this modeling process. The Coulomb limit Tresca law is expressed as:

$$\tau = \mu \sigma_n \qquad \text{if} \qquad \mu \sigma_n < \bar{m} \frac{\sigma_0}{\sqrt{3}} \qquad\qquad \text{Eqn. 5.1 a)}$$

$$\tau = \bar{m} \frac{\sigma_0}{\sqrt{3}} \qquad \text{if} \qquad \mu \sigma_n > \bar{m} \frac{\sigma_0}{\sqrt{3}} \qquad\qquad \text{Eqn. 5.1 b)}$$

Where τ is the shear stress and σ_n is the normal stress. A value of 0.3 for the Coulomb friction factor μ was input into the simulation and the fraction of permissible shear stress, *m* was held at a constant of 1. It is acknowledged that a more detailed consideration of friction processes, particularly the slip-stick contact conditions at the tool nose, would be necessary to accurately model the cutting process. It was elected not to use the environmental window option in DEFORM^{TM}-2D, which facilitates rapid cooling around the tool/chip interface to simulate a coolant fluid, and the simulation was run as a dry-cut.
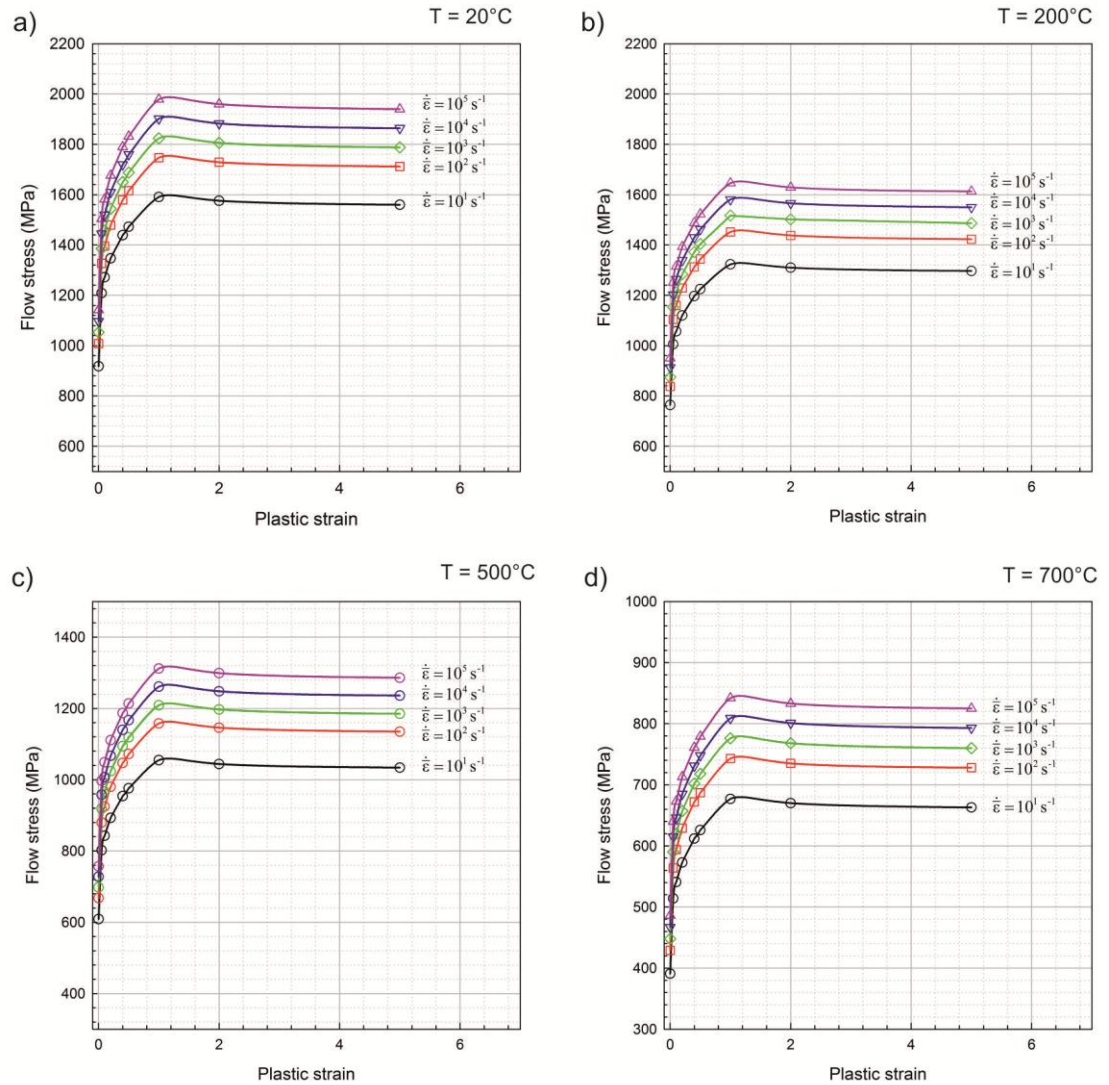
Figure 5.1: Flow data for Ti-6Al-4V in the temperature range 20°C to 700°C. The tabulated data was supplied by Scientific Forming Technologies for use in DEFORM^{TM}-2D orthogonal cutting simulations [8].
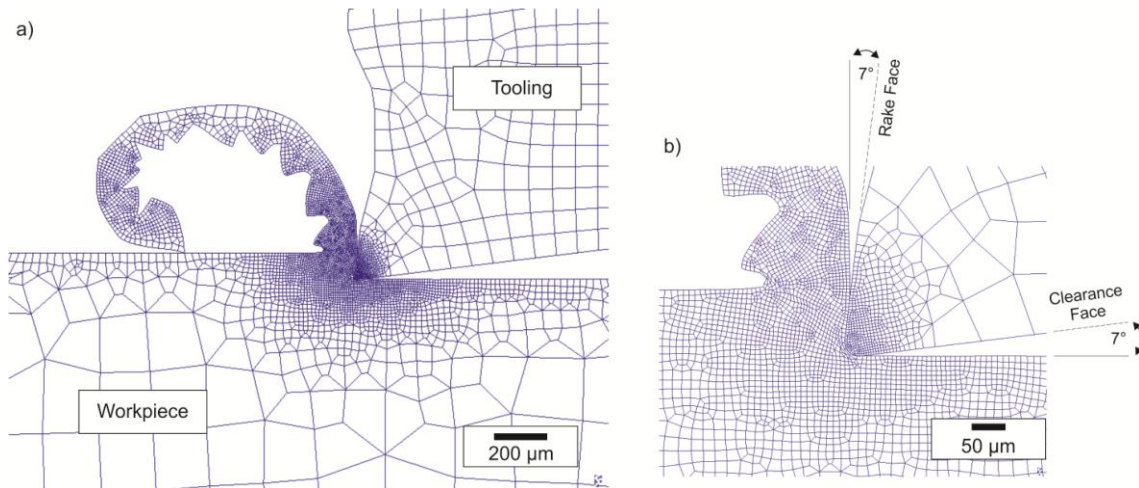
Figure 5.2: Example of the meshing arrangement for the tooling and workpiece during the finite element simulation. A mesh window was inserted around the tool/chip interface to ensure that the number of elements through the un-cut chip thickness remained a constant during continuous re-meshing.

5.2.2 *Milling trials and microstructural characterisation*

Milling trials were performed at the Advanced Manufacturing Research Centre with Boeing (Rotherham, UK) using a MAG Cincinnati Mega 5 machining centre. The two titanium alloys investigated were the near alpha alloy Ti-834 (composition in wt.% is Ti-5.5 Al, 4 Sn, 3.5 Zr, 0.8 Nb, 0.5Mo, 0.3 Si and <0.1 C) and the alpha-beta alloy Ti-6Al-4V, both of which were supplied by Timet UK in forged billet condition. The beta-annealed Ti-6Al-4V alloy possessed a large prior beta grain size and a transformed alpha-colony structure resulting from slow cooling through the beta transus whilst alpha-beta processing of the Ti-834 billet yielded a large volume fraction (approximately 80%) of primary alpha grains in a matrix of transformed beta.

Testpieces of 30 x 40 x 50 mm were held in a hydraulic vice mounted on the 5 axis machine tool table and milled using a Technicut solid carbide uncoated tool with 4 flutes and a 7° rake and 11° relief with a helix angle of 30° and with the spindle in a vertical orientation. An illustration of the Technicut solid carbide tool is shown in figure 5.3. A 16 mm diameter end mill was used to rough out a slot of 25 mm depth in 5 mm steps along the 50 mm length of the testpiece. On one side of the testpiece a finishing cut of 1 mm radial by 25 mm axial was taken at a surface speed of 200 m.min^{-1} and a feed per tooth of 0.05. The radial and tangential milling forces were not measured during the trials. In each case, the end mill was "climb milling", whereby the tool rotation is opposite to the feed direction. Climb milling results in a thick to thin chip which is best practice for titanium milling, yielding better tool life than conventional milling. The thin chip on exit reduces shock load and the chance of built up edge breaking off part of the tool cutting edge.

Specimen coordinates and a schematic arrangement of the high speed milling operation is given in figure 5.4. Following the trials and in reference to figure 5.4, milled testpieces were sectioned along the MD – ND plane and prepared for microscopy. Specimens were progressively ground with silicon carbide grinding papers to initially achieve a planar finish. A two stage polishing schedule was subsequently employed, with preliminary polishing performed using 9 μm diamond suspension and final polishing with a 0.06 μm colloidal silica suspension. Microstructural analysis was

performed using an FEI Sirion field emission gun scanning electron microscope and quantitative crystallographic data was acquired using electron backscatter diffraction (EBSD) with a 15 kV accelerating voltage, 10 nA probe current and a step size of 0.06 µm. Automated indexing and post-processing of the diffraction data was performed using Oxford Instruments HKL Channel 5 software. As the version of Channel 5 software used in this study does not offer a facility to present crystal misorientation data, further post-processing of the EBSD data was undertaken using software based on Visual Basic. NET developed at the Institute of Microstructural and Mechanical Process Engineering: The University of Sheffield (IMMPETUS). Full details of the method to process disorientation data are provided in reference [15].
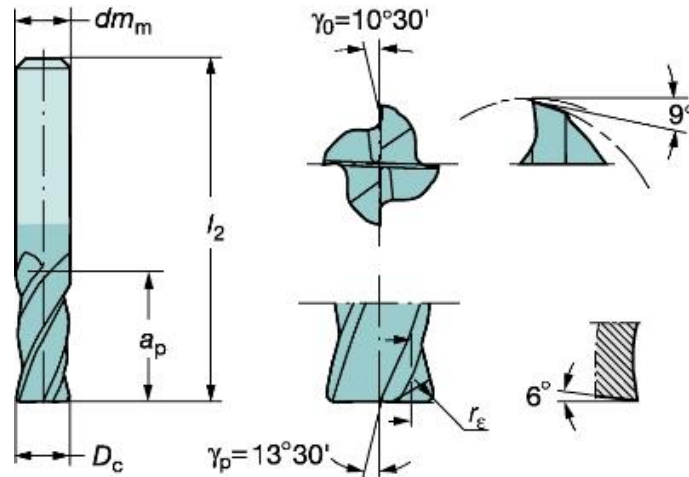
Figure 5.3: Engineering drawing of the Technicut solid carbide tool used in the milling trials of Ti-834 and Ti-6Al-4V.
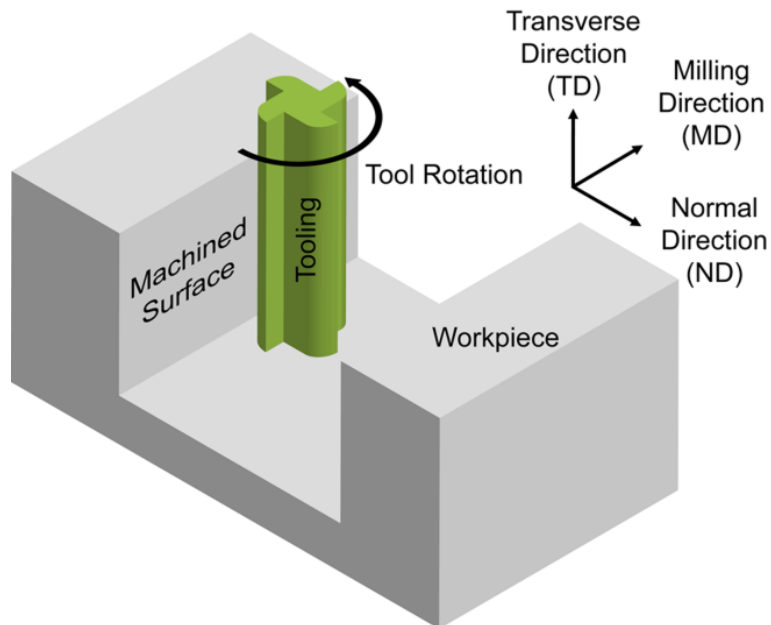
Figure 5.4: Schematic arrangement of the high speed machining set-up employed showing specimen coordinates. The specimen coordinates (x, y, and z) are labelled normal direction (ND), milling direction (MD) and transverse direction (TD) respectively.

5.3   Results and discussion

5.3.1   *Finite element simulations*

Figure 5.5 shows the predicted effective strain, effective strain rate and temperature distributions during orthogonal cutting of Ti-6Al-4V at a surface cutting velocity of 180 m.min^{-1}. Adiabatic shearing at an angle of approximately 45 degrees to the horizontal leads to the formation of serrated (occasionally referred to as "saw-tooth") chips during the machining simulation. Serrated chip formation has been successfully modeled by Calamaz [9] using the FE package FORGE2 and Sima [10], who also simulated orthogonal cutting of titanium using DEFORM^{TM}-2D. In both cases, the chip morphology predicted using the respective FE packages aligned well with experimental results. During the cutting simulation, the DEFORM^{TM}-2D model predicts a maximum temperature of 900°C along the rake face of the tool and peak strain rates approaching 10^5 s^{-1} within the region of shear localization region. A maximum temperature in excess of 600°C is predicted at the flank face/workpiece interface, with rapid cooling to temperatures below 300°C within a 100 – 200 μm lateral distance behind the tool/chip interface. Whilst the predicted strain rates of 10^5 s^{-1} agree with the FORGE2 predictions by Calamaz [9], the maximum predicted temperatures are somewhat higher.

In addition to the predicted plastic strains of ~3 that within the localized shear region of the chip, FE modeling suggests that the machining process introduces residual plastic strain into the surface region of the workpiece. Although a residual plastic strain layer has also been modeled by other researchers [9][10], little analysis of the strain state has been performed, with the focus centring on chip morphology and shear band formation. In order to analyse the magnitude and direction of subsurface plastic strain predicted in the FE simulation, state variable data was extracted along four line profiles. Figure 5.6a) shows the location of the line profiles labelled P1 to P4 with respect to the tool/chip interface.

As the machining simulation was performed under plane-strain conditions, it was possible to determine the direction of the principal strains (ε_1 and ε_3) with respect to the cutting direction and figure 5.6b) shows the sign and angle convention employed in the analysis.
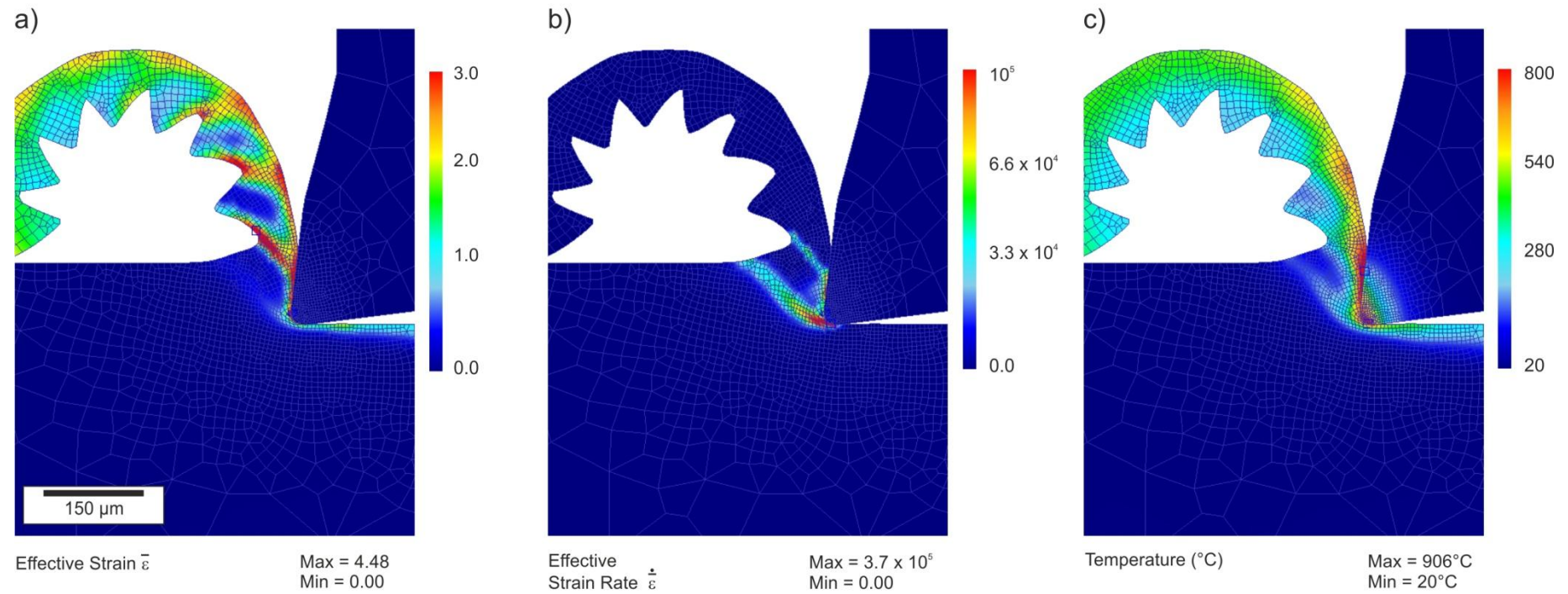
Figure 5.5: DEFORM-2D simulation output for plane-strain orthogonal cutting of Ti-6Al-4V. The effective strain is shown in a), the effective strain rate in b) and the temperature distribution during orthogonal cutting of Ti-6Al-4V is shown in c). The simulation was performed at a surface cutting velocity = 180 m.min^{-1}.
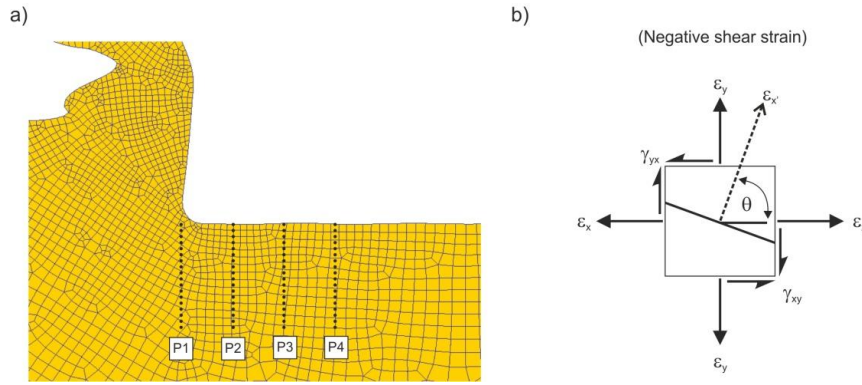
Figure 5.6: The location of line profiles P1-P4 from which strain data was extracted from the FE model is shown in a) and the sign convention for the normal and shear strain acting on an oblique plane is given in b).

Figure 5.7 shows the strain data for line profiles P1 to P4. The normal and shear components of strain at each point are given in addition to the effective strain, which was automatically calculated by the DEFORM^{TM}-2D software in terms of the total plastic strain using:

$$\bar{\varepsilon} = \frac{\sqrt{2}}{3}\sqrt{(\varepsilon_1 - \varepsilon_2)^2(\varepsilon_2 - \varepsilon_3)^2(\varepsilon_3 - \varepsilon_1)^2} \qquad \text{Eqn. 5.2}$$

Where ε_1, ε_2 and ε_3 are the principal strains ($\varepsilon_3 = 0$ in plane strain conditions). Figures 5.7e) and 5.7f) show the direction of maximum shear and the principle strain with respect to the machining direction (horizontal axis). From the normal and shear components of strain (ε_x ε_y and γ_{xy}) at a given point below the machined surface (figure 5.7b) to 5.7d)) and in reference to figure 5.6b), the angle $\theta_{\varepsilon1}$ between the principle strain direction and machining direction is calculated by [16]:

$$\tan 2\theta_{\varepsilon1} = -\frac{\varepsilon_x - \varepsilon_y}{\gamma_{xy}} \qquad \text{Eqn. 5.3}$$

With the direction of maximum shear strain θ_S is subsequently calculated as:

$$\theta_S = \theta_{\varepsilon1} + \frac{\pi}{4} \qquad \text{Eqn. 5.4}$$

The simulation data suggest that the material immediately below the machined surface is subjected to a complex strain path during the machining process. A maximum effective strain in the range 1.7 to 1.9 occurs adjacent to the machined surface in profiles P2 – P4 and decreases in a parabolic manner to zero within the first 50 µm. Inspection of the x and y components of strain suggests that a strain reversal occurs as the machine tool passes over the workpiece surface; with elements in the first 20 µm from the machined surface initially subjected to compressive ε_x and tensile ε_y strains close to the tool nose (Profile 1 in figure 5.7b) and 5.7c)). Elements in the trailing region of the tool (Profiles 2 – 4 in figures 5.7b) and 5.7c)) exhibit tensile ε_x and compressive ε_y strains at all longitudinal distances from the machined surface.
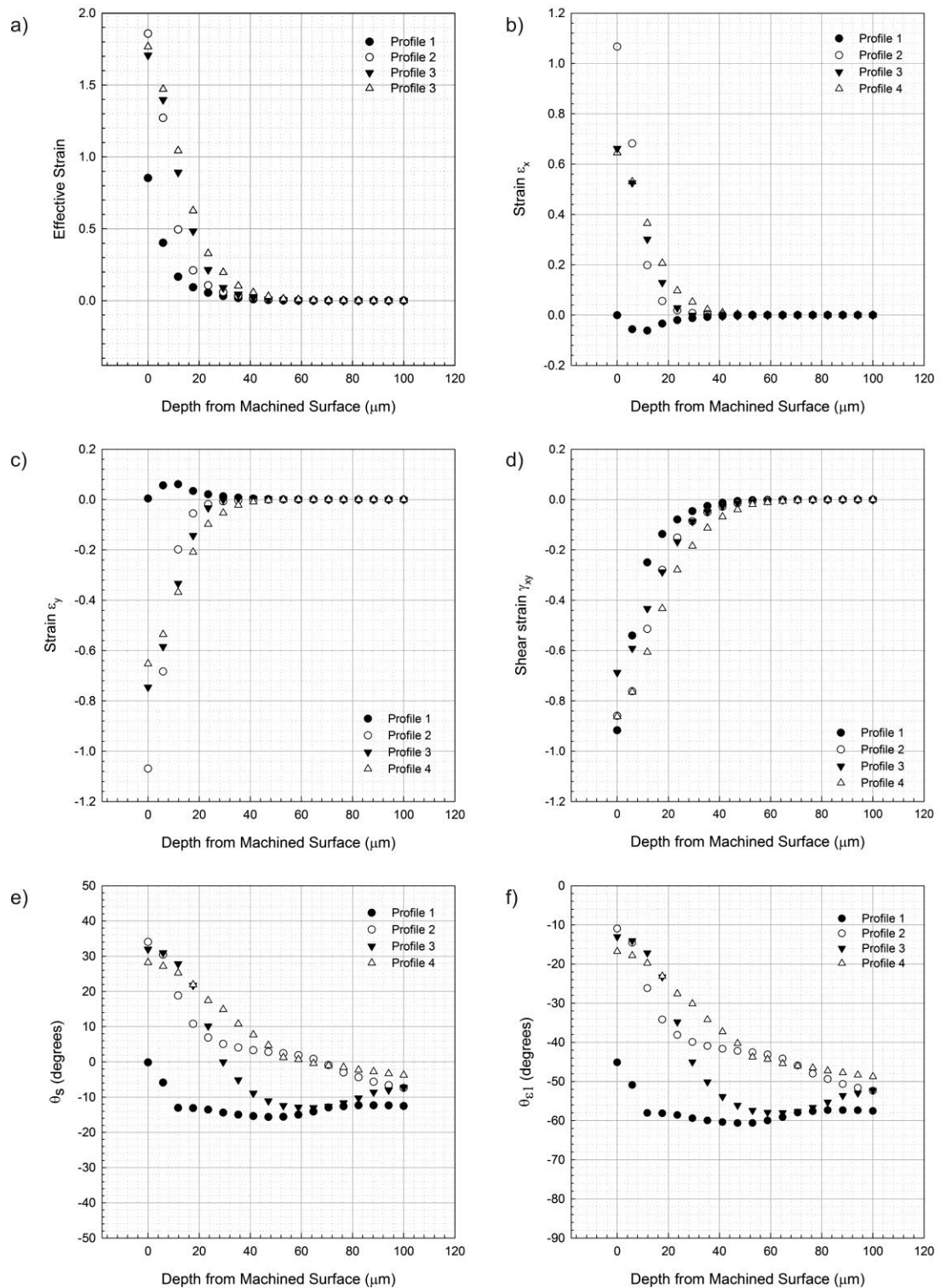
Figure 5.7: DEFORM^{TM}-2D plastic strain predictions for the profile locations P1 to P4 labelled in figure 5.6a). The effective strain is shown along with the normal and shear components of strain as a function of distance from the machined surface in figures a) to d). The direction of the maximum shear strain (θ_S) and the maximum principal strain ($\theta_{\varepsilon 1}$) with respect to the machining direction (MD) are shown in figures f) and e) respectively.

The shearing strain (γ_{xy}) approaches 1 for all elements close to the machined surface with higher shearing strain components in elements close to the tool/chip interface.

The angle of the maximum shear direction θ_S with respect to the machining direction is not constant during the simulated machining process and ranges from 0° to 45°. In elements close to the nose at the tool/chip interface (Profile 1 in figure 5.7e)), the direction of maximum shear is nearly parallel with the machining direction. In the wake of (trailing) the tool/chip interface however, the direction of maximum shear strain approaches 45°, with the angle θ_S decreasing with increasing distance from the machined surface.

Whilst the simulation is able to predict the magnitude and direction of strain during the orthogonal cutting progress, it is assumed that the workpiece is a mechanically isotropic material and the simulation does not account for local variations in modulus that are anticipated to exist in titanium alloys due to microtextural effects. Further to this, the model applies a Von-Mises yielding criteria, which is not modified to account for any anisotropy in yielding that occurs in textured materials [17]. Whilst such assumptions may be acceptable for the simulation of large-scale deformations across an industrial size component during processes such as forging, the size of the tool/chip interface and respective plastic deformation zone are in the region of 100-200 μm. Research using EBSD into the hot working of Ti-6Al-4V performed by Bieler and Semiatin [18] and fatigue fracture mechanisms of Ti-6Al-4V by Bantounas *et al* [19] has shown that the spatial distribution of similarly orientated alpha grains (macrozones) can exceed 100 μm. As the size of the plastic deformation zone during orthogonal cutting of titanium alloys is of similar magnitude to the effective structural unit, it is anticipated that the variations in microtexture will strongly influence the local yielding behaviour of the material.

5.3.2   *Microstructural damage observations*

Figures 5.8a) – 5.8c) are backscatter electron micrographs showing the respective subsurface microstructures of Ti-6Al-4V and Ti-834 following climb milling at a speed of 200 m.min^{-1}. The milling process leads to the introduction of subsurface plastic deformation to a depth of approximately 30 μm Ti-834 and 50 μm in Ti-6Al-4V. Electron channelling contrast from the backscatter micrographs suggest that the plastic strain is principally accommodated by dislocation slip, with regions of closely spaced slip bands visible within the alpha phase grains. Concomitant distortion of the beta-phase toward the cutting direction can also be observed in Ti-6Al-4V, although only to a depth of ~10 μm. Similar measurements have been reported by other researchers using light and scanning electron microscopy. As discussed in the introduction to this chapter, current surface integrity assessment of subsurface damage arising from high speed milling is typically only inferred from distortion of the beta phase, whilst plastic deformation of the alpha phase is not directly observed due to the limitations of the microscopy techniques conventionally employed. Indeed, current practice would suggest that subsurface damage accumulation during high speed milling of Ti-834 is insignificant, as very little distortion of the beta phase is evident from the backscatter electron micrographs (Figure 5.8b)). Therefore, the electron microscopy results from this study suggest that the damage resulting from high speed milling permeates deeper into the material than previously reported by Hughes *et al* [6].

The direct observation of slip bands in the subsurface alpha phase implies that local annealing of the subsurface microstructure does not occur during high speed milling. During high cycle fatigue, the principal mechanism for high cycle fatigue crack

initiation is the intersection of slip bands with the specimen surface or grain boundaries [20] and the nucleation of low cycle fatigue cracks along planar slip bands during four point bend testing [21] and uniaxial loading [22] of Ti-834 have been reported. Therefore, the damage accumulated during high speed milling may be deleterious to the mechanical integrity of engineering components as the presence of near surface slip bands may accelerate fatigue crack initiation. This could be the case if the stress-state during subsequent cyclic loading resulted in high Schmid factors for the slip systems activated during the milling process, although the effect of the pre-existing slip bands on fatigue crack initiation and subsequent fatigue life has not been measured in this study.
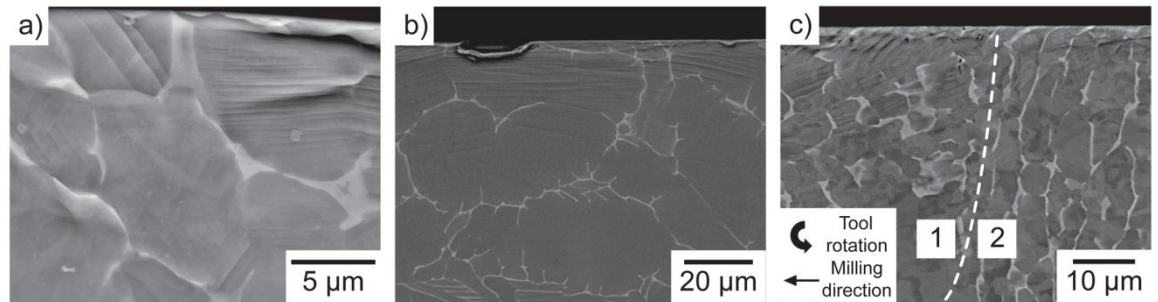
Figure 5.8: Backscatter electron micrographs showing deformation in the form of intense slip bands below the high speed milled surface in a) Ti-6Al-4V and b) Ti-834. An example of the non-uniformity of deformation observed in Ti-6Al-4V is given in c).

A further observation is that the depth to which slip occurs is not uniform below the milled surface. This occurs to a certain degree in Ti-834 (Figure 5.8b)), but Figure 5.8c) gives an example of the more pronounced effect observed in Ti-6Al-4V. It is clear that the response of adjacent alpha-colonies to high speed milling is dissimilar and the depth to which slip occurs is substantially greater in colony 1 than the adjacent colony 2. As each alpha colony can be considered as a single variant of the beta to alpha transformation on cooling, the alpha laths within each colony will have a similar crystallographic orientation and thus behave as a single effective structural unit [23].

Due to the limited number of active slip systems, the crystallographic orientation of the alpha phase will govern the ease of which slip occurs during high speed milling. This is similar to monotonic loading of polycrystalline titanium whereby strain partitioning occurs between "hard" and "soft" grains, although the stress state is less complex and strain rates considerably slower than in high speed milling. The post forging micro-texture of a titanium alloy may therefore have a pronounced effect on the subsequent machinability of a component and degree of subsurface microstructural damage accumulation.

In order to investigate the relationship between slip band intensity and the underlying crystal orientation of the alpha-titanium phase, EBSD analysis was performed on high speed milled Ti-834. The results are presented in the form of a disorientation map referenced against the grain average orientation in figure 5.9a). Figure 5.9b) is a pattern quality (band contrast) map of the area demarcated in figure 5.9a). Slip traces can be observed in both the disorientation and pattern quality maps, and the traces of the crystallographic planes which posses the minimum angular deviation from the slip traces are delineated. The corresponding stereographic projections of the slipped grains in figure 5.9b) are also given.
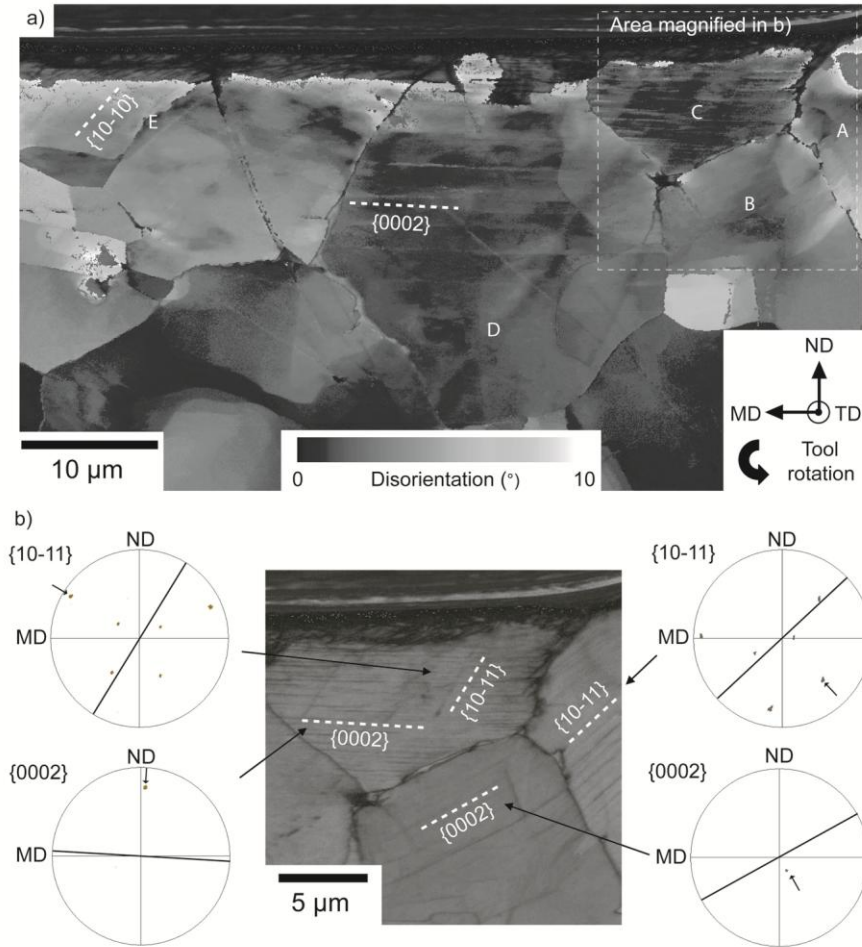
Figure 5.9: Electron backscatter diffraction results of high speed milled Ti-834 (200 m.min^{-1}). The area analysed is immediately below the machined surface and the machining coordinates with reference to figure 2 are labelled. The data is presented in the form of a crystal disorientation map referenced against the grain average orientation in a) and a pattern quality (band contrast) map of the region demarcated in a) is given in b). Slip trace analysis showing the crystallographic planes with the minimum angular deviation from the observed slip traces are also presented.

Full identification of a slip system is normally performed using a combination of slip trace and Schmid factor (*m*) analysis [24][25], but as the stress state immediately below the milled surface is complex, it is not possible to accurately determine the resolved shear stress on each crystal plane and thus a value for *m*. A first approximation may be drawn from the finite element simulations of orthogonal cutting as described in section 5.3.1 however. Here, it is assumed that the onset of plastic deformation occurs slightly ahead of the tool/chip interface (in the region of profile 1 in figure 5.7a)), where the direction of maximum principal strain acts at an angle of 45° to the machining direction (MD). It follows that the direction of maximum shear is parallel (but opposite) to the machining direction (MD).

Since strain can be related constitutively to stress, for the purpose of this analysis it is assumed that the direction of maximum shear stress is parallel to the direction of maximum shear strain. Two limitations to the above assumptions should be mentioned however: First is that as the finite element simulations were performed under a condition of plane-strain, a constraining stress will act in the direction normal to the orthogonal x-y plane. Secondly, in a "real-life" milling operation the state of strain is

likely to be tri-axial due to the helix-angle of the milling tool and it would be expected that considerable plastic deformation occurs in perpendicular to the orthogonal cutting co-ordinates. In view of the limited data an analysis of the machining operation from a microstructural damage perspective, an initial attempt to explain the observed variations in slip band intensity is made based on the above simplifications.

From the EBSD data presented in figure 5.9, two observations can be made. The first is that multiple slip systems are activated during milling with the second being the variation in slip intensity, including slip band spacing, between neighbouring grains. Grains C and D are of similar crystallographic orientation and show the highest intensity of slip, with the slip band traces closely aligned with the machining direction. It is evident from the trace analysis that slip has occurred along the basal plane and in both cases, the grains have a Schmid factor approaching 0.5 for {0002}[11-20] basal slip. Additionally, slip traces aligned with the {10-11} crystallographic plane can be observed in grain C, corresponding to the activation of a secondary slip system; {10-11}[11-20] pyramidal slip, which has a Schmid factor, of 0.46.

From the disorientation and pattern quality maps, the intensity of slip observed in grains A, D, and E is somewhat less than in grains C and D. In the case of grains A and E, the c-axis is oblique to the machined surface and non-basal slip has occurred, with Schmid factors of $m = 0.43$ for {10-11}[11-23] first order pyramidal slip in grain A and $m = 0.46$ for {10-10}[11-20] prismatic slip in grain E. The Schmid factor for {10-11}[11-20] pyramidal slip is in fact slightly greater than that of prismatic slip in grain E ($m_{\{10-11\}[11-20]} = 0.48$), although the angular deviation between the slip trace and the {10-11} crystallographic plane is considerable (~15°), and this discrepancy in m-values may be due to the employed simplification of the stress state during milling.

A more complex situation arises in the case of grain B. Whilst the closest aligned crystal plane to the observed slip trace is the basal {0002} plane, such a slip system possesses a low Schmid factor of <0.3. However, both the {10-10} and {10-11} crystal planes are also closely aligned with the slip trace, and have Schmid factors of $m = 0.45$ and $m = 0.47$ for prismatic and <a>-pyramidal slip respectively and it is likely that either of these systems have been activated. The Schmid factor for 1st order pyramidal slip in grain B is 0.4.

As the adiabatic heat input during machining can lead to an increase in surface temperature for short periods of time, the observation of both <a> and <c+a> pyramidal slip in grains B and C, and A respectively may be due to the significant reduction in critical resolved shear stress for pyramidal slip at temperatures above 400 K [26]. Nevertheless, regardless of what slip system is activated during the milling process, it is clear that the underlying grain orientation with respect to the machining direction (MD) plays a significant role in the degree of damage accommodated.

5.4   Chapter conclusions

Milling trials have been performed on the titanium alloys Ti-834 and Ti-Al-4V at maximum surface cutting velocity of 200 m.min^{-1} and at a feed per tooth of 0.05 mm. Microstructural analysis of the plastically deformed surface regions using scanning electron microscopy and electron backscatter diffraction has shown that the plastic strain is accommodated by dislocation slip within the alpha grains. The intensity of slip bands is non-uniform below the machined surface and it is anticipated that current workpiece surface integrity analysis applied by mechanical engineers for high speed milled titanium alloys could be inadequate, as failure to detect microstructural sub-

surface damage, such as intense slip bands, may have serious implications on in-service performance.

The preliminary data presented in this chapter suggest that the near surface micro-texture has a direct effect on slip band characteristics in the alpha phase following high speed milling. In conjunction with finite element modeling of the orthogonal cutting process, a hypothesis is proposed to explain the variation of slip intensity across alpha grains of differing crystal orientation using Schmid factor (m) analysis. Whilst further model development is required to accurately simulate a milling operation, and incorporate the effect of microtexture into the flow behaviour and yield criterion, the preliminary investigation provides an initial framework to advance the research area.

A better understanding of the upstream thermo-mechanical processing on near surface micro-texture, could potentially aid downstream machining operations. It is hypothesized that a combinatorial improvement in forging practices, milling tool parameters and machining process variables will aid the development of through-process models by mechanical and metallurgical engineers, with a view to facilitate much high production rates (>200 $m.min^{-1}$) of aero-structural titanium components without a reduction in fatigue crack initiation resistance.

References

[1] N. Zlatin, M. Field, in: R.I. Jaffe, H. M. Burke (Eds.), Titanium Science and Technology, Plenum Press, New York, 1973, pp. 489-503.

[2] W. Konig, *"Applied research on the machinability of titanium and its alloys"*, Proceedings of the 47th Meeting on AGARD Structural and Materials Panel, CP 256, 1978, pp. 1.1-1.10.

[3] D. A. Stephenson, A. Ali, J. Eng. Ind. 114 (1992) 127 – 137

[4] M. C. Shaw, Metal Cutting Principles, Clarendon Press, Oxford, 1996

[5] P. -J. Arrazola, A. Garay, L. -M. Iriarte, *et al*, Journal of Materials and Processing Technology 209 (2009) 2223 – 2230

[6] J. I. Hughes, A. R. C Sharman, K. Ridgway, Proceeding of the Institute of Mechanical Engineers, part B: Journal of Engineering Manufacture 218 (2004) 1113 – 1123

[7] B. R. Sridhar, G. Devananda, K. Ramachandra *et al*, Journal of Materials Processing Technology 139 (2003) 628 – 634

[8] DEFORM[TM]-2D Finite Element Modeling Software, Scientific Forming Technologies Corporation, Columbus, OH, USA

[9] M. Armendia, P. Osborne, A. Garay *et al*, Materials and Manufacturing Processes, DOI:10.1080/10426914.2011.585499

[10] S. L. Semiatin, T. R. Bieler, Acta Materialia 49 (2001) 3565 – 3573

[11] M. Calamaz, D. Coupard, F. Girot, International Journal of Machine Tools & Manufacture 48 (2008) 275 – 288

[12] M. Sima, T. Özel, International Journal of Machine Tools & Manufacture 50 (2010) 943 – 960

[13] T. Özel, International Journal of Machine Tools & Manufacture 46 (2006) 518 – 530

[14] P. J. Arrazola, T. Özel, International Journal of Mechanical Sciences 52 (2010) 31 – 42

[15] P. Davies (2009) *Investigation of Microstructure and Texture Evolution in the near-alpha titanium alloy Ti-834*, PhD Thesis, The University of Sheffield.

[16] G. E. Dieter, Mechanical Metallurgy, Second edition, McGraw-Hill, United States, 1976

[17] O. Cazacu, I. R. Ionescu, J. W. Yoon, International Journal of Plasticity 26 (2010) 887 – 904

[18] T. R. Bieler, S. L. Semiatin, International Journal of Plasticity 18 (2002) 1165 – 1189

[19] I. Bantounas, D. Dye, T. C. Lindley, Acta Materialia (2010) 3908 – 3918

[20] G. Lütjering, A. Gysler, in: G. Lütjering, U. Zwicker, W. Bunk (Eds.), Titanium: Science and Technology, Deutsche Gesellschaft für Metallkunde e. V., Oberursel, 1984, pp.2065-2083.

[21] G. J. Baxter, W. M. Rainforth, L. Grabowski, Acta Materialia 44 (1996) 3453 – 3463

[22] H. J. Maier, R. G. Teteruk, H. -J. Christ, Metallurgical and Materials Transactions A 31 (2000) 431 – 442

[23] D. Rugg, M. Dixon, F. P. E Dunne, Journal of Strain Analysis for Engineering Design 42 (2007) 269 – 279

[24] Z. Keshavarz, M. R. Barnett, Scripta Materialia 55 (2006) 915 – 918

[25] B. Zhou, T. R. Bieler, T.-K. Lee, K.-C.Liu, J. Electron. Mater. DOI: 10.1007/s11664-009-0929-6

[26] J.C. Williams, R. G. Baggerly, N. E. Paton Metallurgical and Materials Transactions A 33 (2002) 837 – 850

Chapter 6

Summary, conclusions and further work

6.1   Summary and conclusions

A research programme has been undertaken that investigates subsurface deformation microstructures in aerostructural titanium alloys during shot peening and high performance machining. A range of microstructural characterisation methods have been employed to characterise the micro-mechanisms of microstructural damage, and electron backscatter diffraction analysis has proven to be a powerful tool in understanding the role of underlying microstructure and microtexture on mode of plastic deformation. A summary of the key findings presented in this thesis is listed as follows:

- Shot peening of CP-Ti, Ti-834 and Ti-6Al-4V to an Almen intensity of 9A using R32 steel shot leads to the formation of mechanical twins within the plastically deformed subsurface region. CP-Ti shows the highest propensity for mechanical twinning, with the observed fraction of twinning being the lowest in the heavily alloyed near-alpha alloy Ti-834. The majority of mechanical twins observed of the {10-12} tension type, which corresponds to a ~85° rotation about the <12-10> crystal axis. Such a mechanical twin mode facilitates an extension of the hexagonal crystal along the *c*-axis and is therefore commonly referred to as tensile twins. The fraction of mechanical twins increases with shot peening coverage, although the maximum depth to which twinning is observed remains largely constant.

- The influence of temperature on deformation mode during shot peening was investigated through trials performed at Metal Improvement Company. Coupons of CP-Ti, Ti-834 and Ti-6Al-4V were either initially cooled to cryogenic temperatures in liquid nitrogen or heated in a furnace to 280°C prior to the shot peening process. Control specimens were shot peened at ambient temperatures.

- In the case of CP-Ti, the maximum depth of mechanical twinning was measured to increases with increasing temperature of shot peening. The underlying microtexture also appears to influence the mode of plastic deformation during shot peening; with experimental data from electron backscatter diffraction suggesting that alpha crystals show an increased preponderance for mechanical

twinning if their *c*-axis is aligned close to the peening direction (direction of the shot stream). Preliminary observations from the shot peening trials at Metal Improvement Company suggest that regions of textural heterogeneities have a more pronounced effect than temperature on the mode of plastic deformation in Ti-834, although further research is required to test this hypothesis.

- Following high speed milling of Ti-6Al-4V and Ti-834 using a solid carbide tool, residual slip bands are observed beneath the machined surface and no evidence of twinning was found. This is in contrast with the shot peening process where deformation is additionally accommodated via mechanical twinning. The electron backscatter diffraction data was presented in the form of a crystal disorientation map (referenced against the grain average orientation) and slip mode was indexed through a trace analysis technique. In Ti-834, the intensity of slip bands was observed to be greater in alpha crystals where the basal planes were closely aligned to the cutting direction. Here, the slip was indexed to be long the basal plane and in the <11-20> direction, although prism and pyramidal slip modes were also observed. In milled Ti-6Al-4V, a change in the maximum depth to which slip bands occurred between adjacent secondary alpha colonies was indentified through backscatter electron microscopy. In conjunction with finite element modeling of the orthogonal cutting process, a hypothesis is proposed to explain the variation of slip intensity across alpha grains of differing crystal orientation using Schmid factor (m) analysis.

- The importance of characterising the subsurface deformation structures that occur in titanium alloys following surface finishing processes is highlighted through the measured increase in oxygen uptake kinetics following isothermal exposure of Ti-834 at elevated temperatures in laboratory air. Oxygen embrittles the α-phase of titanium and significant concentrations can promote the formation of surface microcracks during monotonic or cyclic loading. The temperature-time combinations were selected in order to evaluate the thermal stability of the modified surface rather than provide a specific match to service conditions. However, the regimes chosen are sufficiently close to service conditions that trends concerning shot peened versus electrodischarge machined surfaces should be pertinent to the service application of Ti-834 in aero gas turbine engines.

- The increased levels of oxygen content measured by secondary ion mass spectrometry in shot peened Ti-834 following elevated temperature exposure is accompanied by the precipitation of silicides (likely to by S_2 type) along the mechanical twin boundaries and within regions of high dislocation density. The proposed mechanism which accommodates increased oxygen uptake in shot peened specimens is the introduction of short-circuit diffusion pathways through the cold working process.

- Mechanical testing shows that shot peening does not increase the high cycle fatigue life of Ti-834. Evidence exists however, that a decrease in room temperature fatigue performance occurs in shot peened material following prolonged thermal exposure in air at 650°C and shot peening promotes surface microcracking of Ti-834 following long-term thermal exposure in air.

In summary, the use of electron backscatter diffraction and polarized light microscopy to characterise the subsurface deformation microstructures has suggested that the microtexture developed during the thermomechanical processing of titanium alloys influences both the mode and magnitude of plastic deformation during surface finishing processes such as high performance machining and shot peening. Therefore, an improved understanding of both the upstream thermomechanical processing on near surface microtextural development in titanium alloys, coupled with further research to fully qualify the influence of local crystal orientation on the micromechanisms of plastic deformation, could facilitate reliable predictions for microstructural damage during downstream manufacturing processes.

6.2   Further Work

Several key areas of research have emerged from this thesis that merit further investigation. Although the effect of shot peening on the microstructure of Ti-834 following long term thermal exposure has been investigated in detail and preliminary fatigue testing has alluded to a lowering of the high cycle fatigue limit, a comprehensive testing programme should be undertaken in order to ascertain whether a statistically significant lowering of the both the low and high cycle fatigue properties occurs in peened Ti-834 following thermal exposure in air. Such a fatigue testing programme should also investigate the effect of stress ratio on the high cycle strength and mechanisms of crack initiation.

In order to develop more potent predictions for the effect of shot peening on surface oxygen uptake during prolonged thermal exposure, a parametric study should be undertaken which measures oxygen diffusion profiles following exposure at a range of temperatures and times. A suggested experimental matrix for Ti-834 is listed in table 6.1.

Table 6.1: Proposed experimental matrix to determine activation energies for oxygen diffusion in shot peened and as-machined Ti-834

Surface condition	Exposure Temperature (°C)	Exposure Time (hrs)
As-machined/Shot peened	600/650/700	10
As-machined/Shot peened	600/650/700	100
As-machined/shot peened	600/650/700	1000

If the data is of sufficient quality, it will be possible to numerically determine the diffusion coefficients (D_T) for oxygen in Ti-834 at the range of temperatures suggested through fitting the following expression to the experimental data:

$$1 - \frac{C - C_0}{C_s - C_0} = erf\left(\frac{x}{2\sqrt{D_T t}}\right)$$ Eqn. 6.1

Where C is the measured concentration of oxygen at a distance x from the exposed surface, C_s is the surface concentration of oxygen and C_0 is the bulk concentration following exposure in air for a time t. The activation energy for diffusion of oxygen in

either shot peened or machined Ti-834 (*Q*) may be calculated through the Arrhenius equation:

$$D_T = D_0 \exp \frac{-Q}{RT}$$

Eqn. 6.2

By plotting *ln(D$_T$)* as a function of reciprocal temperature (1/T) for all temperatures investigated. The pre-exponential term *D$_0$* is the intercept of the straight line through the y-axis and the gradient is the activation energy for oxygen diffusion (*Q*) in Ti-834.

An opportunity also exists to fully characterise the nature of the mechanical twin boundaries observed in shot peened titanium alloys. In chapter 3, it was proposed that the mechanical twin boundaries act as short-circuit diffusion pathways for oxygen during exposure to air at elevated temperatures. Whilst some evidence in the literature suggests that a high dislocation density is associated with the mechanical twin boundaries, it would be beneficial to characterise the boundary structures in peened material through transmission electron microscopy. Due to the close proximity of the twinned structure to the surface of the specimens, it is recommended that TEM foils are prepared via a focussed ion beam method. Such a specimen preparation strategy could also be employed to obtain TEM foils from thermally exposed specimens, with a view to characterising the crystal structure and orientation relationship between the silicides and the α-titanium matrix.

In terms of understanding the effect of different surface finishing methods on subsurface microstructure, future research should investigate turning (to compliment the high speed milling studies) and low plasticity burnishing. Additionally, milling trials might be performed on unidirectional or cross-rolled plate to investigate whether significant changes in deformation mode occur as the angle between the milling direction and the rolling direction is varied.

Finally, deformation maps similar to those developed by Guo *et al* [1] and discussed in chapter 2 could be generated for the milling and turning operations. Here, the subsurface deformation microstructures would be characterised through electron backscatter diffraction and plotted as a function of the key process variables identified for industrials machining processes e.g. feed rate, depth of cut and surface speed. Such microstructural studies may be complimented with finite element simulations to predict the resulting subsurface microstructure as a function of strain, strain rate and maximum temperature; all three of which are directly related to the key machining variables.

[1] Y. Guo, C. Saldana, W. Dale Compton *et al*, Acta Materialia 59 (2011) 4538 – 4547